



## AN ABSTRACT OF THE THESIS OF

Daniel Way for the degree of Master of Science in Wood Science presented on June 2, 2015

Title: Proof of Concept for a Three-Dimensional Molded Core Wood-Strand Sandwich Panel

Abstract approved:

---

Arijit Sinha

Frederick A. Kamke

Sandwich composites are typically produced from two high strength facings bonded to a lower strength, lightweight core. Sandwich design has proven to be efficient for applications demanding high strength and low weight. Wood-based sandwich composites have been largely limited to non-structural applications with the exception of structural insulated panels and balsa core sandwich composites. This research presents a sandwich composite panel composed of oriented strand board (OSB) facings and a three-dimensional molded core produced from wood strands.

Three-dimensional molded core panels (3DMCPs) were fabricated and subjected to bending, flatwise compression, in-plane shear, mechanical fastener, and small-scale shear wall testing. Results from these tests were compared to code-approved OSB sheathing to determine the feasibility of using this 3DMCP for structural sheathing applications.

© Copyright by Daniel Way  
June 2, 2015  
All Rights Reserved

Proof of Concept for a Three-Dimensional Molded Core Wood-Strand Sandwich Panel

by  
Daniel Way

A THESIS

Submitted to  
Oregon State University

in partial fulfillment of  
the requirements for the  
degree of

Master of Science

Presented June 2, 2015  
Commencement June 2015

Master of Science thesis of Daniel Way presented on June 2, 2015

APPROVED:

---

Co-Major Professor, representing Wood Science

---

Co-Major Professor, representing Wood Science

---

Head of the Department of Wood Science and Engineering

---

Dean of the Graduate School

I understand that my thesis will become part of the permanent collection of Oregon State University libraries. My signature below authorizes release of my thesis to any reader upon request.

---

Daniel Way, Author

## ACKNOWLEDGEMENTS

I would like to express sincere appreciation to the following individuals for their support in my work and personal life throughout this thesis:

- My advisors, Ari and Fred for all of the help they have provided throughout this project and the knowledge they have passed on. The time of my other committee members, Kenny Martin and David Woodruff is greatly appreciated
- Milo Clauson- Milo has the most widespread knowledge base of anyone I have ever met. His clever ideas and teaching ability contributed greatly to my success. Thank you for the coffee, lunches, stories, laughs, and pushing me to expand my critical thinking ability.
- My parents, Rob and Carol, for providing love, a wonderful home, support, and positive outlook on life that made me the person I am today.
- My best friend Camille for always being there and supporting me through the good and the bad.
- My good friends Chris, Dennis, Hannah, Jake, Jenna, Jeff, Molly, Ryan, Sharon Stewart, and Skip for all the good times.
- Shawn Freitas for support and guidance on grad student life and many hours of good laughs in the office.
- Members of the Kamke and Sinha research groups for their guidance and support.

## TABLE OF CONTENTS

	<u>Page</u>
Chapter 1- Introduction.....	1
Chapter 2- Literature Review .....	4
Sandwich composites General Design Provisions .....	4
Common Wood-Based Sandwich Composites .....	6
Wood Structural Panels .....	7
Wood-Based 3DMCP Product Development .....	9
Mechanical Testing Procedures .....	11
Chapter 3- Materials and Methods .....	20
Core Manufacturing.....	20
Sandwich Panel Fabrication.....	23
Bending.....	28
In-Plane Shear.....	29
Flatwise Compression.....	32
Small-Scale Shear Walls.....	33
Mechanical Fastener Performance .....	35
Chapter 4- Results and Discussion .....	40
Phase One Results.....	40
Bending.....	42
In-Plane Shear.....	48
Flatwise Compression.....	52
Mechanical Fasteners.....	55
Yield Mode Comparison.....	58
Small-Scale Shear Walls.....	60

	<u>Page</u>
Chapter 5- Conclusions.....	65
Recommendations.....	68
Literature Cited .....	69
APPENDICES .....	73

## LIST OF FIGURES

<u>Figure</u>	<u>Page</u>
1.1. Typical sandwich composite anatomy .....	1
1.2. Bottom half of the core mold used in this study .....	3
2.1. Common core geometries .....	5
2.2. Investigation of rib repeating patterns .....	10
2.3. Example of rib angle ( $\alpha$ ) .....	10
2.4. Core design used by Voth (2009) .....	11
2.5. Reference coordinate system for in-plane shear .....	13
2.6. Example of the 5% offset method.....	16
2.7. Example EEEP curve .....	19
3.1. Laboratory hot press equipped with custom molds .....	20
3.2. Top view of a core panel.....	21
3.3. Formed mat with no targeted strand alignment .....	22
3.4. Formed mat on aluminum caul plate and Teflon sheet.....	23
3.5. Custom press for bonding sandwiches.....	26
3.6. Cutting pattern for strong axis bending and in-plane shear .....	27
3.7. Cutting pattern for weak axis bending, flatwise compression, and connections .....	27
3.8. Brackets used for clamping specimen during in-plane shear test .....	30
3.9. Apparatus for flatwise compression tests .....	33
3.10. Configuration for small-scale shear walls.....	34
3.11. Nail withdrawal apparatus .....	36
3.12. Half-hole drilled in specimen and apparatus for dowel bearing test .....	37
3.13. Edge and plate connection geometries .....	38

## LIST OF FIGURES (Continued)

<u>Figure</u>	<u>Page</u>
3.14. Apparatus for edge and plate lateral connections .....	39
4.1. Typical failures observed for 3DMCPs in strong axis bending .....	45
4.2. Typical failures observed for 3DMCPs in weak axis bending .....	46
4.3. Load-shear strain plot for 3DMCPs and OSB .....	49
4.4. Shear strain contour maps .....	51
4.5. Comparison of in-plane shear failures .....	51
4.6. Flexural failure in the peak region of a flatwise compression specimen .....	53
4.7. Shear failure in the core of a flatwise compression specimen .....	54
4.8. Buckling failure of the curved rib portion in flatwise compression specimen .....	55
4.9. Comparison of three withdrawal curves between 3DMCPs and OSB .....	57
4.10. Comparison of 3DMCP geometry in lateral connection tests .....	60
4.11. Specimen 3DMCP-1 wall assembly failure .....	62
4.12. Specimen 3DMCP-2 wall assembly failure .....	62
4.13. EEEP curves for all wall assemblies.....	64

## LIST OF TABLES

<u>Table</u>	<u>Page</u>
3.1. Phase one experimental sandwich panel manufacturing matrix .....	24
4.1. Summary of phase one results .....	41
4.2. Mass, volume, and density for facings, cores, and 3DMCPs .....	42
4.3. Summary of bending results for 3DMCPs and OSB .....	42
4.4. Comparison of bending properties .....	44
4.5. Comparison between 3DMCPs and minimum Span-Rating values .....	47
4.6. In-plane shear results .....	49
4.7. Summary of flatwise compression testing .....	53
4.8. Flatwise compression failures .....	53
4.9. Summary of withdrawal testing .....	56
4.10. Summary of dowel bearing test results .....	57
4.11. Summary of lateral connection test results .....	58
4.12. Comparison of predicted yielding behavior and experimental behavior .....	60

## LIST OF APPENDICES

	<u>Page</u>
APPENDIX A.....	74
Core manufacturing .....	74
APPENDIX B .....	81
Bending.....	81
Explanation of Box Plots .....	83
APPENDIX C .....	90
In-Plane Shear.....	90
APPENDIX D.....	92
Flatwise Compression.....	92
APPENDIX E .....	96
Mechanical Fasteners.....	96
APPENDIX F .....	102
Small-Scale Shear Walls.....	102

## LIST OF APPENDIX FIGURES

<u>Figure</u>	<u>Page</u>
A1. Histogram of strand length distribution .....	77
A2. Histogram of strand width distribution .....	78
A3. Histogram of strand aspect ratio distribution .....	79
A4. Histogram of strand thickness distribution .....	80
B1. Load-deflection plot for some 3DMCPs in strong and weak axis bending .....	82
B2. Load-deflection plot for some 3DMCPs in strong and weak axis bending .....	82
B3. Boxplot comparing the bending strength of strong axis specimens .....	84
B4. Boxplot comparing the bending strength of weak axis specimens .....	85
B5. Boxplot comparing strong axis bending strength by failure mode .....	86
B6. Boxplot comparing weak axis bending strength by failure mode .....	87
B7. Comparison of weak axis bending specimens.....	89
C1. In-plane shear load-deflection plot comparing 3DMCPs and OSB .....	91
D1. Boxplot comparing compression strength for compression specimens .....	93
D2. Buckling failure at rounded portion of the rib in flatwise compression specimen ....	94
D3. Core shear failure in flatwise compression specimen .....	95
D4. Flexural failure of bottom peak in flatwise compression specimen.....	95
E1. Nail yielding in lateral connection tests .....	97
E2. Example of main member bearing yielding in lateral connection tests.....	98
E3. Example of nail contacting rib and deflecting upon further insertion.....	98
E4. Boxplot comparing withdrawal resistance .....	99
E5. Boxplot comparing dowel bearing strength of 3DMCPs .....	100

## LIST OF APPENDIX FIGURES (Continued)

<u>Figure</u>	<u>Page</u>
E6. Boxplot comparing dowel bearing strength of OSB vs. bearing direction.....	101
F1. Load-deflection plot for all small-scale shear wall assemblies .....	103
F2. Strain contour plot for specimen 3DMCP-1 at peak load.....	104
F3. Strain contour plot for specimen 3DMCP-2 at peak load.....	105
F4. Strain contour plot for specimen 3DMCP-3 at peak load.....	106
F5. Strain contour plot for specimen OSB-1 at peak load .....	107
F6. Strain contour plot for specimen OSB-2 at peak load .....	108

## LIST OF APPENDIX TABLES

<u>Table</u>	<u>Page</u>
A1. Furnish inputs for producing cores .....	75
A2. Press schedule .....	76
B1. ANOVA output comparing bending strength of strong axis specimens .....	83
B2. Multiple linear regression output comparing bending strength of weak axis specimens .....	86
B3. Multiple linear regression output comparing bending strength of strong axis bending specimens by failure mode.....	87
B4. Multiple linear regression output comparing bending strength of weak axis bending specimens by failure mode.....	88
D1. Multiple linear regression output comparing flatwise compression specimen panel placement to strength .....	94
E1. Multiple linear regression output comparing withdrawal resistance.....	99
E2. Multiple linear regression output comparing dowel bearing strength of 3DMCPs..	100
E3. Multiple linear regression output comparing dowel bearing strength of OSB.....	101

## Chapter 1- Introduction

Sandwich composites utilize an efficient design that permits for optimization of weight-critical structures (Carlsson & Kardomateas, 2011). Produced by bonding a core material between two facings (Fig. 1.1), sandwich composites are structurally analogous to an I-beam (Carlsson & Kardomateas, 2011; Strong, 2008). Relatively thin, strong facing materials act as flanges, while relatively thick, low strength core materials act as the web. Low density, or semi-hollow cores offer advantages in weight reduction, thermal insulation, and acoustical dampening. Structural efficiency has made sandwich composites a vital component for advancing the transportation industries and has potential for use in building and infrastructure construction.

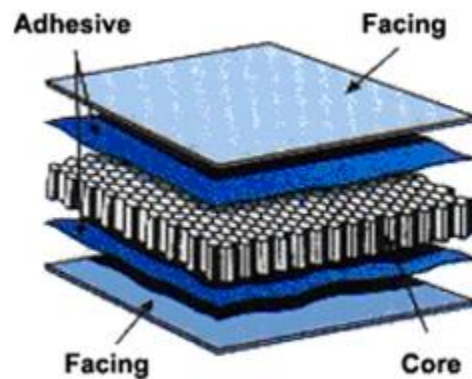


Figure 1.1. Typical sandwich composite anatomy (Engineered Materials Inc., 2015)

In the past, building construction has relied on meeting structural demands by using large, strong materials. These materials don't necessarily foster building material efficiency, both in expense and material utilization. As larger wooden structures emerge, new building products will be necessary to meet the demands associated with larger structures- while minimizing material cost, construction cost and environmental impact of the built environment.

Oriented strand board (OSB) is a popular wood composite used in light-frame construction, due to low cost and favorable structural characteristics. Adhesive is applied to strands from low density species of timber- then strands are oriented, followed by consolidation under heat and pressure. Pressure densifies the strands and with the addition of adhesive for a binder, OSB panels exhibit greater mechanical properties than the strands used to create it.

This study investigates the structural performance of a three-dimensional molded core sandwich panel (3DMCP) produced with OSB facings and a wood-strand molded core (Fig. 1.2). The purpose of this project is to determine if low cost, resource efficient panel inputs used in conjunction with an efficient structural design can create a panel with superior properties for use in building construction.

3DMCPs were fabricated and compared to code approved, Span-Rated OSB sheathing. Since the finished 3DMCPs are a panel product, it was most logical to use a proven commercial panel product for comparison. However, this product is not intended to be a direct replacement for currently produced, code approved, wood structural panels on the market. Instead, if this 3DMCP can meet the demands of wood structural panels as they are currently used, improvements in mechanical properties would allow for 3DMCPs to be used in more demanding engineering applications.

Obtaining code certification for any new structural product is a burdensome process. Numerous mechanical and physical properties of the product must be determined, followed by periodic code conformance and quality assurance testing upon certification. Code approval for structural sheathing requires testing to be performed on both partial and full-size panels. Producing full-size (1.2 m x 2.4 m) 3DMCPs is costly due to fabrication of large press molds. Laboratory size (0.71 m x 0.76 m) 3DMCP panels were produced for selected tests that would be necessary for code conformance. Determining all of the necessary mechanical properties was outside the scope of this project.

Instead, this work is a proof of concept to assess the technical feasibility of this particular 3DMCP for use in building construction. The study was broken up into two phases. First, three different sandwich composite parameters with two treatment levels were investigated for the optimum combination of parameters. Bending, in-plane shear, and flatwise compression tests were performed to quantify the performance of each combination of parameters. Second, additional 3DMCPs were produced using the chosen set of parameters for further mechanical characterization. Bending, in-plane shear, flatwise compression, mechanical connections, and small-scale shear wall performance were then tested and compared to Span-Rated OSB used as facing material. These tests were chosen to better understand crucial mechanical properties necessary for validation as a building construction product.



Figure 1.2. Bottom half of the core mold used in this study

## Chapter 2- Literature Review

### *Sandwich composites General Design Provisions*

Sandwich composites are produced by bonding facings to a core material. Face plies are generally thin compared to the total thickness of the sandwich composite and utilize dense, strong materials (Carlsson & Kardomateas, 2011). Conversely, core materials are typically lower density compared to the faces, relatively thick, and of lower strength and stiffness (Carlsson & Kardomateas, 2011). Sandwich composites are often characterized as double composite structures since utilizing composite components is often most efficient and the combination of components creates another composite (Strong, 2008).

In bending, strong and stiff face plies are responsible for moment resistance while the core carries shear forces and stabilizes the facings (Carlsson & Kardomateas, 2011). Like I-beams, the increased stiffness of sandwich composites is a function of the distance between the higher-strength face plies, instead. Facing materials must also evenly distribute load to prevent localized wrinkling or buckling of the core.

Core materials are classified into two broad categories: “cellular” and “structural,” (Carlsson & Kardomateas, 2011). “Cellular” cores have hollow spaces enclosed by walls, with common examples being foams, honeycomb, and balsa wood. “Structural” cores consist of a continuous web made from a solid material, with a common example being corrugations found in fiberboard packaging. “Structural” cores are often referred to as ribbed, corrugated, or webbed (Fig 2.1).

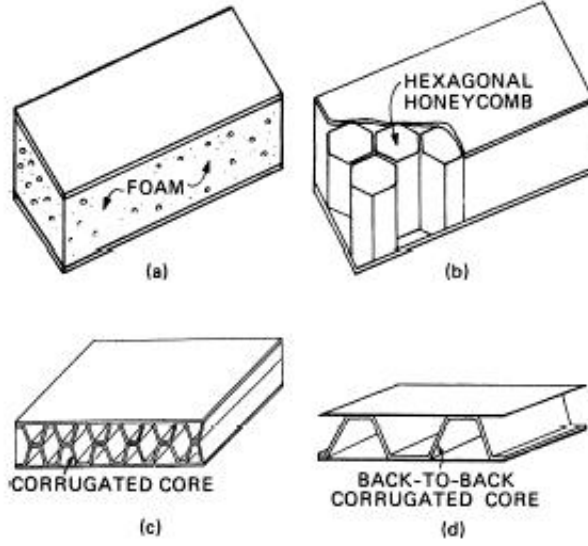


Figure 2.1. Common core geometries. “Cellular core” (a, b) and “Structural Core” (c, d) (Nallagula, 2006).

Carlsson and Kardomateas (2011) provide general equations (equation 2.1 and 2.2) for determining the bending stiffness of a sandwich beam of symmetrical cross-section using the parallel axis theorem. This approach works well with simple core geometries, but a complete analysis of bending stiffness for more complex geometries and material configurations is better accomplished through finite element analysis (Hunt, 2004; Nallagula, 2006).

$$D_x = E_x^f \bar{I}_f d^2 + \frac{h_c^3}{12h_f d^2} \frac{E_x^c}{E_x^f} + \frac{1}{6} \left( \frac{h_f}{d} \right)^2 + \frac{1}{2} \quad (\text{Eq. 2.1})$$

In equation 2.1,  $D_x$  is the bending stiffness about the x-axis,  $E_x^f$  and  $E_x^c$  are the modulus of elasticity of the facings and core respectively,  $h_f$  and  $h_c$  are the thicknesses of the facings and core respectively, and  $d$  is distance between the centroids of the facings.

The first term in the brackets of equation 2.1 represents the core’s contribution to bending stiffness, which is generally small. When facing materials are relatively thick, the second term in the brackets becomes significant. Since facings are generally designed to be thin compared to the core, a limit is reached at which the second term in the

brackets has significance. In an ideal sandwich composite, this limit occurs when the ratio of core thickness to facing thickness is less than 5.35. If the bending stiffness contribution from the core is very small, and the core to facing thickness ratio is satisfied, then equation 2.1 simplifies to:

$$D_x = \frac{E_x^f h_f d^2}{2} \quad (\text{Eq. 2.2})$$

Equation 2.2 shows that the bending stiffness calculation is simplified when the facings are thin compared to the core and the core contributes minimally to bending stiffness. For these reasons, most sandwich composites utilize thin, high modulus materials bonded to a low-density, compliant core (Carlsson & Kardomateas, 2011).

#### *Common Wood-Based Sandwich Composites*

Being the lightest commercially available wood species, balsa (*Ochroma sp.*) is an important core for sandwich design. Balsa possesses considerable strength properties for its weight and has been used heavily in aviation and maritime applications (Easterling et al., 1982). Fiber-reinforced polymer (FRP) wrapped balsa wood has gained attention for use in bridge decks, where it offers increased corrosion resistance, decreased installation time, low maintenance and durability (Cai et al., 2014; Overney, 2012)

Use of wood-based sandwich composites in building construction has been relatively limited. An exception is the use of structural insulated panels (SIPs) that are gaining popularity in the green building materials market because of their favorable insulation properties and fast erection times (Allen & Thallon, 2011). SIPs consist of a foam polymer insulation core bonded to wood structural panel facings (APA- The Engineered Wood Association, 2013). SIPs are designed to replace traditional light-frame diaphragm systems by carrying axial, transverse, and racking loads that are placed on the structure (APA- The Engineered Wood Association, 2013).

The Forest Products Laboratory (Madison, Wisconsin, U.S.), originally introduced the idea of SIPs in the 1930s (Panjehpour et al., 2013). Adoption of SIPs into

the 2007 *International Residential Code* (IRC) allowed for wider spread use since this document provides prescriptive design methods for builders (SIPA, 2015). The use of other facings to substitute wood structural panels is possible (Panjehpour et al., 2013), but the IRC supplies prescriptive methods only for SIPs produced with code-approved wood structural panels (APA- The Engineered Wood Association, 2011; International Code Council, INC, 2011).

SIPs are generally prefabricated with openings for doors, windows, and chases for electrical wiring and utilities, resulting in efficient installation and minimized waste (Panjehpour et al., 2013). Model homes built in the early 2000s have been shown energy efficiency increases of 60-70% compared to traditional light-frame homes that meet the model energy codes (Maynard, 2009).

Despite the benefits that SIPs offer, there have been some concerns and limitations preventing a wider-spread use of the material in residential and light-commercial buildings. Long term durability of the panels is not fully understood and repairs to damaged sections can be limited (Maynard, 2009). Contractors may also be reluctant to use SIPs for the first time because of the added complexity of connections and the limitations of running utilities through prefabricated chases (Maynard, 2009). In addition, the IRC limits the size of a structure produced from SIPs to 40 feet wide, 60 feet long, and two stories in height along with specific wind and seismic zone limitations (International Code Council, INC, 2011). Although these limitations may be insignificant in most parts of the country, light-frame construction practices allow for more design options than SIPs.

### *Wood Structural Panels*

Oriented Strand Board (OSB) is the most common structural panel certified under PS 2-10 (APA- The Engineered Wood Association, 2011). OSB is manufactured by applying a structural adhesive to wood strands and consolidating them together under heat and pressure (Smulski, 1997). Strands are typically produced from a low-density wood species with the most common being aspen (*Populus sp.*). Heat and pressure from

the pressing process densifies the strands, improving their mechanical properties. Since the early 1980s, a width ranging from 0.5-3 inches, length from 4-6 inches, and thickness from 0.023-0.027 inches have been the commercially-targeted strand geometries (Smulski, 1997). Like plywood, favorable mechanical properties of OSB are obtained by creating an odd number of layers oriented perpendicular to each other (APA- The Engineered Wood Association, 2012). The orientation of layers and the orthotropic nature of wood results in a panel exhibiting different properties depending on the loading direction. Perpendicular layer orientation also favors flatwise dimensional stability with changes in moisture content and a reduction of splitting upon insertion of fasteners.

OSB panels are designed to efficiently use resources. Stranding processes are highly controlled, but still result in a distribution of strand sizes (Smulski, 1997). Smaller strands are utilized in the core layer and longer strands in the face layers. A higher aspect ratio of the long face strands improves the ability to orient strands and increases the ultimate bending stress that is seen at the outer fibers. Separate adhesive systems may also be used for the core and face layers where an adhesive with a faster cure time is used in the core and a slower curing adhesive in the face (Smulski, 1997).

In the early days of wood structural panel manufacturing and use, the availability of technology and raw materials was fairly limited, which allowed for prescriptive manufacturing methods to be implemented and design values were determined for each of the few panel lay-up options (APA- The Engineered Wood Association, 2012). As technology advanced and new raw materials were available, the prescriptive method placed constraints on how manufacturers could produce panels. Introduction of performance-based standards offered a solution. Manufacturers now had the flexibility to choose whatever materials they wanted as long as their panels met minimum values for code approval (APA- The Engineered Wood Association, 2012). Through the National Institute of Standards and Technology (NIST), third-party testing organizations, such as APA- The Engineered Wood Association (APA), are responsible for determining the performance criteria and testing protocol for wood structural panels in the U.S.

### *Wood-Based 3DMCP Product Development*

A literature review by Hunt (2004) summarized the current technology and applications of wood-based 3DMCPs, which differed by design, manufacturing technology, and raw material input. Structural efficiency of 3DMCPs can help to offset the demand of fiber resources through selective removal of core material without resulting in significant reductions of mechanical properties. The FPL has worked to develop three-dimensional molded core (3DMCP) sandwich composites using wood fiber in response to the USDA National Fire Plan to utilize small-diameter timber (Hunt & Winandy, 2002, 2003; USDA Forest Service, 2001). Thinning of dense, small-diameter timber stands along with removal of dead surface fuels aids in wildfire management. However, removal is expensive due to lack of a viable market.

In response to the USDA National Fire Plan, Hunt and Winandy (2003) worked to develop a 3DMCP produced from small-diameter timber fiber. Results from previous research were used to determine the best method of refining fiber from tree tops and were used as the material inputs for this study (Hunt & Winandy, 2002). Tree tops were fiberized using mechanical refining and a wet-forming process was used to produce fiber mats. This process was chosen to obtain a more uniform fiber distribution and utilize the natural bonding ability of a wet-formed mat, eliminating the use of adhesives. The design focused on developing a product suitable for use as pallets, bulk bins, heavy duty boxes, shipping containers, wall panels, roof panels, displays, desks, shelves, tables, and doors.

An engineering analysis was conducted to determine the potential performance of their 3DMCP product idea. They investigated the effect of rib angle (Fig 4.2), distance between peaks in the repeating pattern (Fig 4.3), and rib thickness. Using a three-point bending test they compared these factors at the same load per unit width. The bending stiffness in the longitudinal direction (strong axis) for all configurations was found to be very consistent, a result of the facings representing 85-95% of the moment of inertia, meaning that the core contributed minimally to bending stiffness. For the transverse axis (weak axis), the repeating pattern was not uniform, making the moment of inertia calculation difficult. In this case, they simply ignored the contribution of the core

resulting in a conservative estimate of bending stiffness. Results of this study indicated that a 3DMCP from low-value fiber could be designed to be stiffer than minimum particleboard standards with significantly less material usage.



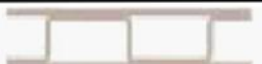
50.8 mm (2.0 in) Pattern Width with 90 degree rib angle shown repeated 3 times.	
76.2 mm (3.0 in) Pattern Width with 90 degree rib angle shown repeated 2 times	
101.6 mm (4.0 in) Pattern Width with 90 degree rib angle shown repeated 1.5 times	

Figure 2.2. Investigation of rib repeating patterns (Hunt & Winandy, 2003)

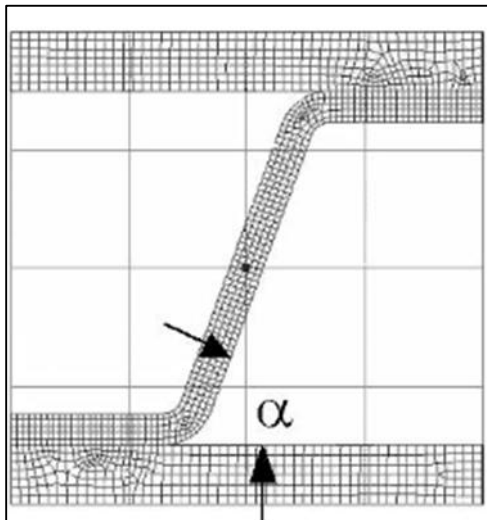


Figure 2.3. Example of rib angle ( $\alpha$ ) (Hunt, 2004)

Hunt investigated the effect of rib geometry on flatwise compression of wood-based 3DMCPs using FEA modeling (Hunt, 2004). Depending on the geometry and elastic properties of the rib structure, failure in compression normal to the surface may occur as buckling or compression of the ribs. When the rib length-to-thickness ratio increases, the ribs act as miniature columns and fail prematurely in buckling. Short, thick ribs tended to favor compressive failure, where compressive deformation occurs instead of structural failure.

Voth (2009) designed a bi-directional molded core panel (Fig. 2.4) using two different wood-based raw materials for the core and OSB facings and found that bending failures were governed by the shear strength of the core-facing interface- meaning that the design did not have core-facing bonding interface area. Failure was consistent between 3DMCPs produced with wood strands and old newsprint cores.

The greatest success has been for non-structural applications (ECOR, 2015; Neucor, 2015). SingCore (McCleary, WA, U.S.) produces a wood-based sandwich composite product that utilizes a vertical veneer honeycomb design, which is filled in with synthetic foam. This product has had the greatest success for doors (SingCore, 2015).

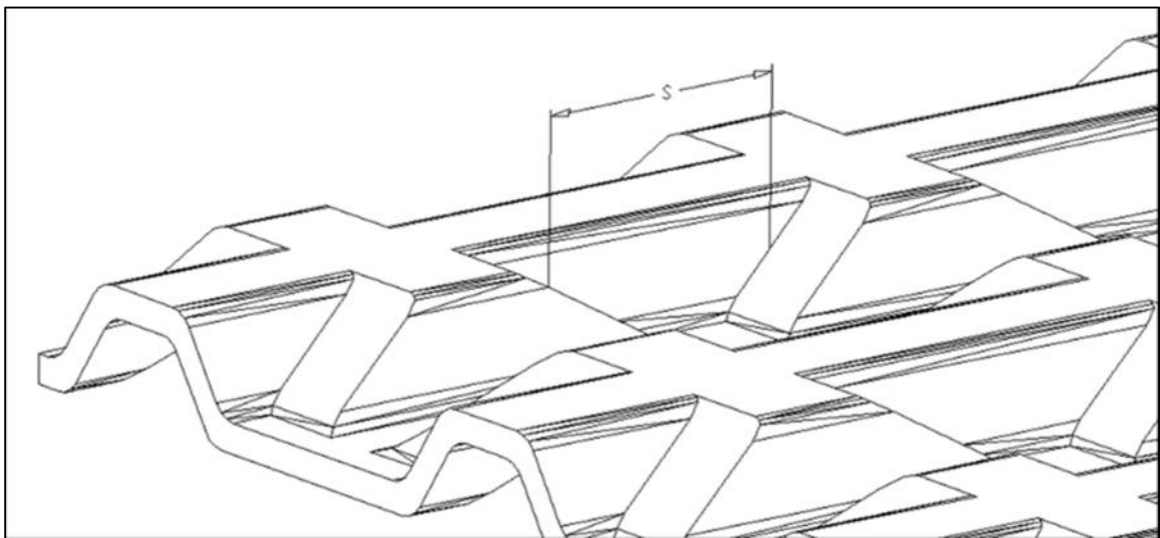


Figure 2.4. Core design used by Voth (2009)

### *Mechanical Testing Procedures*

Using a three-point bending test, Nallagula (2006) found that experimental deflections were less than those predicted with FEA on a balsa wood core and glass fiber polyester facing sandwich composite. Both Nallagula (2006) and Voth (2009) reported maximum failure load but did not report the ultimate bending stress, although both studies analytically derived equations for doing so. Shear failure in the core material was

the limiting failure in bending for both studies, which may have been why maximum flexural stress was not reported.

ASTM D7249 subjects a long sandwich beam to a bending moment normal to the plane of the sandwich and is meant to determine the facing properties of the structure (ASTM, 2012c). Internal facing failure is the only acceptable failure mode making it necessary to have a sufficiently long specimen to reduce the likelihood of failure at the core-facing interface or within the core. Limitations to this standard are that results are intended to be specific of the facing material, not the sandwich composite as a whole. ASTM D7250 allows for calculating the flexural stiffness, shear rigidity, and core shear modulus of a sandwich beam (ASTM, 2012a). The drawback to this method is the requirement to use data from at least two different testing configurations.

ASTM D3043 is used to determine the flexural properties of wood structural panels (ASTM, 2011). The center-point loading method (Method A) from this standard was developed to investigate many variables and to test small, defect-free specimens. The drawback to this method is a relatively constant presence of shear across the cross-section, and thus flexural properties tested are not from pure bending. It is also limited to relatively uniform materials.

In-plane shear (or shear-through-the thickness) occurs when loads are applied on opposite edges of the panel causing shear stress and distortion about the x-y plane (Fig. 2.3) (Alldritt, 2013; APA- The Engineered Wood Association, 2012; ASTM, 2013b). In-plane shear strength and stiffness are important properties for panels used in I-joist webs and lateral force resisting systems in light-frame construction (Alldritt, 2013; Breyer et al., 2015). ASTM D2719 (2013) calls for bonding a panel to heavy wood or metal rails and loading them in tension to induce a shearing force. Several researchers have obtained favorable results by avoiding the cumbersome process of bonding the panels to the rails, instead bolting the panel between two sets of rails (Alldritt, 2013; Shrestha, 1999).

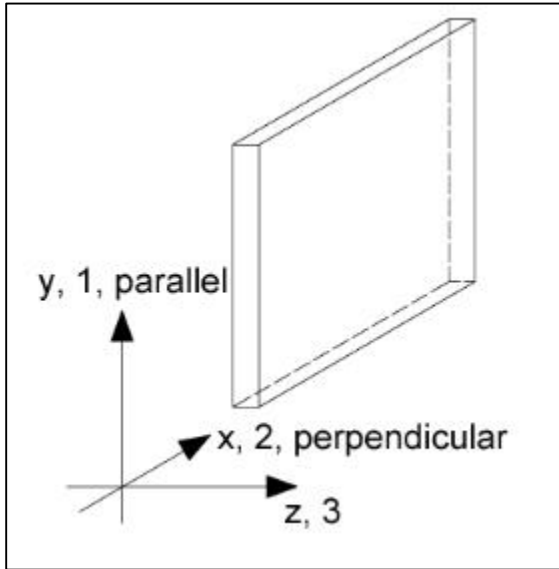


Figure 2.5. Reference coordinate system for in-plane shear (Alldritt, 2013).

Digital image correlation (DIC) is an optical, non-contact method to measure two-dimensional deformation on a surface. DIC uses an algorithm to simultaneously track targets on a specimen surface and has been used extensively in material science (Schwarzkopf et al., 2013; Sutton et al., 2009). Blocks (subsets) of contrasting pixels are tracked relative to a reference image throughout specimen deformation (Sutton et al., 2009). Tracking the multiple targets during testing with two cameras allows for full-field information on topography ( $x$ ,  $y$ , and  $z$  coordinates) as well as surface displacements and strain components (Schwarzkopf et al., 2013).

As a non-contact deformation measurement tool, DIC has many advantages compared to deformation measurements requiring contact with the specimen (e.g. strain gauges). The user is able to analyze full field strain measurements and generate a strain contour map of the specimen. Two dimensional (2D) DIC using one camera can quantify deformation and rotation in solids, but is limited to in-plane displacements and strains (Sutton et al., 2009). Constrained to in-plane deformations, 2D DIC is sensitive to errors caused by small out-of-plane motions (Sutton et al., 2009). To combat these issues, two cameras capture images of the specimen, allowing for deformation measurement in three-

dimensions (Sutton et al., 2009). Three-dimensional (3D) DIC greatly expanded the use of DIC in mechanical systems that are subject to out-of-plane motions (Sutton et al., 2009).

In 3D DIC, a pair of high resolution cameras capture images of a specimen during testing. Cameras are calibrated based on a known reference target. The software then tracks blocks of pixels (the subset) in relation to a reference image. Principle strain calculations are made based on a grid of correlation points. The distance between these points is known as the step size (Correlated Solutions, 2010). Next, each point in the grid is considered separately and a local mesh of triangles are created. Each triangle is considered separately and rigid body motion is determined. The remaining deformation provides enough information to create a strain tensor for that single triangle, and then the process is repeated for all triangles.

Painting structural wood panels with either a black or white background followed by application of a contrasting speckle pattern (either black or white) has been used successfully to measure strains by several researchers (Alldritt, 2013; Sinha & Gupta, 2009). The software used does not differentiate color, but only the binary contrast between the speckles and the background (Correlated Solutions, 2010). Effective speckle patterns are non-repetitive and have high contrast to the background (Correlated Solutions, 2010). Speckle size is also important. If the speckles are too large, then there may be certain subsets that contain all black or all white resulting in poor matching. Large speckles can be dealt with by increasing the subset size at the sacrifice of spatial resolution. If the speckles are too small, then very high resolution cameras are required to distinguish movement.

Flatwise compressive strength is generally not a controlling mechanical property for wood structural panels. However, when a column (such as a stud) or appliances rest on a piece of sheathing, the flatwise compressive strength becomes important due to deflection limits (APA- The Engineered Wood Association, 2012). The presence of voids in 3DMCPs leads to failures that are not typical of solid panel products. Ribbed structures

are subjected to localized rib buckling, localized rib compression failure, and localized compression failure of the facings (Carlsson & Kardomateas, 2011; Gibson & Ashby, 1997; Hunt & Winandy, 2003; Voth, 2009).

The ability to make connections of adequate strength and ductility is imperative for using wood structural panel products in construction applications to provide lateral support of the structure. Analysis of building failures following hurricanes and earthquakes has shown time and time again that inadequately fabricated connections lead to premature failure (Breyer et al., 2015). Because of the importance of connections in a structure, connection properties of any new panel product must be determined and compared with baseline values given in the *National Design Specification for Wood Construction* (NDS) (AFPA, 2012). In light-frame construction, the most common lateral force resisting system is composed of wood structural panels attached to framing members through dowel-type fasteners (e.g. nails). Connections between sheathing and wood framing members are generally the weakest link in a shear wall assembly and are of significant design concern (Sinha et al., 2011).

Dowel bearing strength is a measure of the resistance to embedment, (i.e. crushing of wood fibers) of a dowel-type fastener in wood or wood composites and is directly correlated with the specific gravity of the material and fastener diameter (Breyer et al., 2015; Wilkinson, 1991). Dowel bearing strength is determined experimentally using the 5% offset method. Using the 5% offset method, yield load is determined by offsetting a line of the same slope as the linear region from experimental load-deflection plot, and determining the load at which the offset line and curve intersect (Fig. 2.6) (AFPA, 2012; Breyer et al., 2015; Sinha et al., 2011; Wilkinson, 1991). For small diameter fasteners (e.g.  $D < 0.25$ -in) the direction of fastener loading with respect to the grain in wood is considered the same whether it is parallel, perpendicular, or different angle (ASCE, 1996; AFPA, 2012; Breyer et al., 2015). Dowel bearing strength is the material property of the connection members that is used to predict the connection yield capacity.

Three common connection geometries exist for wood structural panels to framing members in shear wall assemblies- plate, edge, and field (Sinha et al., 2011). Plate and edge connections are made around the perimeter of the panel and have been found to be the first connections to fail (Sinha & Gupta, 2009). This can be deduced from the NDS, where the fastener edge spacing influences unit shear capacity for a given panel thickness/fastener diameter (AFPA, 2012). The main difference between edge and plate connections is that the dowel loads the framing member parallel to the grain in the edge connection, whereas the loads are perpendicular to the grain in the plate connection when resisting pure overturning moment. Edge and field connection have been found to have similar ultimate strengths, yield loads, and yield modes (Kent, 2004; A Sinha et al., 2011).

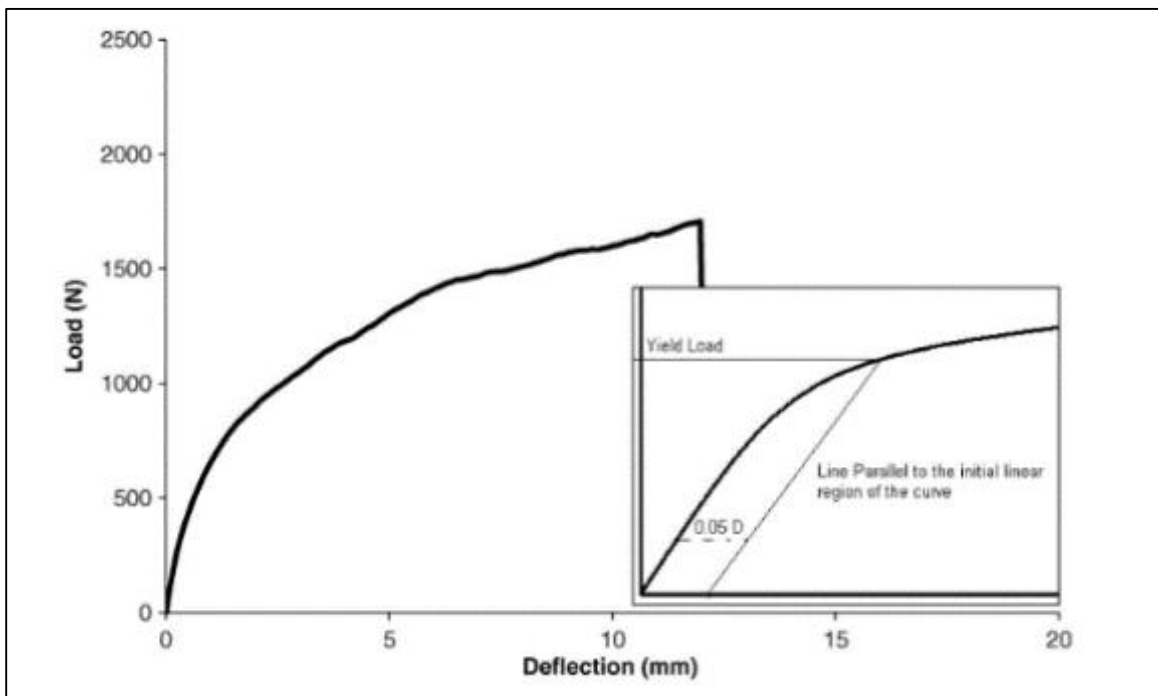


Figure 2.6. Example of the 5% offset method (Sinha et al., 2011)

An engineering mechanics approach for determining the design value of a dowel-type connection between solid wood-to-solid wood, wood-to-metal, wood-to-concrete, or wood structural panels-to-solid wood is given in the NDS and is known as the *yield limit model for dowel-type fasteners* (AFPA, 2012; Breyer et al., 2015). These yield limit

models were first developed by Johansen (1949) to provide a predictive method for assessing the capacity of connectors based on geometry and material property inputs (A Sinha et al., 2011). Deformation of the assembly depends on which member of the connection yields and is dependent on the stiffness of the dowel and bearing strength of the wood (ASCE, 1996). Six possible yield modes are given in the NDS for two-member, or single shear, connections (AFPA, 2012). Factors affecting the load capacity of these connections include the embedment strength of each constituent, the thickness of each constituent, the diameter of the fastener, and the material properties of the fastener (ASCE, 1996; Breyer et al., 2015).

Yield limit models have been successfully implemented for predicting the behavior of typical shear wall connections exposed to biological decay (Kent, 2004) and elevated temperatures (Sinha et al., 2011). This was done by experimentally determining the dowel bearing strength after subjecting the specimens to degradation conditions and using this dowel bearing strength in the yield limit models.

Isolated characterization of mechanical properties is important for understanding performance of individual components in a structural system. However, wood structural panels are rarely used on their own and are generally an assembly component. Wall racking is the tendency for a sheathed wall to distort from forces applied in-plane (parallel) to the length of the wall (ASTM, 2012b). The result of the distortion is horizontal displacement of the wall (McCutcheon, 1985). The objective of racking tests is to determine the shear stiffness and strength of the wall configuration, which are important considerations for designing shear wall assemblies (ASTM, 2012b).

To fully understand racking performance of a particular wall assembly, dimensions of the test wall must be similar to that of a typical section of two full-size panels (2.4 m x 2.4 m) that would be used in service. Testing of a full-size wall section is a taxing process from a materials, expense, labor, and data analysis stand-point. For proof of concept testing the use of full-size panels may not be possible. Characterizing the performance of a shear wall assembly as it would respond in a seismic event is also

difficult because it requires difficult loading procedures and statistical analysis. Beall et al. (2006) tested 1.2 m x 1.2 m wood-frame shear wall assemblies and found that wall assemblies at this dimension provided good sensitivity to variations in materials, assemblies, and moisture exposure and could help to screen variables to minimize the amount of full-scale testing needed.

McCutcheon (1985) performed a study to better understand the racking performance of wood shear walls at load levels typical of design loads. As mentioned by Price and Gromala (1980), load-slip characteristics of nailed connections are generally assumed to be linear, but in reality these interactions are nonlinear. McCutcheon presented an analytical model to calculate nonlinear racking deformation of wood shear walls. Results indicated that at low load, the shear stiffness of the panel is responsible for wall deformation, where at higher loads the load-slip (yielding) behavior of the connections becomes more significant in the total deformation of the wall.

Equivalent energy elastic-plastic (EEEP) curves are a perfectly elastic-plastic representation of the response seen in a shear wall (Sinha & Gupta, 2009). EEEP curves are plotted such that the curve is equal to the area under the load-deflection plot obtained from small-scale (or large) shear wall testing. First, load and deflection are determined for 40% of peak load, peak load, and 80% of post-peak load. Next, a line with slope equal to 40% peak load over its corresponding deflection is plotted from point (0,0) through the point of 40% peak load- stopping at a load equal to 80% post-peak load. Next, a line with slope equal to zero continues from the linear line until the point of 80% post peak load. This method allows direct quantitative comparison of total energy absorption until failure for different wall assemblies (Sinha & Gupta, 2009). Important characteristics of EEEP curves are the load at 40% peak load, 80% peak load, and peak load (Fig. 2.7).

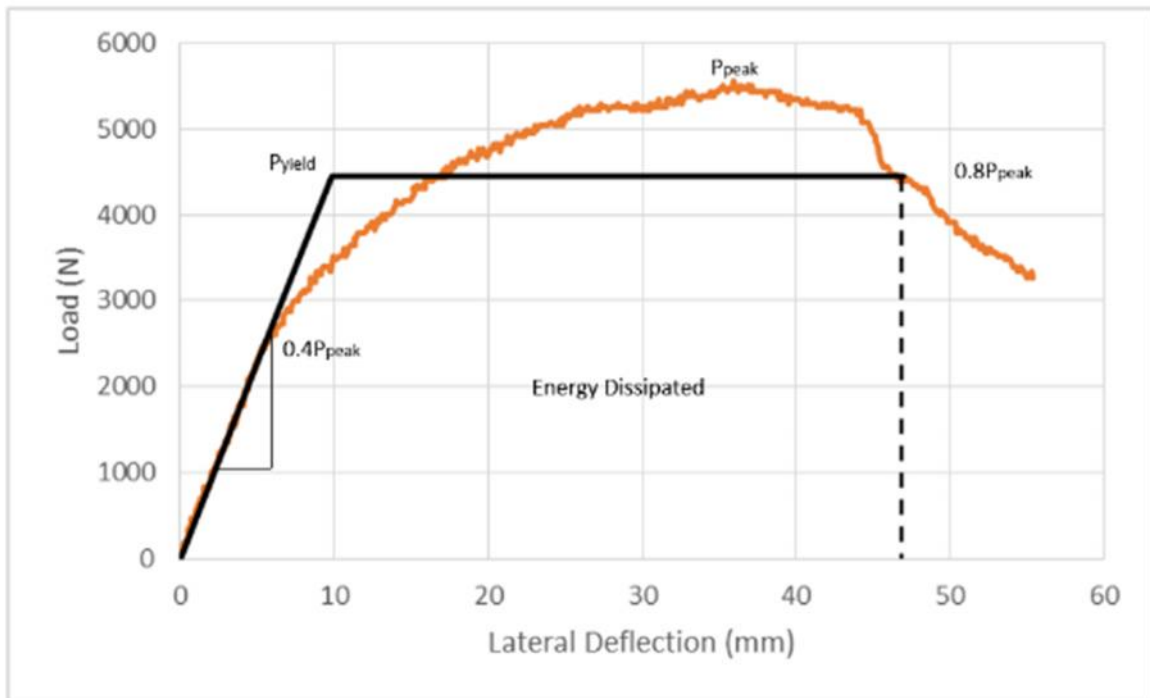


Figure 2.7. Example EEEP curve

## Chapter 3- Materials and Methods

### *Core Manufacturing*

Cores were manufactured using proprietary aluminum molds (Fujii, 2014) supplied by the sponsoring company. The molds were attached to a 0.91 m x 0.91 m hot-press with the top half of the mold bolted to the hot press and the bottom half floating freely on the press platen (Fig. 3.1). The mold was 749 mm wide and 800 mm long. The contoured rib areas lead to an increased surface area compared to a flat panel of the same width and length. A surface area modification factor of 1.3 for the molded core was determined using image analysis software (ImageJ). The repeating corrugation structure varied both in the length and width directions and was at an angle of 30 degrees to the length direction (Fig. 3.2) with a 19 mm rib depth.



Figure 3.1. Laboratory hot press equipped with custom molds

Target core densities of  $0.56 \text{ g/cm}^3$  and  $0.64 \text{ g/cm}^3$  were chosen since this represents a fairly average range of commercial OSB densities. Two core adhesive contents of four and six percent were used to represent the average and high end of commercial OSB. Commercial OSB strands were donated by a manufacturer in the Great Lakes Region. Species mix was predominately aspen with a small percentage of assorted hardwood species. Strands were screened at the facility to a geometry distribution typical of strands used in the core layer of three-layer OSB. No additional screening was performed to remove fines. Strands were dried before shipping to a moisture content of approximately 6% and placed into plastic bags upon delivery, remaining sealed until processing.

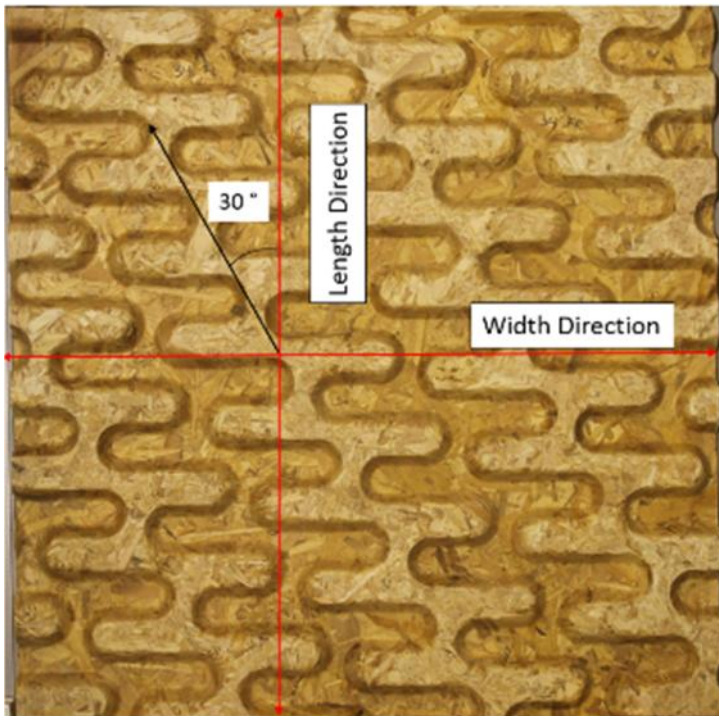


Figure 3.2. Top view of a core panel

Strands were placed in a rotating drum blender measuring 1.83 m in diameter and 0.89 m in depth. The blender was set to rotate at 5 rpm while a spinning disk atomizer (Coil Model EL4, Surrey, British Columbia) spinning at 10,000 rpm applied adhesive to the strands. A phenol formaldehyde adhesive blended specifically for use in OSB face layers was used for the cores (GP Chemicals, Atlanta, GA, USA) with a weight based

resin solids content of 55%. Blending occurred in batches of three panels with 15% additional furnish to account for blending and forming loss.

After blending, furnish for a single panel was weighed. Mats were hand formed, targeting a random orientation of strands (Fig. 3.3). Several trials were performed to make the core panels as uniform as possible and eliminate the presence of voids. Strands were placed in a 711 mm by 762 mm forming box one handful at a time. Strands were dropped using a shaking motion from approximately 50 mm above the level in the forming box. Forming started at one corner of the forming box and a level layer of strands was laid across the entire surface until reaching the opposite corner. This occurred four times until all of the strands were used.



Figure 3.3. Formed mat with no targeted strand alignment

When approximately half of the strands remained, the mat was rotated 90 degrees and prepressed by hand with two people using an OSB panel. The purpose of this procedure was to look for high and low areas of strands in the mat and achieve a uniform distribution of strands. The mats were formed on a sheet of Teflon to aid in transferring to the mold (Fig. 3.4). Prepressing occurred once more when all of the strands had been used. Once inside the mold, a board was used to hold the mat in place and the Teflon and aluminum caul plate were removed.



Figure 3.4. Formed mat on aluminum caul plate and Teflon sheet for transferring into the hot press

Platen temperature was set to 165°C and the temperature of the mold surface was verified with an infrared thermometer. No significant heat loss of the surface of the mold was observed after removing a pressed panel. Panels were pressed using displacement control until the press reached the desired thickness of 6.33 mm. The press was set to reach set-point in 24 seconds. Panels were held at 6.33 mm for a period of 240 seconds and vented at a rate of 0.05 mm/sec for 40 seconds. The same pressing schedule was used for all panels and no blow outs were observed during venting.

#### *Sandwich Panel Fabrication*

For the first phase of the project, two nominal thicknesses of commercial OSB were used as sandwich panel facings. Half of the sandwich panels were produced using 9.5 mm nominal (3/8 in) thick 24/0 Span-Rated OSB and the other half were produced using 11.1 mm thick nominal (7/16 in) 24/16 Span-Rated OSB. Average density for the 9.5 mm thick panels was 0.66 g/cm<sup>3</sup> with a coefficient of variation (COV) of 6.7% while the average density for the 11.1 mm thick panels was 0.60 g/cm<sup>3</sup> with a COV of 6.1%. Table 3.1 contains the test matrix of sandwich panel inputs used for the first phase of the project. The purpose of this test matrix was to determine the best combination of chosen manufacturing parameters for producing panels for the second phase of testing to complete a broader mechanical characterization of the 3DMCPs.

Table 3.1. Phase one experimental sandwich panel manufacturing matrix for determining the set of panel parameters to be used for phase two of the project.

<b>Group</b>	<b>Target core density (g/cm<sup>3</sup>)</b>	<b>Core adhesive content (%)</b>	<b>Nominal facing thickness (mm)</b>	<b>Replications</b>	<b>Average core density (g/cm<sup>3</sup>)</b>
<b>1</b>	0.56	4	9.5	12	0.56
<b>2</b>	0.56	6	9.5	12	0.62
<b>3</b>	0.56	4	11.1	12	0.62
<b>4</b>	0.56	6	11.1	12	0.55
<b>5</b>	0.64	4	9.5	12	0.65
<b>6</b>	0.64	6	9.5	12	0.65
<b>7</b>	0.64	4	11.1	12	0.62
<b>8</b>	0.64	6	11.1	12	0.64
<b>Total panels produced in phase one</b>				<b>96</b>	

After cooling, 25 mm was removed from each edge of the panel to negate edge effects. Final dimensions were 660 mm wide by 711 mm long. Both the facings and cores were sanded to create a uniform bonding surface and remove strands that came into direct contact with the mold during pressing. A 15 HP, 3-phase drum sander was used for all sanding activities (Grizzly Industrial, USA). The sander was equipped with two sanding drums with the second drum set 0.38 mm below the first drum. 60-grit paper was placed on the first drum and 80-grit paper was placed on the second drum. To minimize material waste and limit excess removal of the orientated strands of the facings, all panels were sanded the least amount as possible. Panels that required excess sanding were not used in fabrication. Cores were sanded on both sides and had an average thickness of 6.3 mm after sanding. The average thickness of the 9.5 mm and 11.1 mm panels after sanding were 8.9 mm and 10.7 mm, respectively.

Density of the cores and facings were determined after sanding by measuring core thickness to the nearest 0.1 mm and weight to the nearest gram. A total of six thickness measurements were taken: four were taken on all edges of the panel in the middle of the peak region and two were taken on each side of the width edges of the core using long-reach calipers. Length and width were determined and the area was multiplied by the surface area modification factor of 1.3.

Phenol resorcinol formaldehyde adhesive, typical of that used for glued-laminated timber, was used for bonding the facings and core to create the sandwich structure. The long dimension of the core was laminated parallel to the strong axis of the facings. The adhesive was a two part mixture consisting of a hardener and resin (Hexion Specialty Chemicals, Columbus, OH, USA). The hardener was mixed at a 2:1 ratio of water to powder based on weight. The resin and hardener were then mixed at a weight-based ratio of 2.5:1. After mixing, 94 g of the mixture was applied to each side of the core with a 101 mm long paint roller at a spread rate of  $0.061 \text{ g/cm}^2$ . Excess adhesive remaining on the roller was rolled onto the facings in an attempt to keep the spread rate on the cores uniform. Open assembly time averaged 35 minutes at room temperature.

After adhesive application, panels were pressed using a custom press for 24 hours (Fig. 3.5). Sandwiches produced with the 8.9 mm facings were pressed in stacks of five, while sandwiches with 10.7 mm facings were pressed in stacks of four. High density rubber mats were placed on the top and bottom of the panels to aid in uniform load transfer. Three pieces of 152 mm C-channel were used to transfer load from the bolting assembly to the panels. Applied pressure was approximately 0.69 MPa. Total load needed for achieving 0.69 MPa was calculated using the core laminating area, which is 30% of the facing surface area. Load cells were used to determine the bolt torque necessary in each threaded rod to achieve the desired load.

Panels were cut into smaller specimens for mechanical testing. Limitations on maximum panel length and minimum panel thickness made it necessary to produce twice as many panels than would be necessary for the same tests on flat OSB. Half of the

panels produced for each combination of panel parameters were used for strong axis bending and in-plane shear tests (Fig. 3.6), while the other half were used for flatwise compression, weak axis bending, and mechanical fastener tests (Fig. 3.7). Six panels of each cutting pattern were produced for each combination of panel parameters for a total of 12 panels per parameter set for phase one.



Figure 3.5. Custom press for bonding sandwiches

Twenty-seven panels with 8.9 mm facings, 4% core adhesive content, and 0.64 g/cm<sup>3</sup> target density were produced for the second phase of the project. Thirteen were cut using the first cutting pattern (Fig 3.6), eleven were cut using the second cutting pattern (Fig. 3.7), and three were used for small-scale shear wall tests.

All specimens were placed in a conditioning chamber at 20 °C and 65% relative humidity for at least two weeks prior to testing. The same bending, in-plane shear, and flatwise compression tests were performed on panels produced for both phases of the project. In addition, panels produced for the second phase of the project were tested for mechanical fastener performance and small-scale shear wall performance. Control specimens consisting of the commercial OSB facings were subjected to all tests with the exception of flatwise compression.

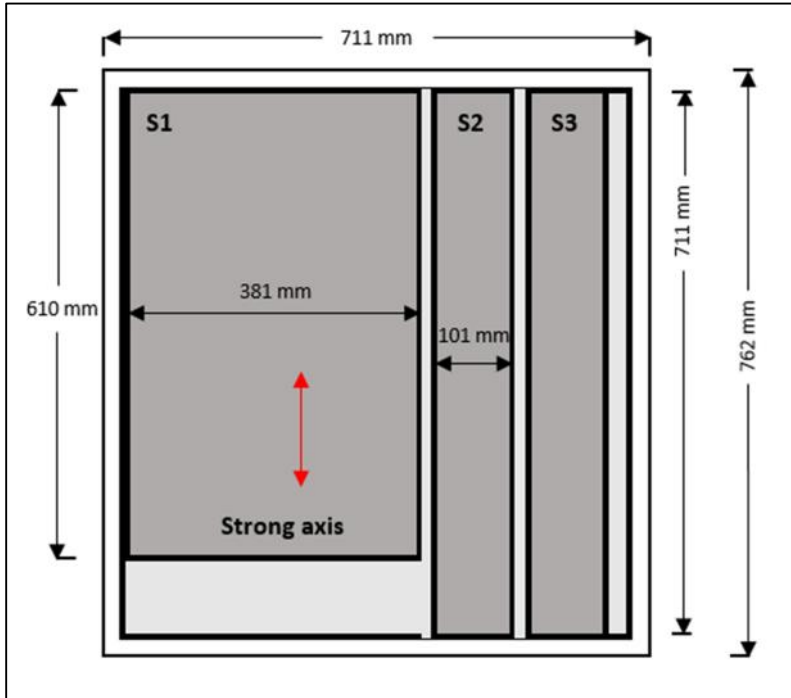


Figure 3.6. Cutting pattern for strong axis bending and in-plane shear

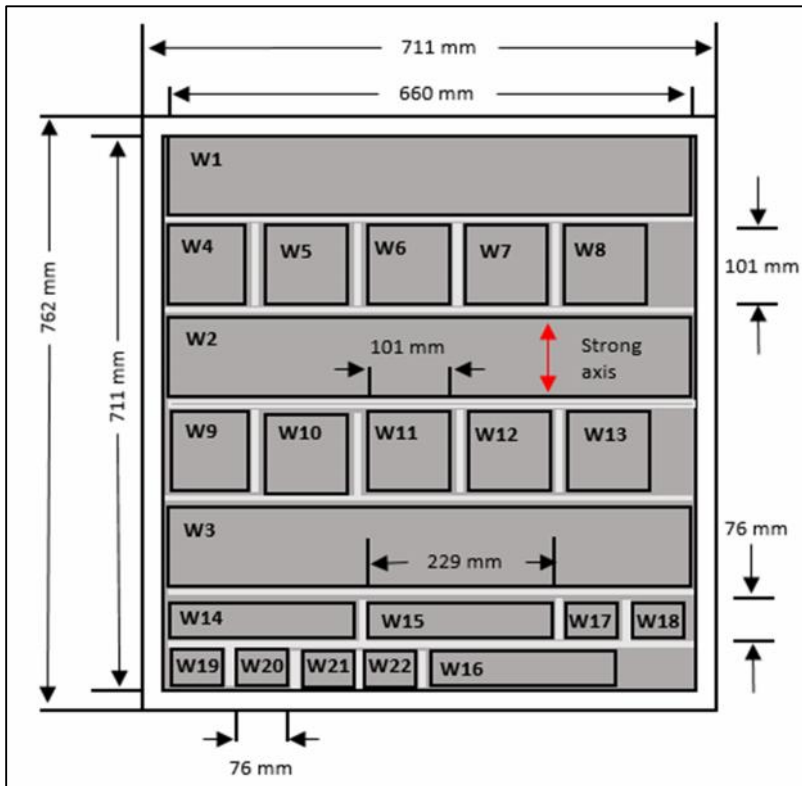


Figure 3.7. Cutting pattern for weak axis bending, flatwise compression, and connections

### *Bending*

Bending tests were conducted on an INSTRON Series 5582 universal testing machine (UTM) using displacement control. The UTM was equipped with a  $\pm 100$  kN load cell. Sandwich specimens were loaded at a rate of 2.54 mm/min and control specimens were tested at a rate of 2.00 mm/min to achieve failure in three to five minutes. Load and cross-head displacement were continuously recorded during testing. Beam supports were capable of rotating in both the length and width direction of the specimen to prevent eccentricities during loading and provide simply supported boundary conditions. Specimens were tested at an average moisture content of 8.2%.

Strong axis bending specimens were cut to 101 mm wide by 711 mm long and were specimens S2 and S3 from the 3DMCPs (Fig. 3.6). A three-point bending test following ASTM D3034 (2011) was used with a span of 660 mm. This method calls for a 50 mm wide specimen, however due to the angle of the corrugations in the core, it was chosen to use a 101 mm wide specimen to reduce variability caused by offset ribs across the specimen width. The span-to-depth ratio was 15.4 for panels with 8.9 mm facings and 14.3 for the panels with 10.7 mm facings. Depth was computed as the total thickness of the sandwich. For the first phase of the project, 12 strong axis bending specimens were tested for each combination of panel parameters. Twenty-six specimens were tested in total for the second phase of the project.

OSB control specimens were subjected to the same testing procedure as the 3DMCPs. Two specimens were randomly cut from 10 panels for a total of 20 specimens per thickness. Both facing thicknesses were cut to a width of 50 mm per ASTM D3043 (2011). The span for the 9.5 mm facings was 165 mm and 178 mm for the 11.1 mm facings- chosen so that the span-to-depth ratio was consistent with their respective sandwich thicknesses.

Weak axis bending specimens, specimens W1-W3 (Fig. 3.7), were prepared to the same width as their respective strong axis counterparts and tested following the same method. Specimens were cut to 660 mm in length and tested at a span of 610 mm. The

span-to-depth ratio for 3DMCPs with 8.9 mm facings was 14.4 and 13.3 for 3DMCPs with 10.7 mm facings. For phase one, 18 weak axis bending specimens were tested for each combination of panel parameters. For phase two, 33 specimens were tested in total. 50 mm wide weak axis control specimens were sampled like the strong axis specimens and tested in bending. The span for the 9.5 mm OSB was 152 mm and 165 mm for the 11.1 mm OSB.

Because of the difficulties involved with determining the moment of inertia of the core, it was chosen to report the bending stiffness (EI) instead of the modulus of elasticity (equation 3.1).

$$EI = \frac{P * L^3}{\Delta * 48} * \frac{1}{b} \quad (\text{Eq. 3.1})$$

EI is the bending stiffness per millimeter of panel width (N-mm<sup>2</sup>/mm), P/Δ is the slope of the linear region of the load-deflection plot (N/mm), L is the span length (mm) and b is the width (mm) of the specimen. Modulus of rupture (MOR) was determined for each specimen according to equation 3.2.

$$MOR = 1.5 \frac{PL}{bd^2} \quad (\text{Eq. 3.2})$$

MOR is the maximum bending stress (MPa), P is the ultimate load (N), L is the span length (mm), b is the thickness (mm) and d is the total depth of the panel (mm).

#### *In-Plane Shear*

In-plane shear tests were conducted using a method based on ASTM D2719 (ASTM, 2013b) with some variations. Pairs of steel rails similar to those used successfully for testing in-plane shear on wood structural panels (Alldritt, 2013; Shrestha, 1999) were bolted to the test specimen instead of the adhesive attached lumber rails called for in the standard. The rails were made from 19 mm thick, A36 grade steel plates with 15 holes in each for 13 mm diameter bolts to clamp the rails to the specimen (Fig. 3.8).

Specimens were tested using a UTM equipped with a MTS 407 Hydraulic Controller linked to a MTS 160 kN Hydraulic Actuator (model # 244.23) on a MTS Load Unit test bed. One of the clamped sides was attached to the test bed and the other was attached to the hydraulic cylinder. Tensile load was applied at a rate of 1.91 mm/min to exert a shearing force on the panel.

Shear specimens (S1, Fig. 3.6) were 381 mm in width by 610 mm in length. Bolt holes were drilled for clamping the specimen to the steel rails and the distance between the rails after clamping was 203 mm. Distance between holes was 38 mm and they were offset by 25 mm in the horizontal direction. To prevent localized crushing of the core, small solid wood blocks were placed in the hollow portions of the core near each bolt and the bolts were tightened to 88 N-m.

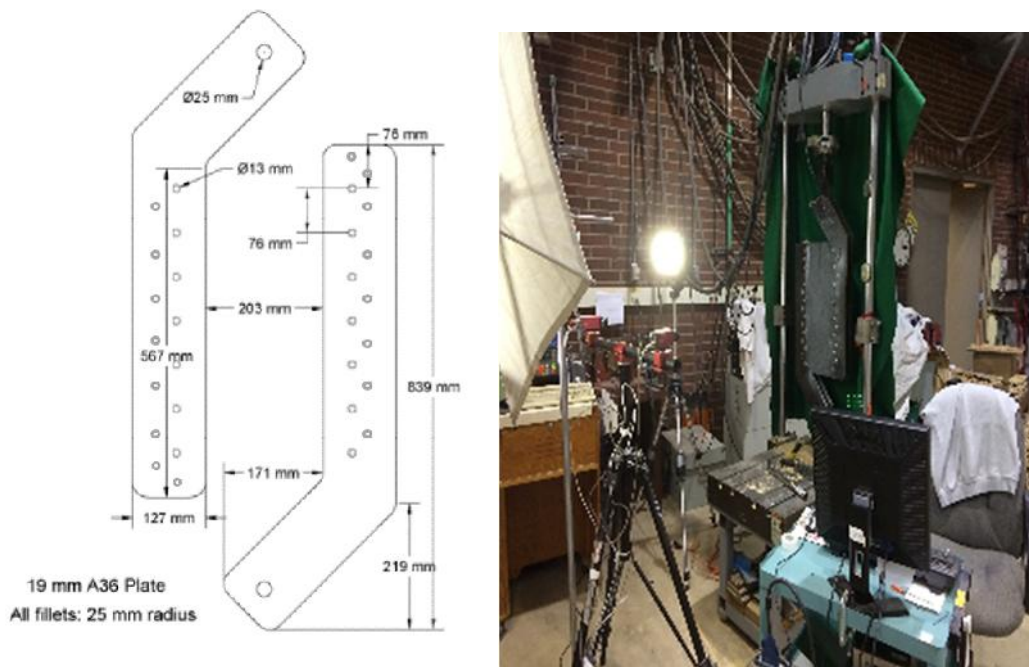


Figure 3.8. Brackets used for clamping specimen during in-plane shear test (Alldritt, 2013)

For phase one of the study, six shear specimens were tested for each combination of parameters and twelve specimens were tested during phase two. All specimens were

aligned so that the strong axis of the facings was parallel to the applied load. The average moisture content for in-plane shear specimens was 8.4%.

DIC was used to optically measure shear strain. DIC tracks blocks of contrasting pixels and correlates their movement to a reference image taken at the start of the test (Alldritt, 2013; Schwarzkopf et al., 2013). Each panel was roll coated with black paint followed by application of white speckles using a texture gun to create contrasting pixels for tracking deformation during testing. A set of high resolution cameras was calibrated using a calibration plate.

Shear strain ( $\gamma_{xy}$ ) for each panel was determined using Vic-3D (2009) software (Correlated Solutions, Inc. Irmo, SC, USA). The software is capable of averaging shear strain over a specified area, known as the area of interest (AOI). AOI for these tests was limited to the area between the brackets and the outer bolts to avoid the areas of very low strain near the edges. The size of the pixel blocks (subset) used was 33 and the step size was 7. Cameras were set to acquire one image per second with data from the MTS UTM tagged to each image. Shear strain was then extracted using the software and coupled with the corresponding load for each image to create a load-shear strain plot.

The resolution of the shear strain measurement was 0.02% strain, which would be achieved with optimum camera settings, calibration, and speckle pattern. Since DIC only measures surface deformation, based on the principle of strain compatibility it was assumed that the strain on the surface of the facing being photographed was the same throughout the entire thickness of that facing. Local variations in surface strain may be caused by voids, strand alignment, strand size, resin distribution, and density distribution.

Shear modulus ( $G_{xy}$ ) for each panel was determined from DIC strain data and the corresponding load data over the linear elastic-region of the load-shear strain curve (equation 3.3). Shear strength ( $\tau_{xy}$ ) was calculated following equation 3.4

$$G_{xy} = \frac{P}{\varepsilon_{xy}} * \frac{1}{2Ld} \quad (\text{Eq. 3.3})$$

$P/\varepsilon_{xy}$  is the slope from the load-shear strain diagram (N/mm/mm) in the linear region, which was the load between 20 kN and 48kN for the sandwich panels and 11 kN and 35 kN for the control specimens. L is the total length of the panel (mm) and d is the total thickness of the panel (mm).

$$\tau_{xy} = \frac{P_{max}}{Ld} \quad (\text{Eq. 3.4})$$

Where  $P_{max}$  is the maximum load (N) carried by the specimen.

#### *Flatwise Compression*

Flatwise compression was performed following ASTM D143, which is intended for small-clear wood specimens perpendicular to the grain (ASTM, 2009). Load was applied at 1.0 mm/min at a total test time of three minutes. Specimens were cut to 101 mm by 101 mm and loaded through two thick circular steel plates (Fig. 3.9). The bottom plate measured 152 mm in diameter and rested on a base equipped with a spherical seat to eliminate eccentricities during loading. The top loading plate was 125 mm in diameter and was attached directly to the crosshead. The same UTM and load cell were used as in the bending tests. Specimens were tested at an average moisture content of 7.8%. For the first phase of testing, 10 specimens were tested from each of the 48 panels (W4-W13, Fig. 3.7). For the second phase of testing, 10 specimens from 11 panels were tested.

After testing, the load at 2.5 mm of compressive displacement was determined. The cross sectional area of each specimen was taken as the total surface area of the facing. Compressive stress was computed following equation 3.5.

$$\sigma = \frac{P_{2.5}}{A} \quad (\text{Eq. 3.5})$$

is compressive stress (MPa),  $P_{2.5}$  is the load at 2.5 mm of compressive displacement (N) and A is the total cross-sectional area of the facing (mm<sup>2</sup>).

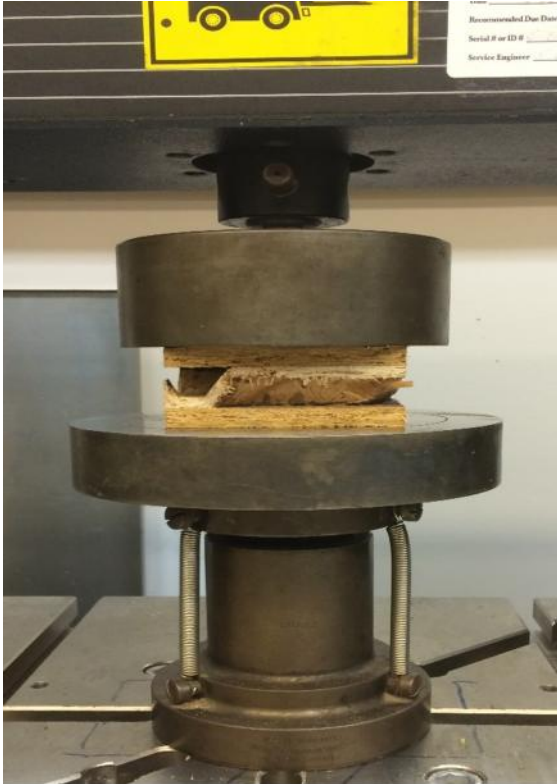


Figure 3.9. Apparatus for flatwise compression tests

#### *Small-Scale Shear Walls*

610 mm x 610 mm small-scale shear walls were constructed for both 3DMCP and OSB control panels. The tests were based on ASTM E564 (ASTM, 2012b) and modified for reduced specimen size. Framing consisted of a top and bottom plate and two vertical studs (Fig. 3.10). No. 2 and better, 2 x 4 nominal (38 mm x 90 mm) kiln dried Douglas-fir was used for framing lumber. The top and bottom plates were 610 mm long and the studs were 533 mm long. Sheathing was attached to the frame with bright, full round head 10d nails measuring 3.8 mm in diameter and 75 mm in length [(0.148 in. x 3 in) (Senco Brands, Inc. Cincinnati, OH)]. Nails were hand driven and spaced at 75 mm around the entire wall and 19 mm from the edge of the framing members. Specimens were painted black and a white speckle pattern was applied for DIC measurement.

The bottom plate was mounted on a rigid base via two, 13 mm diameter bolts equipped with Simpson Strong-Tie BP 5/8, 76 mm square washers and tightened until

snug. Bolt holes were drilled 45 mm from the top and bottom plate edges. The top plate was attached to the UTM hydraulic cylinder by two, 13 mm diameter bolts and equipped with Simpson Strong-Tie BP 5/8, 50 mm square base plates and tightened until snug. A monotonic racking force was applied at 6.35 mm/min. Top plate deflection was measured directly from the MTS hydraulic cylinder and images were captured every second for deformation measurement and analysis.



Figure 3.10. Configuration for small-scale shear walls

No stud hold downs were used in the test. The test was ceased when the load-deflection plot reached its peak and plateaued. A total of three, 3DMCP panels were tested with two having the strong axis perpendicular to the studs and the other with the strong axis oriented parallel to the studs. Two OSB assemblies were tested. OSB sheathing was oriented so the strong axis was parallel to the studs in one assembly while the other had the strong axis oriented perpendicular to the studs.

Maximum load for each panel was determined from the load-deflection plot, which was also used to produce equivalent energy elastic-plastic (EEEP) curves for wall assembly performance comparison. The region of interest for these curves was from the time of load initiation until the point of 80% post peak load. Surface deformation of each panel was determined using DIC imaging with a subset of 33 and step size of 7. AOI for the small-scale shear walls included the entire wall.

### *Mechanical Fastener Performance*

Three different tests were conducted to characterize the mechanical fastener performance of 3DMCPs produced in phase two. These tests were withdrawal, dowel-bearing, and lateral connections. All tests were performed on the same UTM as bending and compression tests and the nails were the same as those used in small-scale shear wall fabrication.

3DMCPs have three different portions of the core in which the fastener may pass through. These areas are the top peak, rib section, and bottom peak (Fig. 3.11). Nail location was noted for each specimen to determine if position in the core affected connection properties.

Withdrawal tests were performed following ASTM D1761 (ASTM, 2012d). Both 3DMCPs and OSB were cut to 75 mm x 75 mm and the nails were inserted in the center of each specimen. Nails were driven completely through the specimen by hand leaving at least 13 mm of the nail remaining on the insertion side of the specimen. A nail withdrawal device attached to the UTM crosshead passed through a frame attached to the base of the UTM with a 25 mm diameter hole in the top to place a tensile force on the nail, while keeping the specimen stationary (Fig. 3.11). The withdrawal device had a pivoting joint for reducing eccentricities during loading. Tensile force was applied at a rate of 0.75 mm/min with time to failure of approximately 90 seconds. Testing was stopped once a peak load followed by a plateau region was observed. Twenty-one 3DMCP specimens and ten OSB specimens were tested in withdrawal. No lead holes were drilled and all tests were performed within one hour of nail insertion.

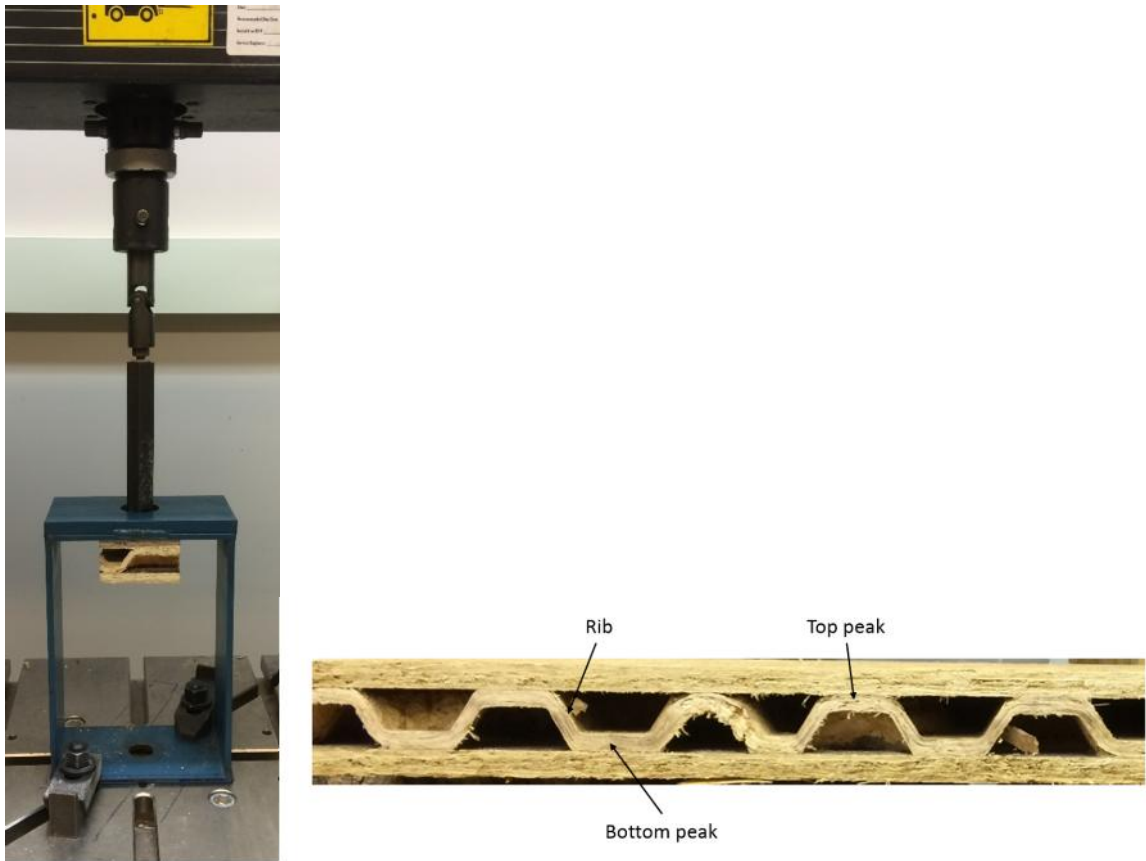


Figure 3.11. Nail withdrawal apparatus (left) and different core regions (right)

Dowel bearing tests were performed following ASTM D5764 (ASTM, 2013a). Both 3DMCPs and OSB control specimens were cut to 75 mm x 75 mm. A 3.56 mm lead hole was drilled 13 mm from the edge (Fig. 3.12). Specimens were then cut so that approximately half of the hole was remaining. Two sets of specimens were prepared for both the 3DMCPs and OSB. One set of specimens was prepared so that dowel embedment occurred parallel to the strong axis with the other set embedding into the weak axis. Eleven specimens for each embedment direction were prepared for the 3DMCPs and seven were prepared for each embedment direction of the OSB specimens. Experimental apparatus consisted of a vice for securing the specimen and a 50 mm x 100 mm steel loading block attached to the UTM crosshead (Fig. 3.12) for embedding the dowel into each specimen.



Figure 3.12. Half-hole drilled in specimen (left) and apparatus for dowel bearing test (right)

Embedment occurred at a rate of 1.5 mm/min and testing concluded when the loading block contacted the surface of the specimen, which was approximately 90 seconds. For the 3DMCPs, specimen W16 was used for embedment into the strong axis while specimen W17 was used for embedment into the weak axis (Fig. 3.7). Dowel bearing strength was calculated using the 5% offset method for determining yield load and the total bearing area of the nail (AFPA, 2012).

Two lateral connection geometries were tested following ASTM D1761 (ASTM, 2012d). The two geometries were edge and plate (Fig. 3.13), both single-shear plane connections. Nails, which were the same as the other connection tests, were hand-driven and main member (framing lumber) penetration depth was 32 mm for both geometries. Yield load was determined from the load-deflection plot using the 5% offset method (AFPA, 2012).

Edge connections were prepared by overlapping a 75 mm x 229 mm portion of 3DMCP (side member) onto the edge of a 305 mm long 2x4 (38 mm x 89 mm) nominal framing lumber piece. Framing lumber was No. 2 and better kiln-dried Douglas-fir and specimen W16 was used as the sheathing member (Fig. 3.7). A 2.8 mm diameter lead hole was drilled into the sheathing 50 mm from the bottom and 19 mm from the edge.

The same diameter lead hole was also drilled 50 mm from the end of the framing member and centered at 19 mm on the edge for a total overlap of 100 mm. A 21 mm hole was centered 50 mm from the opposing end of the sheathing and 19 mm from the edge. The purpose of this hole was to attach the specimen to the UTM crosshead using a clevis and 19 mm bolt in place of compression grips to prevent crushing of the sandwich structure (Fig. 3.14). The clevis was equipped with an extension that had a pivoting joint to reduce eccentricities during loading. A tensile load was applied at 2.54 mm/min with an average test time of one minute. Tests were ceased after the load-deflection plot began to peak.

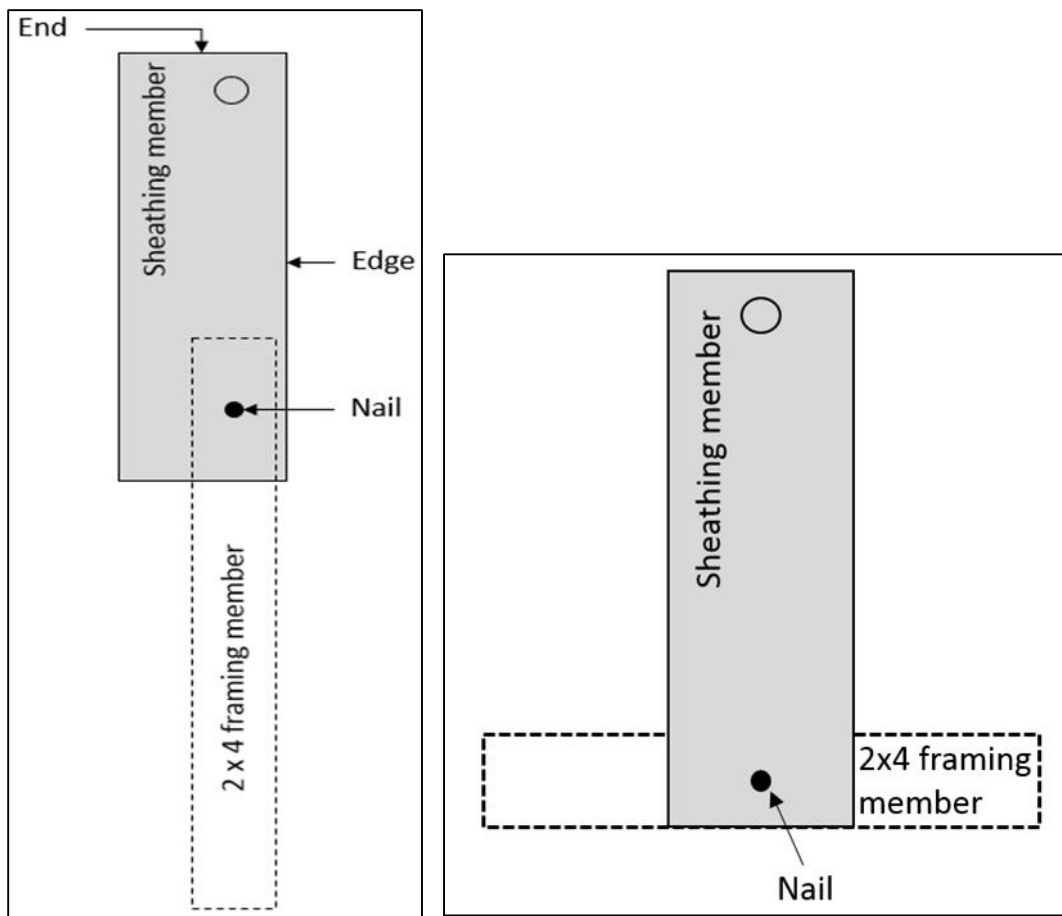


Figure 3.13. Edge (left) and plate (right) connection geometries

Plate connection tests were prepared from specimen W14 (Fig. 3.7) in a similar manner except the lead hole on the sheathing was drilled 38 mm from the edge and 19 mm from the end. Framing members were 203 mm long with a lead hole drilled 19 mm

from the edge and 100 mm from the end. The framing member portion of the edge connection assembly was clamped to a stand attached to the UTM base (Fig. 3.14).

Control specimens were prepared in the same manner for each connection geometry with the exception of the 21 mm hole, since crushing of the OSB was not a concern. Instead, OSB was attached to the crosshead using a compression grip. All other loading procedures remained the same between the two sheathing types. Penetration depth into the main member was approximately 65 mm.

After post-test visual examination, sheathing was removed from the assembly with a bandsaw. The area of the framing member surrounding the nail was examined and nails were removed with pliers or a chisel. Yield modes were characterized using the European Yield Models as presented in NDS (AFPA, 2012) for a single shear connection.

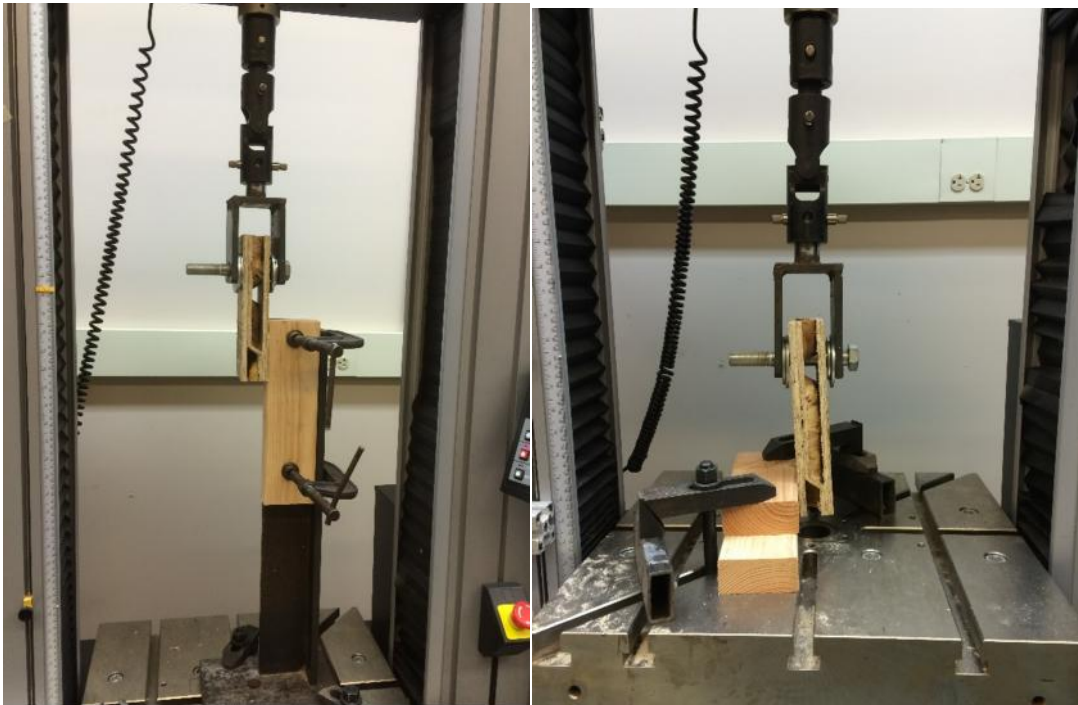


Figure 3.14. Testing apparatus for edge (left) and plate (right) lateral connections

## Chapter 4- Results and Discussion

### *Phase One Results*

Upon completion of phase one testing, each combination of manufacturing parameters was ranked based on flexural, in-plane shear, and flatwise compression values (Table 4.1). The values located underneath the group title are the nominal facing thickness used, adhesive content, and target density, respectively. Group 5 was the top performing group and its parameters were used to produce panels for phase two. It was interesting that 3DMCPs produced with the thinner facing performed better than those with the thicker facings. However, the thinner OSB facings had greater density.

Results discussed herein pertain specifically to the 3DMCPs produced for the second phase of the project where 9.5 mm nominal 24/0 Span-Rated OSB was used as a control for comparison. Table 4.2 summarizes mass, volume and density of the facings, core, and 3DMCP as seen in the sandwich panel after fabrication. Density was determined at an oven-dry moisture content of 10.7% for the facings and 10.1% for cores. Two different volumes were computed for 3DMCPs, which were the actual volume (the volume sum of each constituent) and the total volume which included void space.

Table 4.1. Summary of phase one results

Group		Strong axis bending		Weak axis bending		In-plane shear		Compression Strength (MPa)	Rank
		Strength (MPa)	Stiffness (N-mm <sup>2</sup> /mm)	Strength (MPa)	Stiffness (N-mm <sup>2</sup> /mm)	Max load (kN)	Strength (MPa)		
<b>1</b>	Average	9.70	1.67E+07	12.15	1.15E+07	99.81	3.80	0.56	<b>8</b>
9.5 mm	St. Dev	0.58	8.89E+05	0.33	6.68E+05	2.85	0.26	0.03	
4%	COV (%)	6.0%	5.4%	2.7%	5.8%	2.9%	6.9%	4.5%	
0.56 g/cm <sup>3</sup>	n	12		21		6		70	
<b>2</b>	Average	11.80	1.81E+07	11.94	1.19E+07	95.75	3.61	0.71	<b>6</b>
9.5 mm	St. Dev	0.88	1.29E+06	0.48	8.56E+05	4.23	0.30	0.04	
6%	COV (%)	7.5%	7.1%	4.1%	7.2%	4.4%	8.2%	5.2%	
0.56 g/cm <sup>3</sup>	n	9		18		5		60	
<b>3</b>	Average	10.98	2.10E+07	9.26	1.18E+07	97.03	3.43	0.57	<b>7</b>
11.1 mm	St. Dev	0.86	1.14E+06	0.48	7.02E+05	4.03	0.13	0.04	
4%	COV (%)	7.8%	5.5%	5.2%	6.0%	4.2%	3.8%	6.6%	
0.56 g/cm <sup>3</sup>	n	10		18		6		59	
<b>4</b>	Average	10.96	1.98E+07	10.47	1.24E+07	92.40	3.28	0.76	<b>4</b>
11.1 mm	St. Dev	0.86	1.53E+06	0.48	8.59E+05	4.23	0.40	0.04	
6%	COV (%)	7.8%	7.7%	4.6%	6.9%	4.6%	12.3%	4.9%	
0.56 g/cm <sup>3</sup>	n	10		18		5		60	
<b>5</b>	Average	13.16	1.86E+07	12.76	1.29E+07	106.14	4.01	0.75	<b>1</b>
9.5 mm	St. Dev	0.82	9.25E+05	0.48	6.98E+05	4.03	0.27	0.04	
4%	COV (%)	6.2%	5.0%	3.8%	5.4%	3.8%	6.8%	5.0%	
0.64 g/cm <sup>3</sup>	n	12		18		6		56	
<b>6</b>	Average	15.14	1.95E+07	12.31	1.30E+07	104.67	3.97	0.70	<b>2</b>
9.5 mm	St. Dev	0.82	9.56E+05	0.48	8.93E+05	4.03	0.17	0.04	
6%	COV (%)	5.4%	4.9%	3.9%	6.8%	3.8%	4.2%	5.2%	
0.64 g/cm <sup>3</sup>	n	12		18		6		60	
<b>7</b>	Average	12.60	2.20E+07	9.51	1.22E+07	94.37	3.34	0.65	<b>5</b>
11.1 mm	St. Dev	0.82	1.12E+06	0.48	7.06E+05	4.23	0.19	0.04	
4%	COV (%)	6.5%	5.1%	5.1%	5.8%	4.5%	5.8%	5.6%	
0.64 g/cm <sup>3</sup>	n	12		18		5		60	
<b>8</b>	Average	12.05	2.15E+07	9.72	1.29E+07	100.08	3.50	0.67	<b>3</b>
11.1 mm	St. Dev	0.86	1.09E+06	0.48	1.04E+06	4.23	0.24	0.04	
6%	COV (%)	7.1%	5.2%	5.0%	8.1%	4.2%	6.7%	5.5%	
0.64 g/cm <sup>3</sup>	n	10		18		5		60	
11.1 mm facing	Average	30.02	2.73E+07	12.88	9.26E+06	57.53	7.61		
	St. Dev	6.94	4.79E+06	2.94	1.74E+06	5.61	1.05		
	COV (%)	23.1%	17.6%	22.9%	18.8%	18.8%	18.8%		
	n	20		20		6			
9.5 mm facing	Average	36.81	2.13E+07	17.10	7.10E+06	57.61	9.12		
	St. Dev	8.60	4.03E+06	4.55	1.71E+06	6.68	1.06		
	COV (%)	23.4%	18.9%	26.6%	24.0%	24.0%	24.0%		
	n	20		20		6			

Table 4.2. Mass, volume, and density for facings, cores, and 3DMCPs

	<b>OSB facing (1 piece)</b>	<b>Core</b>	<b>3DMCP, actual volume</b>	<b>3DMCP, including voids</b>	<b>3DMCP actual/OSB</b>
<b>Mass (g)</b>	2679	2464	7823	7823	2.92
<b>Volume (cm<sup>3</sup>)</b>	4253	3791	12297	20536	2.89
<b>Density (g/cm<sup>3</sup>)</b>	0.63	0.65	0.64	0.38	1.02

### *Bending*

Average bending stiffness per millimeter of specimen width (EI) and strength (MOR) were determined for specimens loaded in the strong and weak axis directions (Table 4.3). A two-way ANOVA found a significant difference between the facing orientation on EI and MOR for the 3DMCPs ( $p < 0.001$ )

Table 4.3. Summary of bending results for 3DMCPs and OSB

<b>Panel type</b>	<b>Facing orientation</b>	<b>n</b>	<b>EI (N-mm<sup>2</sup>/mm)</b>	<b>COV (%)</b>	<b>MOR (MPa)</b>	<b>COV (%)</b>
<b>3DMCP</b>	Strong axis	26	$1.91 \times 10^7$	5.0	12.7	12.3
	Weak axis	33	$1.21 \times 10^7$	7.5	10.7	14.6
<b>OSB</b>	Strong axis	20	$4.17 \times 10^5$	18.9	36.8	23.4
	Weak axis	20	$1.39 \times 10^5$	26.6	17.1	24.1

The large difference in stiffness between 3DMCPs and OSB was expected and was approximately 46 times and 87 times greater for the strong and weak axis orientations, respectively. Due to the repeating corrugations that are offset in the core, the core geometry was different between specimens S2 and S3 for strong axis bending and specimens W1, W2, and W3 for weak axis bending. Influence of specimen position in the

panel was insignificant ( $p = 0.20$ ) for the strong axis specimens while significant for the weak axis specimens ( $p = 0.01$ ). Specimen W1 had the greatest MOR, followed by specimen W2, and finally specimen W3. Specimen W2 showed evidence of having an average MOR less than specimen W1 ( $p = 0.05$ ) while specimen W3 showed convincing evidence that the mean MOR was different than that of specimen W1 ( $p = 0.003$ ).

In the immediate vicinity of the loading head, specimen W1 tended to have core geometry that favored load transfer. Specimen W2 had similar core geometry in the vicinity of the loading head, except that the peak region tended to be slightly offset from the center of the specimen, stressing one edge, which resulted in predominate failure of the bottom facing. Many of the W3 specimens were cut through a rib on the edge of the panel, reducing the amount of material in which to transfer load in the vicinity of the loading head, thus causing failure at lower loads. In the weak axis orientation, cores were twice as stiff as the facings, meaning that if the peaks and ribs of the core were offset to one side of the specimen near the loading point, significant load could be placed on the core without failure, instead transferring load to the weaker facings.

Comparing MOR for 3DMCPs and OSB, OSB appears to be much stronger in bending but also more variable. Directly comparing the two based on MOR alone may not be a fair comparison, since the depth used to compute MOR for the 3DMCPs was the total depth of the sandwich, which contains void area due to the hollow core. Comparing the maximum load per unit width, 3DMCPs carried 1.5 times greater load in the strong axis bending orientations and 2.8 times greater load in the weak axis orientation (Table 4.4). Another method for comparing the bending performance is by analyzing the average facing stress of the 3DMCPs. If core materials are considered compliant and do not contribute significantly to bending rigidity then the average bending stress in the facings of a sandwich composite can be found using equation 4.1 (Carlsson & Kardomateas, 2011):

$$\sigma = \frac{M}{bdh_f} \quad (\text{Eq. 4.1})$$

M is the maximum moment, b is the width, d is the distance between the centroids of the faces ( $d = h_c + h_f$ ) where  $h_c$  and  $h_f$  are the core and face thicknesses, respectively (Carlsson & Kardomateas, 2011). Assuming that the core did not contribute significantly to bending strength, the average stress in the facings for the 3DMCPs was computed for each orientation and compared to the actual bending stress determined for control specimens (Table 4.4). Results show that the 3DMCPs use 35% of their facing capacity in the strong axis orientation and 64% in the weak axis orientation. This means that if the strength and stiffness properties are adequate for a given application, then reducing the facing thickness may be possible. However, in the weak axis orientation, the core was considerably stiffer than the facings- meaning that the assumption of cores not contributing significantly to bending is invalid for the weak axis specimens. Strong axis specimens predominately exhibited shear failure in the core, meaning that the core strength did contribute to overall strength of 3DMCPs.

Table 4.4. Comparison of bending properties

Panel type	Facing orientation	Max load/unit width (N/mm)	Average facing stress (MPa)
<b>3DMCP</b>	Strong axis	23.9	13.0
	Weak axis	22.0	11.0
<b>OSB</b>	Strong axis	15.9	36.8
	Weak axis	7.9	17.1

Two predominant failure modes were observed for the 3DMCPs during strong axis bending- shear failure of the core and localized flexural failure of the top facing (Fig. 4.1). Core shear failure is not surprising because of the low span-to-depth ratio of the 3DMCPs ( $S:D = 15.3$ ). Core shear generally occurred in the outer third of the sandwich beam originating at the rounded portion of the rib and propagating along the length

portion of a peak. It was observed through three-point bending of the cores at the same span-to-depth ratio that failures tended to propagate across the width of the rib/peak boundary area, likely due to stress concentrations.

Localized flexural failure of the top facings occurred when the loading head was positioned above a void area in the core causing a shear type failure of the top facing due to the peaks adjacent to the loading area acting as supports and the facing being placed in very short span bending. A two-way ANOVA presented evidence that the average bending strength for specimens failing in core shear was 1.42 MPa greater than specimens failing in localized compression of the top facing ( $p = 0.02$ ). Half of the strong axis specimens failed this manner, meaning that the average bending strength was lower than it would have been if a loading head with a larger radius of curvature was used.

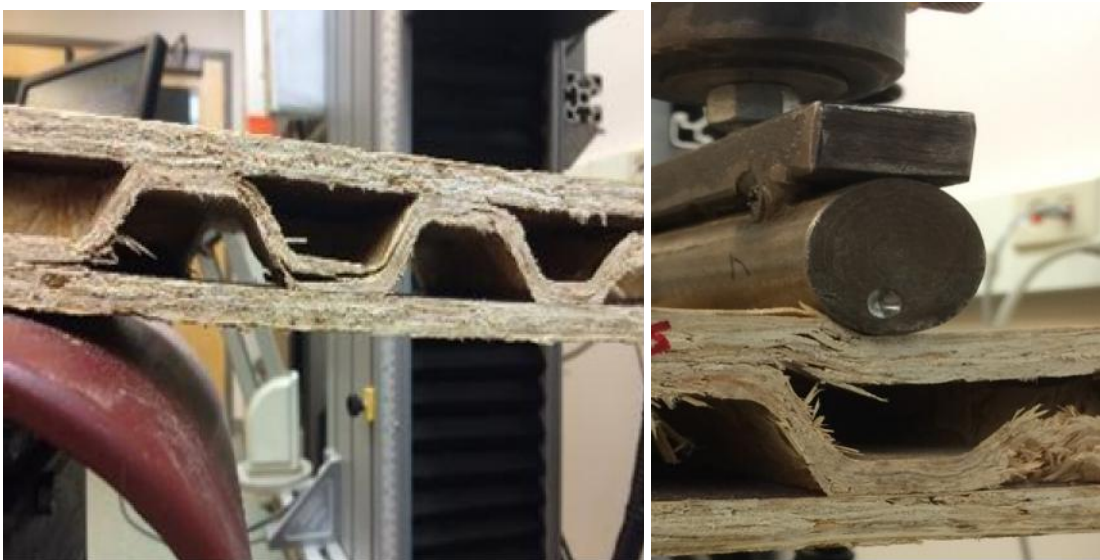


Figure 4.1. Typical failures observed for 3DMCPs in strong axis bending. Core shear failure (left) and localized flexural failure in the top facing (right)

Weak axis specimens also exhibited two predominant failure modes which were localized flexural failure of the top facing and flexural failure of the bottom facing (Fig. 4.2). Localized flexural failure in the top facing was similar to that observed in the strong axis specimens and tended to occur when the loading head was between two peaks in the core, despite the low span-to-depth ratio ( $S:D = 14.0$ ). Flexural failure in the bottom

facing tended to occur directly beneath a bottom peak since the core acts as a load path between the facings and the facings are relatively weak in this direction. Flexural failure in the bottom facing was expected, however no significant difference in MOR was observed between failure modes ( $p = 0.84$ ).

EI and MOR were more equalized for the 3DMCPs between the strong and weak axis orientation compared to OSB. The presence of shear failures in the core for 3DMCPs in the strong axis orientation indicates that the core was either not compliant enough to transfer load to the facings or the span-to-depth ratio favored shear failure. To better understand flexural properties of the core, eight specimens for the strong and weak axis orientation were tested at the same span-to-depth ratio seen in the 3DMCPs. It was found that the core was 3.8 times stiffer in the width direction (weak axis) than the length direction (strong axis). Comparing the facings to the core in the strong axis direction, the facings were 6.2 times stiffer than the core, meaning that the core likely does not contribute significantly to 3DMCP bending rigidity. However, since core failure was a predominate failure mode, than the core most certainly contributed to the overall bending strength of the specimen..

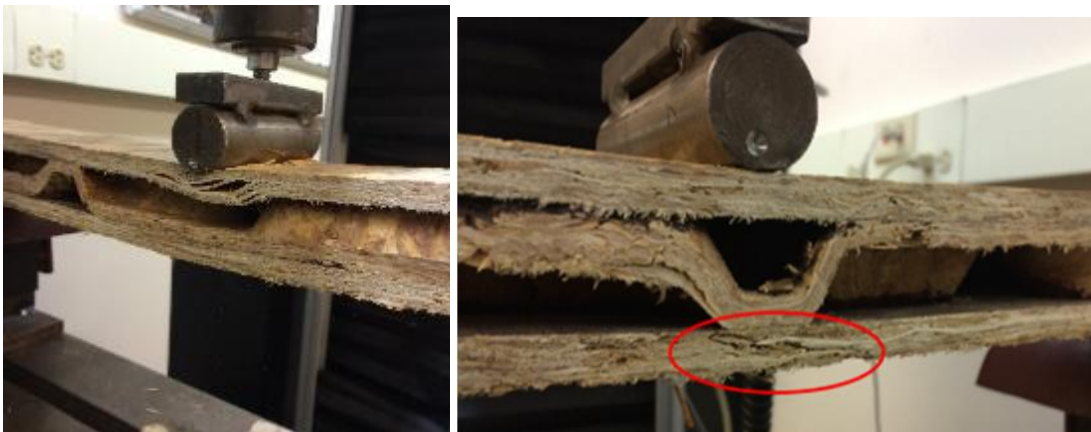


Figure 4.2. Typical failures observed for 3DMCPs in weak axis bending. Localized flexural failure in top facing (left) and flexural failure in bottom facing (right).

Bending results were compared to minimum reference values from PS 2-10 to gain an understanding of how 3DMCPs and the 9.5 mm OSB values compare to selected Span-Rated wood structural panels (Table 4.5). Quality assurance minimum reference values for dry, small specimen bending stiffness and strength were chosen for the thickest panel in each Span Rating or Performance Category from Table 8 in PS 2-10 (APA- The Engineered Wood Association, 2011). The average maximum moment per millimeter of specimen width was computed for both 3DMCP and OSB orientations for comparison to PS 2-10 values.

Table 4.5. Comparison between 3DMCPs and minimum Span-Rating values

<b>End Use-Span Rating or Performance Category</b>	<b>Bending stiffness, EI x 10<sup>3</sup></b>		<b>Maximum bending moment</b>	
	Parallel to strong axis	Perpendicular to strong axis	Parallel to strong axis	Perpendicular to strong axis
	N-mm <sup>2</sup> /mm	N-mm <sup>2</sup> /mm	N-mm/mm	N-mm/mm
<b>3DMCP</b>	19,100	12,100	3,950	3,353
<b>9.5 mm OSB</b>	417	139	657	301
<b>Roof-48/ subfloor-24*</b>	1,790	763	920	510
<b>Structural 1- 3/4*</b>	1,790	716	920	650
<b>Single floor- 48*</b>	8,660	2,110	2,080	820

\*Values obtained from PS 2-10, Table 8 (APA- The Engineered Wood Association, 2011)

Values from Table 8 in PS 2-10 follow ASTM D3043- Method D, which is a three-point bending loading procedure (ASTM, 2011). The loading procedure in this study deviated from the standard since a minimum span of 24 times the nominal panel thickness was not achieved and load application occurred at a slower rate. Since 3DMCPs are designed to have superior bending properties opposed to solid material of the same weight and the loading procedure deviated from the standard, values from PS 2-10 cannot be directly compared. Instead, the comparison is presented to give a coarse comparison of the flexural performance of 3DMCPs compared to minimum Span-Rating requirements.

#### *In-Plane Shear*

Average in-plane shear stiffness ( $G_{xy}$ ) and strength ( $\tau_{xy}$ ) were computed for 3DMCPs and OSB (Table 4.6). Strictly comparing  $G_{xy}$  and  $\tau_{xy}$ , OSB appears to perform better. Both of these calculations require using full sandwich depth of the 3DMCP, meaning they are negatively biased from the presence of void space. Examining the average slope in the linear region from the load-shear strain plot, 3DMCPs have nearly twice the stiffness of OSB while the average maximum load reached for the 3DMCPs was 1.7 times greater than OSB.

An important note is that of the twelve 3DMCP specimens tested, six failed locally around the bolts used for clamping the specimens, while none of the OSB specimens failed in this manner. The only acceptable failure mode is shear failure between the rails so those failing around the bolts were not used for further data analysis. Interestingly, the average failure load for the specimens failing at the bolts was 1.4 kN less than those failing between the rails, with similar COV. Failure in the bolts may have occurred due to inadequate clamping force, reducing the frictional force between the panel and rails; or inadequate load sharing of the bolts, resulting from eccentricities during drilling bolt holes.

Comparing load-shear strain plots of the 3DMCPs and OSB (Fig. 4.3), OSB has a much smoother curve. 3DMCPs were more difficult to attach to the in-plane shear apparatus, and their added thickness made it more difficult to align holes in the rails.

Bumps in the curve may be from connection slack in the bolt holes decreasing as load increased. The curves stop abruptly near peak load since the specimen rapidly deforms at the breaking point and the DIC software is unable to properly recognize the subsets.

Table 4.6. In-plane shear results

Panel type	Statistic	$G_{xy}$ (GPa)	$\tau_{xy}$ (MPa)	Slope (N/mm/mm)	Max load (kN)	Avg. strain @ max load (%)
<b>3DMCP</b>	Average	0.58	3.68	$3.08 \times 10^7$	97.29	0.40
	Std. dev	0.08	0.23	$4.44 \times 10^6$	6.15	0.07
	COV (%)	14.6	6.4	14.4	6.3	17.6
<b>OSB</b>	Average	1.24	9.12	$1.56 \times 10^7$	57.18	0.44
	Std. dev	0.10	1.06	$1.32 \times 10^6$	6.63	0.04
	COV (%)	8.3	11.6	8.5	11.6	10.1

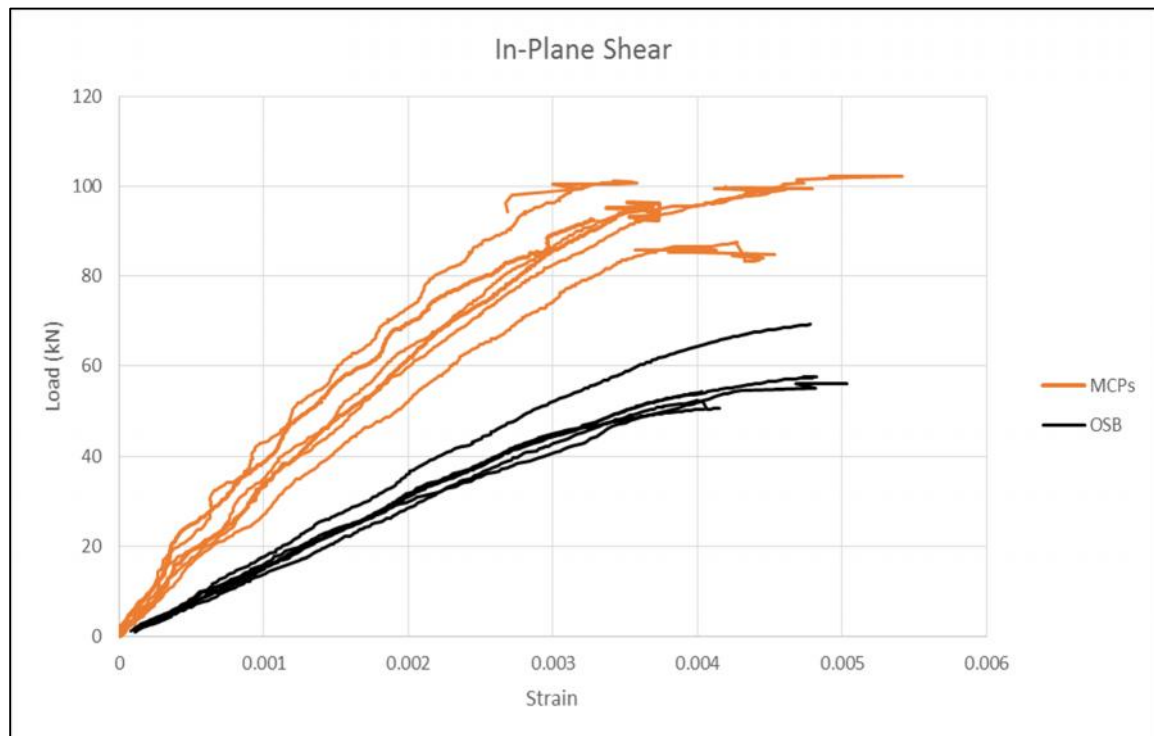


Figure 4.3. Load-shear strain plot for 3DMCPs and OSB

Shear strain contour maps were produced using Vic-3D and compared between the 3DMCPs and OSB. OSB panels reached a proportional elastic limit at approximately 35 kN, well within the proportional limit for the 3DMCPs (Fig. 4.4a). At a load of 48 kN, OSB panels had significant areas of strain between 0.002 and 0.0045 while 3DMCPs were nearing their proportional limit (Fig. 4.4b). OSB failure occurred at an average of 57 kN. At 90 kN, 3DMCPs had developed significant areas of strain between 0.002 and 0.0045 (Fig. 4.4c) and failed at an average load of 97 kN (Fig. 4.4d). Areas of high strain, blue and purple areas (0.006 to 0.008), of the strain contour maps occurring near the failure point were in the exact location of failure.

Fractures in the 3DMCP panels tended to propagate diagonally across the panel and would often deviate either vertically or horizontally for short distances which was similar to those observed for the OSB panels. An important note is that 3DMCP fractures tended to be less catastrophic with the ability to hold approximately 25% of maximum load after fracture where the OSB panels failed completely (Fig. 4.5). This can be seen by the lack of a plateau region at peak load for OSB compared to 3DMCPs (Fig. 4.3)

The catastrophic failure of OSB compared to 3DMCPs indicates core participation holding the panel together and limiting the severity of crack propagation. Fractures on one 3DMCP facing generally did not match the fracture location on the other facing, which may be a result of core reinforcement or the inherent variability of OSB. Shear forces act predominately at a 45 degree angle to the primary surface in which the force is exerted, meaning that if the strongest orientation of a material coincides with the 45 degree angle, the material performs better. Having the ribs in the core at a 30 degree angle to the primary axis reinforces the 3DMCP's shear strength and its ability to withstand shear forces.

Modifications to the in-plane shear apparatus may benefit future testing. An increased number of smaller diameter bolts would likely help to distribute load more evenly to the panel and reduce likelihood of failure near the bolts, while serrated rails would help to increase friction between the panel and rails. Another option would be to

remove core material in the area of the rails, and replace it with lumber so as to obtain greater clamping pressure.

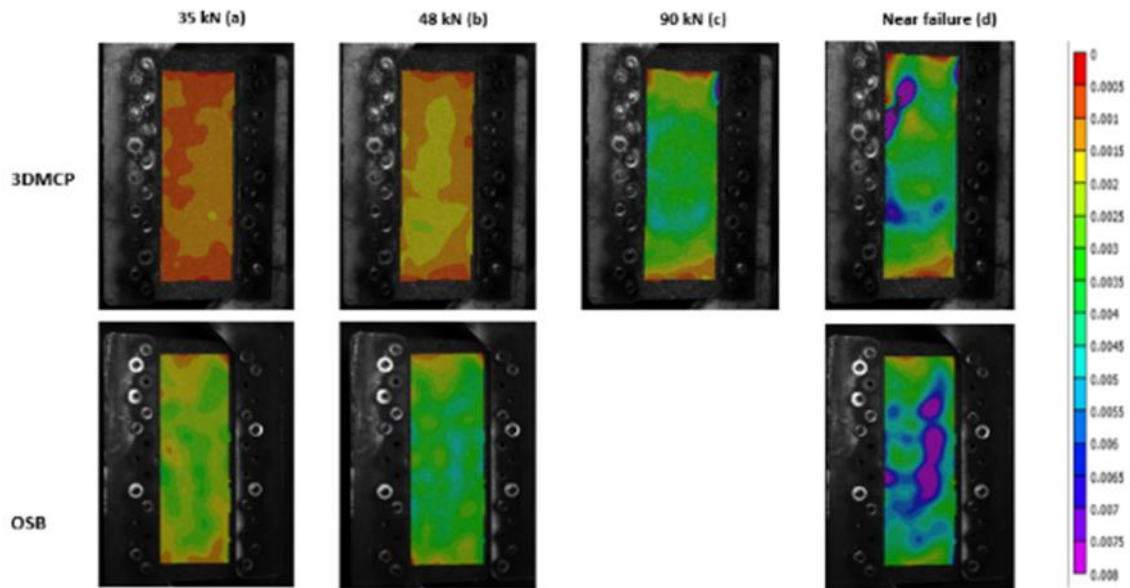


Figure 4.4. Shear strain contour maps at 35 kN (a), 48 kN (b), 90 kN (c), and near failure (d), which was 96 kN for 3DMCPs and 57 kN for OSB.



Figure 4.5. Comparison of in-plane shear failure of 3DMCP (left) and OSB (right)

### *Flatwise Compression*

Data from flatwise compression tests was highly variable, likely a result of the specimen size (Table 4.7). The offset ribs and slight geometry differences in the cores from different placement in the molds during pressing and slight deviations during sandwich fabrication made it nearly impossible to obtain flatwise compression specimens with the same core geometry, making it necessary to increase the sample size for these tests. ASTM D143 for compression perpendicular to the grain for small, clear solid wood specimens was chosen in favor of ASTM C365, which is the standard test method for flatwise compressive properties of sandwich cores. Two different behaviors were observed during initial trials: some specimens reached a maximum load, where ASTM C365 would have been applicable, while some did not. The specimens that didn't reach a maximum load performed more like solid wood in that densification of the ribbed structure created a region of sharp uprise in the load-deflection curves.

Load at 2.5 mm of deflection was taken as the maximum compressive load, which would be applicable in floor and roof sheathing applications where deflection limits can govern structural design. Five different failure modes were observed (Table 4.8). Delamination between the core and facings and shear failure of the facings was rare. Flexural failure in the peak region of the core occurred when the top or bottom peak was relatively centered in the specimen (Fig. 4.6). This type of failure was similar to those seen by Voth (2009), where the peaks were always centered in the specimen. Shear failure in the peak region of the core typically occurred when a portion of the peak was near the edge of the specimen (Fig. 4.7). Here, the ribs were strong enough to withstand the load and the partially supported peak acted like a small cantilever beam.

Table 4.7. Summary of flatwise compression testing

Statistic	Load at 2.5 mm (kN)	Compression strength (MPa)
Average	9.57	0.92
Std. dev	2.73	0.27
COV (%)	28.5	28.9

Table 4.8. Flatwise compression failures

Failure mode	Description	n
1	Delamination between core and facings	2
2	Flexural failure in peak region of core	24
3	Rib buckling	72
4	Shear failure in peak region of core	9
5	Shear failure of the facings	3



Figure 4.6. Flexural failure in the peak region of a flatwise compression specimen

Ribs tended to buckle at the rounded portion of the rib (Fig. 4.8). Strands would then separate and the fracture would travel a short distance towards the top or bottom of the rib depending on which rounded portion buckled. Using FEA modelling, Hunt (2004) found that rib buckling was expected to occur over rib compression at angles less than 80 degrees, although a stiffer response was achieved with a rib angle of 60 degrees. The angle of the ribs in this study was 60 degrees and the failure mode predicted through FEA performed by Hunt (2004) aligns with predominate failure modes observed for the flatwise compression specimens, and those seen by Voth (2009).

A pair-wise comparison was performed for all specimen locations in the cutting pattern. Using a Tukey-HSD method with a 95% family-wise confidence level, 4 out of 45 pairs were found to have an adjusted p-value less than 0.05. These pairs were: W5-W4, W7-W5, W10-W5, and W10-W6. Many of the W4 and W10 specimens had little core support on one half of the specimen, placing greater load on the remaining portion, causing core shear or buckling of the ribs. Specimen W5 typically had greater support from the core and failed in flexure at the peak.



Figure 4.7. Shear failure in the core of a flatwise compression specimen



Figure 4.8. Buckling failure of the curved rib portion in flatwise compression specimen

### *Mechanical Fasteners*

The average withdrawal resistance per millimeter of nail penetration depth ( $W$ ) of the 3DMCPs was significantly greater than OSB ( $p \ll 0.001$ ), despite the 3DMCPs having higher variability (Table 4.9). 3DMCP load-deflection plots exhibited load-slip characteristics before reaching a maximum load, which was not observed for OSB (Fig. 4.9). 3DMCPs reached maximum load at greater deflection than OSB.

Increased withdrawal resistance may have occurred from the presence of the adhesive used in creating sandwich structures or the ability of the core to compress. Having a hollow core, it is necessary for the nail to pass through three different regions before exiting through the bottom of the panel, which are the top facing, core, and bottom facing. Inserting the nail through a rib in the core was difficult and often caused the nail to deflect laterally upon contact. To prevent this issue, nails were intentionally driven through the top or bottom peak region of the core. Nails passing through the bottom peak

of the core had 16% greater withdrawal resistance than those passing through the top peak ( $p = 0.002$ ), although the withdrawal strength was nearly twice as variable.

No significant difference in mean dowel bearing strength was observed between 3DMCPs and OSB in either bearing direction, despite 3DMCPs having slightly larger mean values and lower variability than OSB (Table 4.10). 3DMCP bearing area was approximately 2.7 times that of the OSB and the average yield load for the 3DMCPs was 2.7 and 3.0 times greater than the OSB for strong and weak axis embedment directions, respectively. General load-deflection behavior was similar between 3DMCPs and the control, indicating the composite sandwich structure had little effect on dowel bearing strength, and the increase in yield load was proportional to the added bearing area of the sandwich structure compared to OSB.

Table 4.9. Summary of withdrawal testing

<b>Panel type</b>	<b>n</b>	<b>W (N/mm)</b>	<b>COV (%)</b>
<b>3DMCP-Top peak</b>	11	29.1	20.0
<b>3DMCP- Bottom peak</b>	11	33.7	38.0
<b>3DMCP- Average</b>	22	31.5	31.4
<b>9.5 mm OSB</b>	10	11.3	14.0

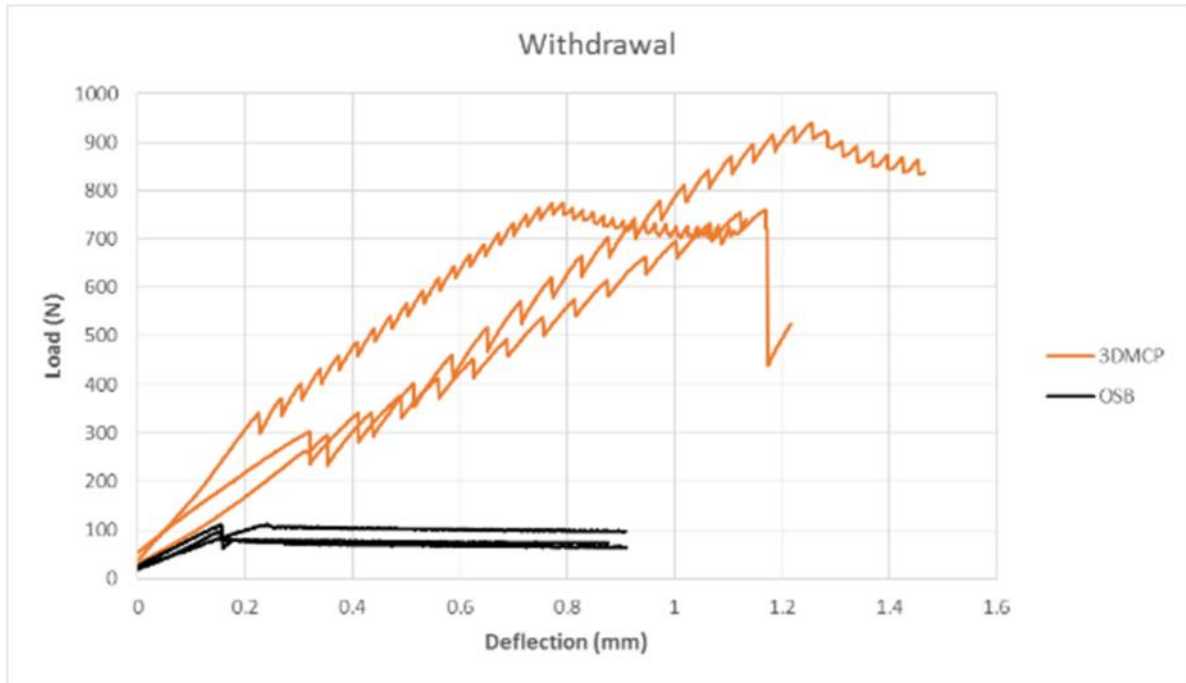


Figure 4.9. Comparison of three withdrawal curves between 3DMCPs and OSB to illustrate 3DMCP load-slip behavior

Table 4.10. Summary of dowel bearing test results

Panel type	Bearing direction	n	Yield load (N)	Dowel bearing strength (MPa) (COV, %)
<b>3DMCP</b>	Strong axis	11	3710	40.9 (19.4)
	Weak axis	11	3468	38.2 (18.4)
<b>OSB</b>	Strong axis	7	1352	37.8 (24.0)
	Weak axis	7	1169	32.6 (28.0)
<b>Framing lumber</b>	Parallel to grain	7	5426	38.2 (16.0)
	Perpendicular to grain	7	3626	25.2 (21.0)

Lateral connection tests exhibited significant evidence that the mean yield load for 3DMCPs was greater than that of OSB for edge ( $p = 0.02$ ) and plate ( $p < 0.001$ ) connection geometries (Table 4.11). Yield load variability was also reduced for 3DMCPs

compared to OSB and different yield modes were observed. No significant difference in yield load between edge and plate geometries was observed for either sheathing type, agreeing with design values in the NDS where connections utilizing dowels less than 6.35 mm in diameter are independent of the grain direction.

Table 4.11. Summary of lateral connection test results

Sheathing type		Geometry	
		Edge	Plate
<b>3DMCP</b>	Yield load (N) (COV,%)	1034 (22.2)	1094 (9.9)
<b>OSB</b>	Yield load (N) (COV,%)	764 (28.5)	785 (19.4)

3DMCP edge connections predominantly yielded by bending of the fastener (Mode III) where in OSB it was crushing of the sheathing (Mode I<sub>s</sub>). Half of the 3DMCP edge assemblies yielded by bending of the nail in the side member (Mode III<sub>m</sub>), while 25% showed nail yielding in the main member (Mode III<sub>s</sub>), and the remaining 25% yielded through crushing of the main member. All of the OSB edge assemblies failed through crushing of the side member (Mode I<sub>s</sub>). 3DMCP plate connections produced the same trend of yielding as that of edge assemblies through bending of the nail. Unlike the edge assemblies, half of the OSB plate connections exhibited yielding of the nail while the other half yielded through crushing of the sheathing.

#### *Yield Mode Comparison*

Understanding connection design capacities and yield modes are imperative for any product intended to be used as part of an assembly. The process simplifies if design values can be reasonably predicted using proven yield limit design value equations. Dowel bearing strength for 3DMCPs and framing lumber were determined for both loading directions and input into the yield limit equations provided in the NDS (AFPA,

2012). The average value for dowel bearing into the weak axis of 3DMCPs was used for both connection geometries, since this was the sheathing configuration tested. Nail bending strength was assumed to be 621 MPa as recommended in the NDS for 3.75 mm diameter nails (AFPA, 2012). The six possible yield modes for a single shear connection were computed and multiplied by a load duration factor of 1.25 to adjust for experimental loading time. Each yield limit equation has a reduction factor ( $R_d$ ) of 2.2 to account for the factor of safety, so average experimental values were also reduced by a factor of 2.2. The yield limit equations assume the two members in the connection are solids, so the sum of the facing thickness and core wall thickness were input into the equations as the thickness of the side member, opposed to using the total depth of the sandwich structure.

The six yield limit equations proved to be inadequate for predicting yielding behavior (Table 4.12). Not only were the predicted loads higher than experimental yield loads, but the predicted yield mode was Mode IV, which was only observed in one specimen. Mode IV failures are typical for thick sheathings where adequate bearing area in both members causes yielding in the nail.

Void space accounts for 44% of the total depth of the sandwich structure (Fig. 4.10). The force on the nail at the bottom of the head is proportional to the distance from the shear plane. The presence of void space during the actual test would cause a greater force at the base of the nail head, leading to a lower yield load than predicted by the yield limit equations. Average experimental values were 29% and 16% less than predicted yield loads for the edge and plate geometries, respectively. Adjusting for the increased distance to the bottom of the nail head from the presence of void space may be able to reasonably predict the yield load for 3DMCP connections. Since the force on the fastener is greater in reality compared to the predicted yield load, it makes sense that the predominant failure mode for 3DMCPs was plastic hinge formation of the nail in the side member as opposed to mode IV failure predicted by the yield limit equations.

Although the yield load of 3DMCPs was greater than OSB, OSB specimens had a greater slope for both edge and plate connections. The average slope for OSB was 2.4

times and 2.1 times greater for the edge and plate geometries, respectively. Higher elastic stiffness of the OSB connections can likely be attributed to the greater penetration depth into the main member and nail yielding in the 3DMCPs due to the greater thickness and presence of void space.

Table 4.12. Comparison of predicted yielding behavior and experimental behavior

Geometry	Predicted yield load [Z(N)]	Adjusted predicted yield load (N)	Predicted mode	Actual yield load (adjusted) (N)	Observed mode	Estimation Index
Edge	529.5	661.8	IV	470.0	III <sub>m</sub>	0.71
Plate	472.1	590.1	IV	497.5	III <sub>m</sub>	0.84

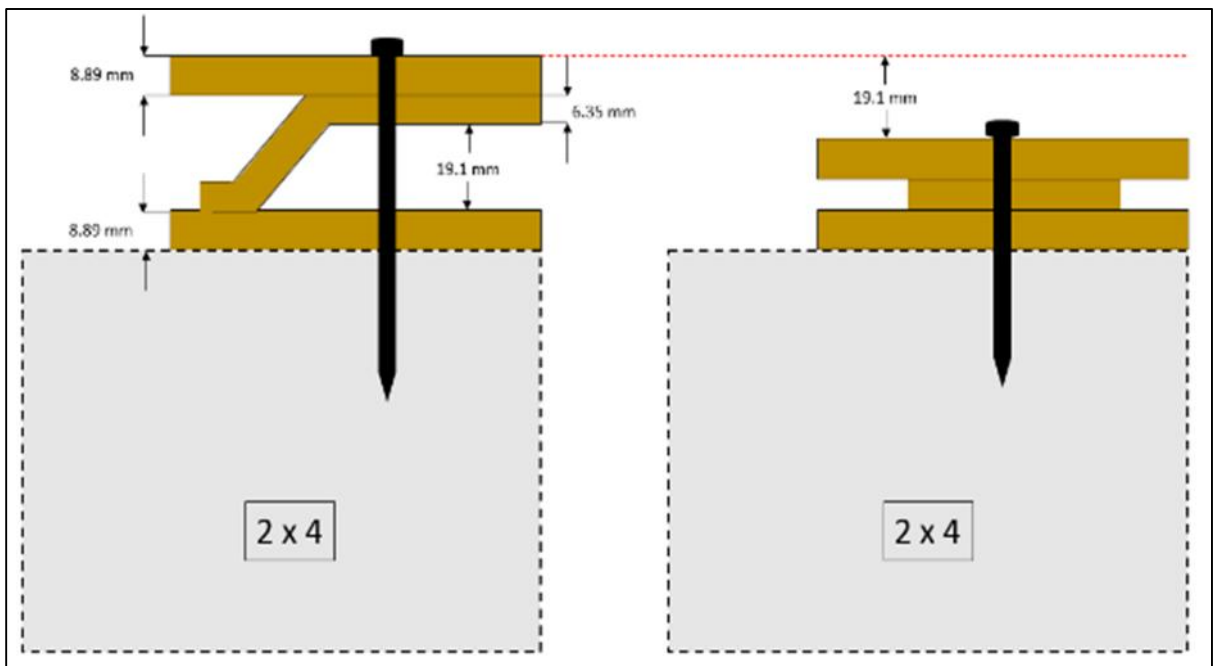


Figure 4.10. Comparison of 3DMCP geometry in lateral connection tests (left) compared to the geometry input used in yield limit equation (right)

#### *Small-Scale Shear Walls*

Results from the small-scale shear wall tests were inconclusive due the variation for each sheathing type caused by bearing failure perpendicular to the grain in the bottom plate. Specimen 3DMCP-1 absorbed the most energy of any wall assembly and failure

occurred as bearing failure perpendicular to the grain in the bottom plate and bearing failure of the bottom facing (Fig. 4.11). Specimen 3DMCP-2 absorbed the lowest amount of energy of any wall assembly and was limited by early splitting of the bottom plate with no noticeable deformation of the sheathing (Fig. 4.12). Specimen 3DMCP-3 had third highest energy absorption and failure occurred through splitting of the bottom plate, although it was much later in the test than the other two assemblies where splitting of the bottom plate occurred.

For the two OSB wall assemblies, specimen OSB-1 had the second lowest energy absorption, failing early through splitting in the bottom plate. The nail at the corner of the bottom plate and bottom stud had slight pull out, but no pull through of the nails in the sheathing was observed. Specimen OSB-2 had the second highest energy absorption of the wall assemblies and experienced bearing failure in the bottom plate and pull through/shear failure in the sheathing.

Two of the tests were stopped before the wall assembly reached 80% post peak load. To compare the data, energy absorption for all assemblies was found using 90% post peak load opposed to 80% post peak load typically used for producing EEEP curves. Specimens failing through early splitting of the bottom plate had much lower energies than the other panels. Large separation between the bottom plate and stud in the uplift corner due to no stud hold downs being used means that nails connecting sheathing to the bottom plate were heavily stressed limiting wall performance to the bearing capacity of the bottom plate.



Figure 4.11. Specimen 3DMCP-1 wall assembly failure. Bearing failure in the bottom plate (left) and bearing failure in the bottom facing of the 3DMCP (right)



Figure 4.12. Specimen 3DMCP-2 wall assembly failure. Failure through splitting of the bottom plate loaded perpendicular to the grain.

Due to the variety of failure modes, EEEP curves were highly scattered (Fig. 4.13). Constructing the curves based on the load at 90% of maximum load biased some of the specimens where the slope of the curve dropped rapidly for a brief period after reaching peak load then slowly tapered off. Panel orientation (strong vs. weak axis) had no noticeable effect on total energy absorption, possibly a result of the highly scattered energy absorption values and low number of wall assemblies tested. The behavior up to the yield point (40% of peak load) was different for OSB and 3DMCPs. 3DMCP assemblies had an average slope, or elastic shear stiffness, 2.1 times greater than the wall assemblies made with OSB. Large deflections due to bearing failure and splitting of the bottom plate provided inconclusive results in terms of average strain in the panels at maximum load.

It is interesting that the elastic stiffness was greater for 3DMCPs than OSB for the small-scale shear wall tests, since lateral connection tests showed OSB having higher elastic stiffness. Since the shear wall assemblies were largely governed by the bearing strength perpendicular to the grain in the bottom plate, the loads may have not been great enough to cause early nail yielding in the presence of additional nails. McCutcheon (1985) found that at lower loads sheathing shear stiffness contributes more to shear wall deformation than nail slip. Slopes of the elastic region of the load-shear strain curve for 3DMCPs were double that of OSB during in-plane shear tests and load limitation from bottom plate bearing failure may have kept the loads small enough to where the elastic stiffness of shear walls was governed by the shear stiffness of the panel.

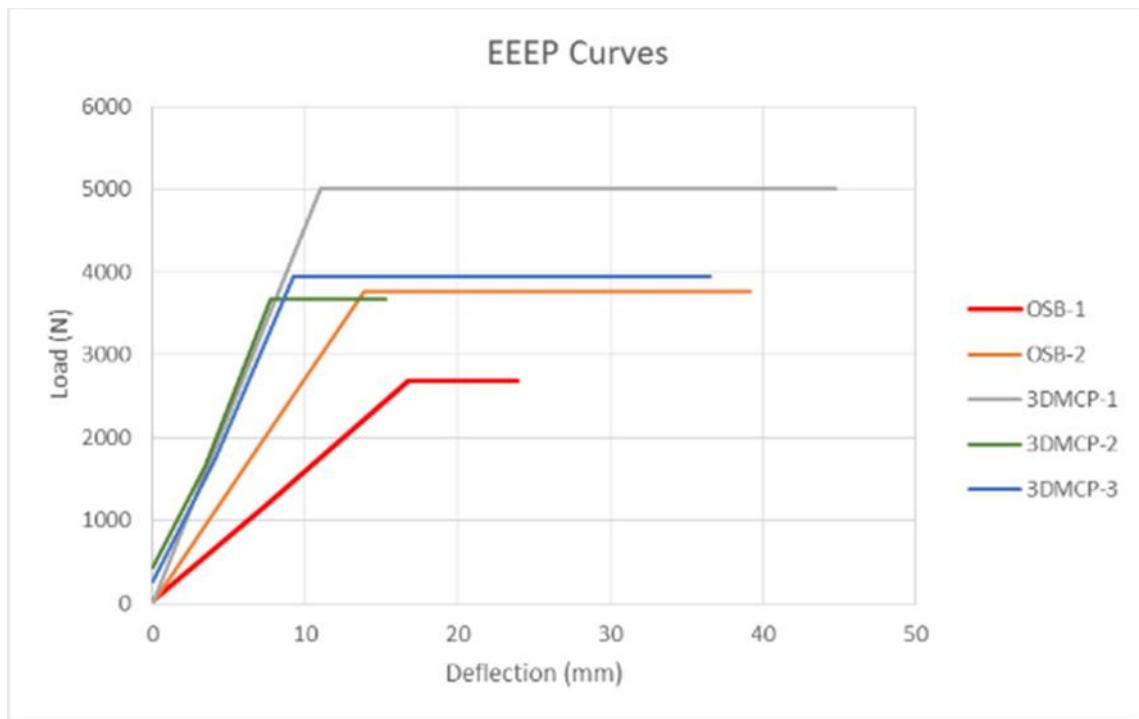


Figure 4.13. EEEP curves for all wall assemblies

## Chapter 5- Conclusions

A large increase in bending stiffness occurred for 3DMCPs compared to OSB used as facing material for both specimen orientations. The width direction of the core, which was laminated parallel to the weak axis of the facings was stiffer than the length direction of the core. Reinforcement from the core in weak axis bending assisted in more nearly equalizing differences 3DMCP strong and weak axis bending values compared to OSB, although a defined strong axis still existed.

Using conventional MOR calculations, void space in the hollow core biased a comparison of 3DMCPs to OSB in favor of OSB. Comparing maximum load and maximum moment per unit width of the specimen, 3DMCPs performed better than OSB in both orientations. Many of the specimens failed locally at the loading head in the top facings, a result of the small loading head that was used and void space in the core. Specimens not succumbing to localized facing failure, experienced shear failure in the core- likely a result of the low span-to-depth ratio. Longer specimens tested with a larger loading head are anticipated to yield results more indicative of pure flexural properties.

Both in-plane shear strength and stiffness of 3DMCPs were less than OSB. Like bending strength, these calculations were influenced from using the total depth of the sandwich structure. 3DMCPs carried 1.7 times more load than OSB and had twice the stiffness in the elastic region of the load-shear strain plots. Average strain at peak load was less for 3DMCPs than OSB, confirming that 3DMCPs were stiffer.

3DMCP fractures were less catastrophic and the panel was still able to hold over 25% of its maximum load after failure. This behavior was not observed for OSB. The fracture behavior may be influenced by the ribs running at a 30 degree angle, reinforcing the panel in the shearing direction. Failure around the bolts used to clamp panels to the in-plane shear apparatus suggests that future work should look to modify the apparatus used to enhance load distribution.

Compression strength was highly variable, influenced by the small specimen size and portion of the panel in which specimens were taken. Rib buckling, originating at the rounded transition of the rib was the predominant mode of failure. Compression strength was computed following a method used for determining the compression strength of wood perpendicular to the grain, since many of the 3DMCP specimens did not reach a defined maximum load. Increased load sharing, reduction of localized failures, and reduced variability are expected for a larger specimen size.

3DMCPs exhibited much greater withdrawal resistance than OSB. Though both were normalized for withdrawal resistance per millimeter of penetration depth, the added depth of the 3DMCPs contributed to load sharing along with the presence of adhesive from creating the sandwich structure, bolstering 3DMCP withdrawal performance. Dowel bearing strength was independent of bearing direction for both 3DMCPs and OSB. Increased dowel bearing load for 3DMCPs was proportional to the additional bearing area, indicating that the sandwich structure had no effect on dowel bearing strength.

Lateral yield load for 3DMCPs was greater than OSB connections with solid wood for both edge and plate geometries, although the increase was not proportional to the additional thickness of the panel. Connections made with 3DMCPs were less variable and no significant difference in yield load between edge and plate geometries was observed. Yielding tended to occur in the nail, with nail yielding in the side member (3DMCP) being most common. NDS yield models were unable to predict the experimentally determined yield load and mode. The increased distance from the shear plane to the bottom of the nail head due to void space is not properly accounted for in the model, resulting in overestimated yield loads. A factor to account for void space when used in conjunction with the yield limit models could perhaps predict dowel-type connection design values for 3DMCPs. Modelling the connection geometry as a two shear plane connection could possibly be used to more accurately model connection behavior.

Results from small-scale shear wall tests were inconclusive due to high variability resulting from bearing failure of the bottom plate from not using stud hold downs. Peak load for nearly all of the wall assemblies was affected by bearing failure perpendicular to the grain in the bottom plate. Assembly stiffness was twice as large for 3DMCPs, which was also observed for the in-plane shear tests. At lower loads (i.e. in the elastic region), sheathing rigidity governs wall deflection. Reduced penetration depth into the framing members in wall assemblies sheathed with 3DMCPs increased stress in the bottom plate, explaining the lack of noticeable nail deformation. During connection tests, no splitting of the framing member was observed due to yielding of the single fastener. Increased stress in the bottom plate and load sharing due to presence of more nails likely caused the bottom plate to fail before large enough forces were generated to cause bending of the fasteners.

In order for this particular 3DMCP to be used as a replacement for flat wood structural panels an increase in performance is necessary to justify the costs of using nearly three times the material. 3DMCPs performed at least as well as the OSB if not better in certain tests. However, with the exception of bending stiffness, dowel bearing, and withdrawal, increased performance was not proportional to the additional volume of raw materials required for sandwich construction. Bending results indicate that if a larger loading head and longer specimen had been used, then significantly more capacity in the facings may exist.

The true benefits of this 3DMCP will not be apparent until full-size panels are produced. Based on the results, it is logical to move forward and produce full-size panels for a more realistic mechanical performance characterization. Evaluating the anticipated increase in thermal and acoustical resistance would also improve the economics of using this 3DMCP for structural sheathing. When bending and compression specimens failed in the core region, fractures tended to originate at the rounded portion of the rib, indicating that a better understanding of the optimum strand geometry and alignment may be beneficial to the mechanical properties of 3DMCPs produced from wood strands.

*Recommendations*

1. Produce larger panels using similar strand geometry and alignment to grasp how full-size 3DMCPs produced with wood strands perform.
2. If core failures in full-size panels originate around the rounded rib transition, then future work should investigate the impact of strand geometry and alignment pattern on the strength of the core. A fracture mechanics based approach would be beneficial in comparing different strand geometries and alignment patterns.
3. Mechanical fastener properties warrant further investigation. A larger fastener may be necessary to procure the benefits of a thicker sheathing material, since lateral connection tests were largely governed by yielding of the nail. Determining ideal fastener placement through the core would also be beneficial.
4. A major benefit of using 3DMCPs as sheathing material would be the anticipated improvement of thermal and acoustical transmission resistance. Characterization of these properties would be important in determining economic feasibility of the panels.

## Literature Cited

- AFPA. (2012). ASD/LRFD Manual for Engineered Wood Construction. *National Design Specification for Wood Construction* (p. 98). American Forest and Paper Association. Washington D.C., USA.
- Alldritt, K. (2013, June 18). *Designing a Strand Orientation Pattern for Improved Shear Properties of Oriented Strand board* (M.S. Thesis). Oregon State University, Corvallis, OR, USA.
- Allen, E., & Thallon, R. (2011). *Fundamentals of Residential Construction* (3<sup>rd</sup> ed.). Hoboken, NJ, USA. John Wiley & Sons, Inc.
- APA- The Engineered Wood Association. (2011). PS 2-10: Performance Standard for Wood-Based Structural-Use Panels. Tacoma, WA, USA.
- APA- The Engineered Wood Association. (2012). Panel Design Specification. Form No. D510C.
- APA- The Engineered Wood Association. (2013). Standard for Performance-Rated Structural Insulated Panels in Wall Applications.
- ASCE-American Society of Civil Engineers. (1996). Mechanical Connections in Wood Structures. *ASCE Manuals and Reports on Engineering Practice No. 84*. New York, NY, USA
- ASTM. (2009). *Standard Test Methods for Small Clear Specimens of Timber*. ASTM D143. ASTM International. West Conshohocken, PA, USA
- ASTM. (2011). *Standard Test Methods for Structural Panels in Flexure*. ASTM D3043–00.
- ASTM. (2012a). *Standard Practice for Determining Sandwich Beam Flexural and Shear Stiffnesses*. Vol. ASTM D7250/D7250M-06.
- ASTM. (2012b). *Standard Practice for Static Load Test for Shear Resistance to Framed Walls for Buildings*. ASTM E564.
- ASTM. (2012c). *Standard Test Method for Facing Properties of Sandwich Constructions by Long Beam Flexure*. ASTM D7249/D7249M-12..
- ASTM. (2012d). *Standard Test Methods for Mechanical Fasteners in Wood*. ASTM D1761.
- ASTM. (2013a). *Standard Test Method for Evaluating Dowel-Bearing Strength of Wood and Wood-Based Products*. ASTM D5764.

- ASTM. (2013b). *Standard Test Methods for Structural Panels in Shear Through-the-Thickness*. ASTM D2719.
- Beall et al. (2006). Small-Scale Rack Testing of Wood-Frame Shear Walls. *Wood and Fiber Science*, 38(2), 300–313.
- Breyer et al. (2015). *Design of Wood Structures- ASD/LRFD* (7th ed.). USA: McGraw Hill Education.
- Cai et al. (2014). Development and Performance Evaluation of Fiber Reinforced Polymer Bridge. Technical Report No. FHWA/LA.10/472. Department of Civil and Environmental Engineering. Louisiana State University.
- Carlsson, L., & Karamateas, G. (2011). *Structural and Failure Mechanics of Sandwich Composites*. USA. Springer.
- Correlated Solutions. (2010). VIC-3D 2010: Testing Guide. Correlated Solutions. Irmo, SC, USA.
- Easterling et al (1982). On the mechanics of balsa and other woods. *Proceedings of the Royal Society of London*, 383(1784), 31–41.
- ECOR. (2015). Noble Environmental Technologies. Retrieved from <http://ecorusa.com/>
- Engineered Materials Inc. (2015). Structural Composites and Sandwich Panels. Retrieved from <http://www.engineeredmaterialsinc.com/>
- Fujii, J. (2014, June 5). Dry Forming Three Dimensional Wood Fiber Webs. US Patent No. 11,570,745. Allowed June 5<sup>th</sup>, 2015.
- Gibson, L., & Ashby, M. F. (1997). *Cellular Solids: Structure and Properties*. Cambridge, NY, USA. Cambridge University Press.
- Hunt, J. (2004). 3D Engineered Fiberboard: Finite Element Analysis of a New Building Product. Proceedings from the 2004 International ANYSY Conference, Pittsburg, PA.
- Hunt, J., & Winandy, J. E. (2002). 3D Engineered Fiberboard: A New Structural Building Product. Proceedings from the 6<sup>th</sup> European Panel Products Symposium. (pp. 106–117). Llandudno, Wales.
- Hunt, J., & Winandy, J. E. (2003). 3D Engineered Fiberboard: Engineering Analysis of a New Building Product. *Proceedings Paper 8.02* (pp. 1–8). EcoComp 2003. Queen Mary, University of London.
- International Code Council, INC. (2011). *2012 International Residential Code*. USA.

- Johansen, K. (1949). Theory of Timber Connectors. *Int. Assoc. of Bridges and Structural Engineering, Publication No. 9*, 249–262.
- Kent, S. (2004). *The Effect of Biological Deterioration on the Performance of Nailed Oriented Strand Board Sheathing to Douglas-fir Framing Member Connections* (PhD Thesis). Oregon State University, Corvallis, OR, USA.
- Maynard, N. F. (2009). Construction Products Review: Structural Insulated Panels. *Architect Magazine*. Retrieved from [http://www.architectmagazine.com/technology/products/construction-products-review-structural-insulated-panels\\_o](http://www.architectmagazine.com/technology/products/construction-products-review-structural-insulated-panels_o)
- McCutcheon, W. (1985). Racking Deformation in Wood Shear Walls. *Journal of Structural Engineering*, 111(2), 257–269.
- Nallagula, S. (2006). *Behavior and Flexural Analysis of Balsa Wood Core Sandwich Composites: Experimental, Analytical, Finite Element Approaches* (M.S. Thesis). University of New Orleans, New Orleans.
- Neucor. (2015). Retrieved from <http://www.neucorpanels.com/>
- Overney, J. (2012). Balsa bridges- with a twist. *Ecole Polytechnique Federale Lausanne*. Retrieved from <http://actu.epfl.ch/news/balsa-bridges-with-a-twist/>
- Panjehpour et al. (2013). Structural Insulated Panel: Past, Present, and Future. *Journal of Engineering, Project, and Production Management*, 3(1), 2–8.
- Price, E., & Gromala, D. (1980). Racking Strength of Walls Sheathed With Structural Flakeboards Made From Southern Species. *Forest Products Journal*, 30(12), 19–23.
- Schwarzkopf, M., Muszynski, L., & Nairn, J. (2013). SteroMicroscopic Optical Method for the Assessment of Load Transfer Patterns Across the Adhesive Bondline Interphase. (pp. 100–109). Presented at the International Conference on Wood Adhesives, Toronto, Ontario, Canada: Forest Products Society.
- Shrestha, D. (1999). Shear Properties Test of Oriented Strand board Panels. *Forest Products Journal*, 49(10), 41–46.
- SingCore. (2015). Retrieved from <http://singcore.com/>
- Sinha, A., & Gupta, R. (2009). Strain Distribution in OSB and GWB in Wood-Frame Shear Walls. *Journal of Structural Engineering*, 135(6), 666–675.

- Sinha, A., Gupta, R., & Nairn, J. (2011). Thermal Degradation of Lateral Yield Strength of Nailed Wood Connections. *Journal of Materials in Civil Engineering*, 23(6), 812–822.
- SIPA. (2015). Structural Insulated Panels. *SIPA- Structural Insulated Panel Association*.
- Smulski, S. (1997). *Engineered Wood Products: A Guide for Specifiers, Designers, and Users*. Madison, WI, USA. PFS Research Foundation.
- Strong, A. B. (2008). *Fundamentals of Composites Manufacturing: Materials, Methods, and Applications* (2nd ed.). Dearborn, MI: Society of Manufacturing Engineers.
- Sutton, M., Orteu, J.-J., & Schreier, H. (2009). *Image Correlation for Shape, Motion and Deformation Measurements: Basic Concepts, Theory and Applications*. Springer.
- USDA Forest Service. (2001). *Forest Service National Fire Plan Implementation*. Audit Report No. 08601-26-SF. USDA Forest Service.
- Voth, C. (2009). *Lightweight sandwich panels using small-diameter timber wood-strands and recycled newsprint cores* (M.S. Thesis). Washington State University, Pullman, WA.
- Wilkinson, T. (1991). Dowel Bearing Strength. *FPL-RP-505*, USDA Forest Service Forest Products Laboratory, Madison, WI, USA.

## APPENDICES

**APPENDIX A***Core manufacturing*

Table A1. Furnish inputs for producing cores with target density of 0.56 g/cm<sup>3</sup> and 4% adhesive content (a), target density of 0.56 g/cm<sup>3</sup> and 6% adhesive content (b), target density of 0.64 g/cm<sup>3</sup> and 4% adhesive content (c), and target density of 0.64 g/cm<sup>3</sup> and 6% adhesive content (d).

	<b>a</b>	<b>b</b>	<b>c</b>	<b>d</b>
<b>Length (cm)</b>	76.2	76.2	76.2	76.2
<b>Width (cm)</b>	71.1	71.1	71.1	71.1
<b>Thickness (cm)</b>	0.64	0.64	0.64	0.64
<b>Surface area multiplier</b>	1.3	1.3	1.3	1.3
<b>Volume (cm<sup>3</sup>)</b>	4508	4508	4508	4508
<b>Strand MC, OD (%)</b>	6.1	6.1	6.1	6.1
<b>Adhesive % solids</b>	55	55	55	55
<b>Adhesive content (%)</b>	4	6	4	6
<b>Target density (g/cm<sup>3</sup>)</b>	0.56	0.64	0.56	0.64
<b>OD wood (kg)</b>	2.41	2.35	2.75	2.69
<b>Adhesive solids (g)</b>	99.8	149.7	113.4	172.4
<b>Furnish loss (%)</b>	15	15	15	15
<b>To blender</b>				
<b>Strands (kg)</b>	2.92	2.85	3.33	3.26
<b>Adhesive (g)</b>	172.4	267.6	195.0	290.3
<b>To press</b>				
<b>Blended furnish (kg)</b>	2.62	2.64	3.00	3.02

Table A2. Press schedule

Segment	Control	Set point (mm)	Segment time (s)
1	Close, -5.4 mm/s	76.33	24
2	Hold	76.33	240
3	Vent, 0.05 mm/s		40
4	Open, 5.4 mm/s	200	24

Phenol Formaldehyde Adhesive for Core Manufacturing:

Manufacturer: Georgia Pacific Chemicals

Product: 320C02 Resi-Stran OSB face adhesive

Phenol-Resorcinol Adhesive System Instructions and Use:

- Manufacturer: Hexion Specialty Chemicals (Columbus, OH, U.S.)
- Product: CASCOPHEN LT-5210J Resin and CASCOSSET FM-6210 Phenol Resorcinol Adhesive System
- Spread rate: 125 lbs/1000 ft<sup>2</sup> (0.06 g/cm<sup>2</sup>)
- Total laminating area per side of core: 1550 cm<sup>2</sup>
- Adhesive per side: 94 g
- Maximum recommended open assembly time at 70-75 °F and spread rate of 90-100 lbs/1000 ft<sup>2</sup>: 60 minutes
- Recommended pressure: 100-150 psi (0.69-1.0 MPa) for 5 hours at 70-75 °F
- Final adhesive mix ratio by weight: 2.5:1 resin to hardener mixture
- Hardener mixing: 2:1 water to powdered hardener

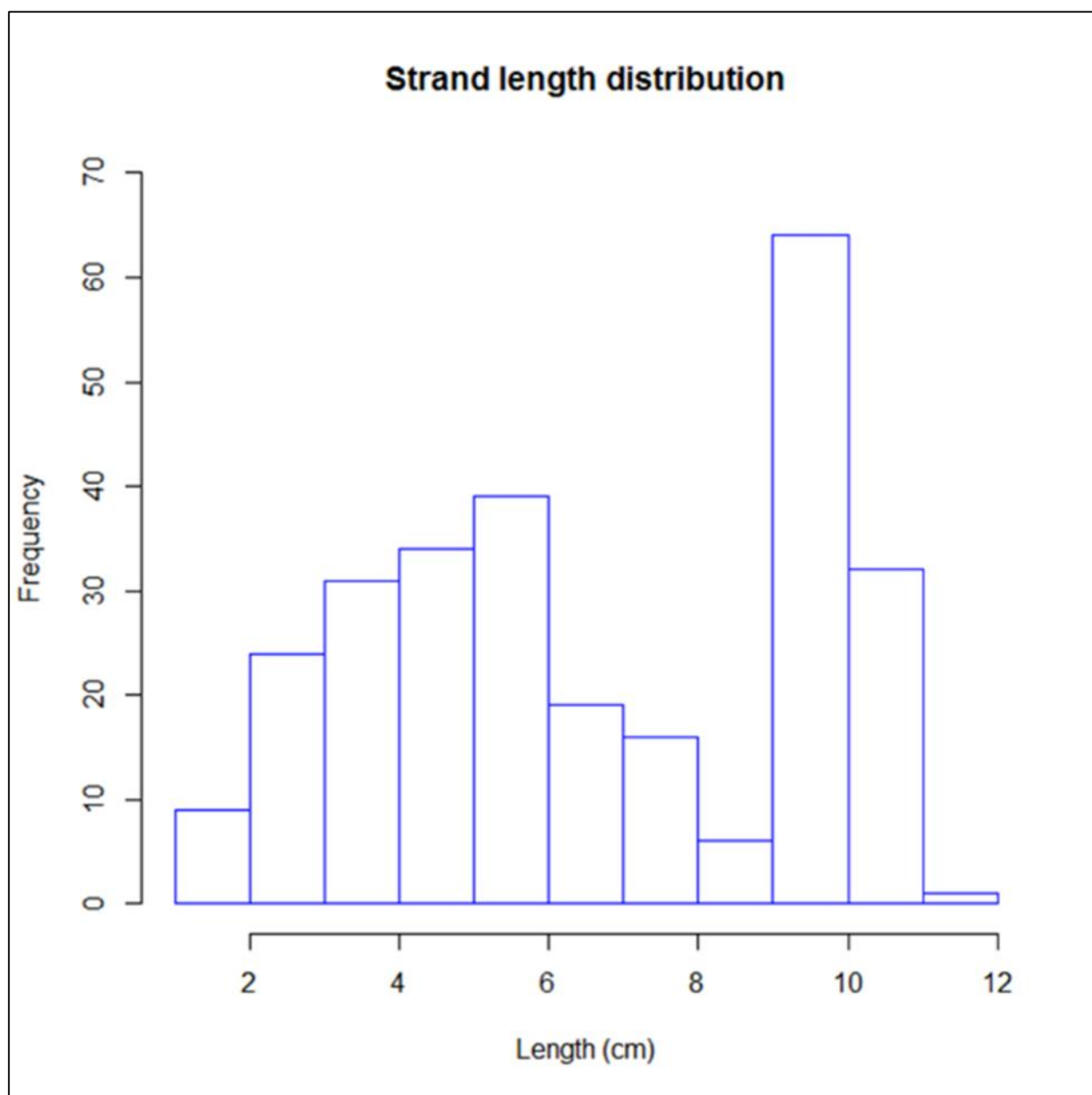


Figure A1. Histogram of strand length distribution

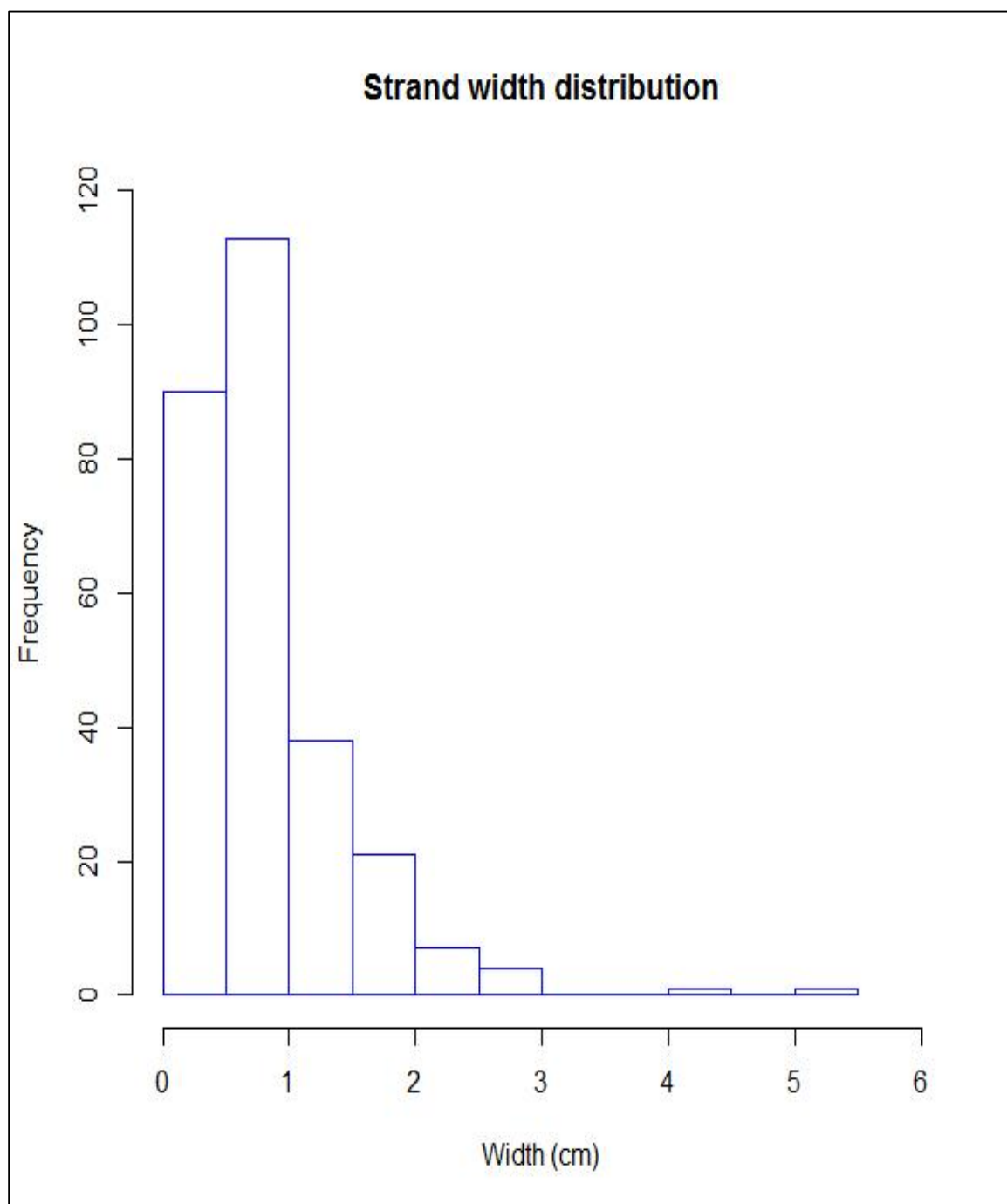


Figure A2. Histogram of strand width distribution

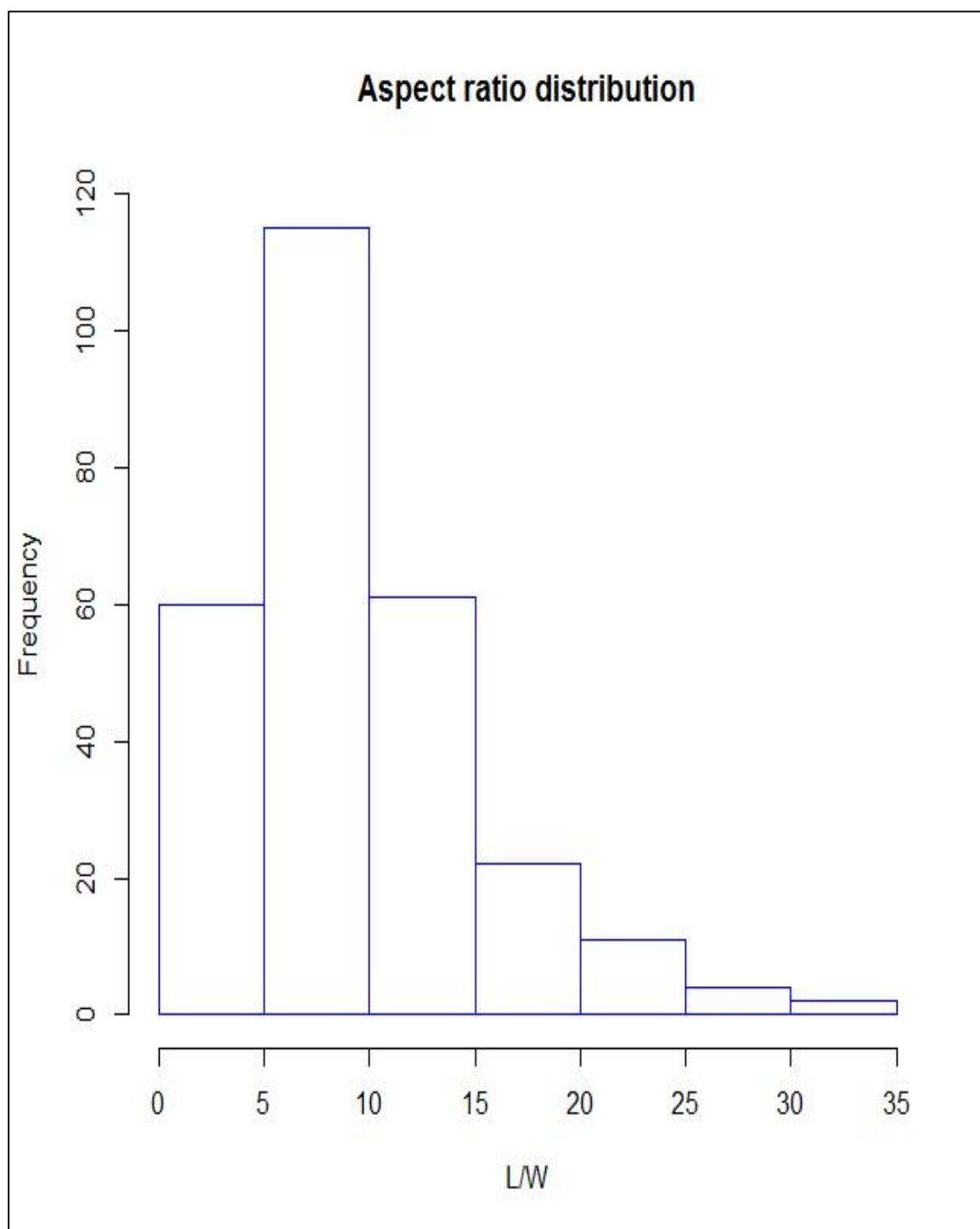


Figure A3. Histogram of strand aspect ratio (length/width) distribution

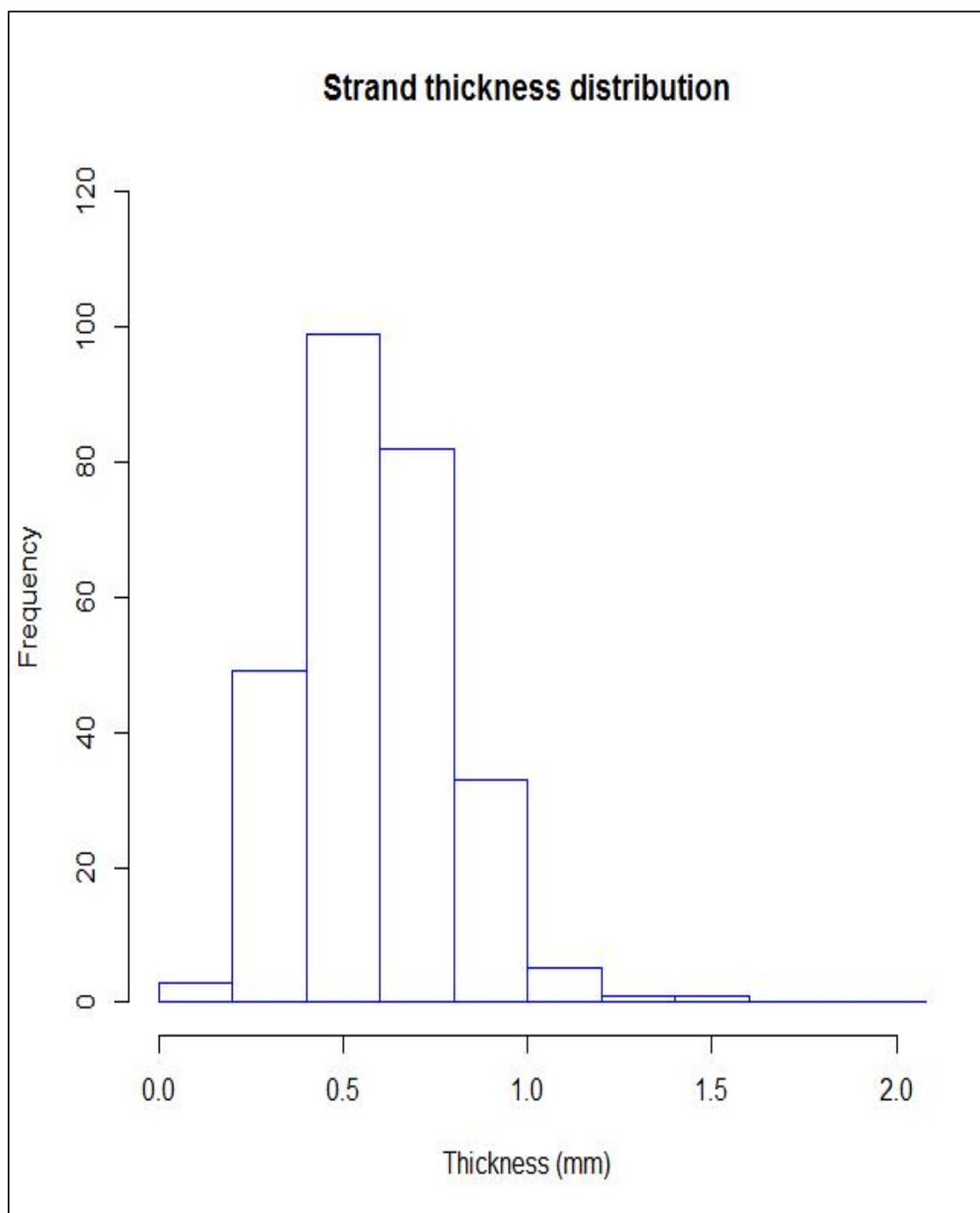


Figure A4. Histogram of strand thickness distribution

**APPENDIX B***Bending*

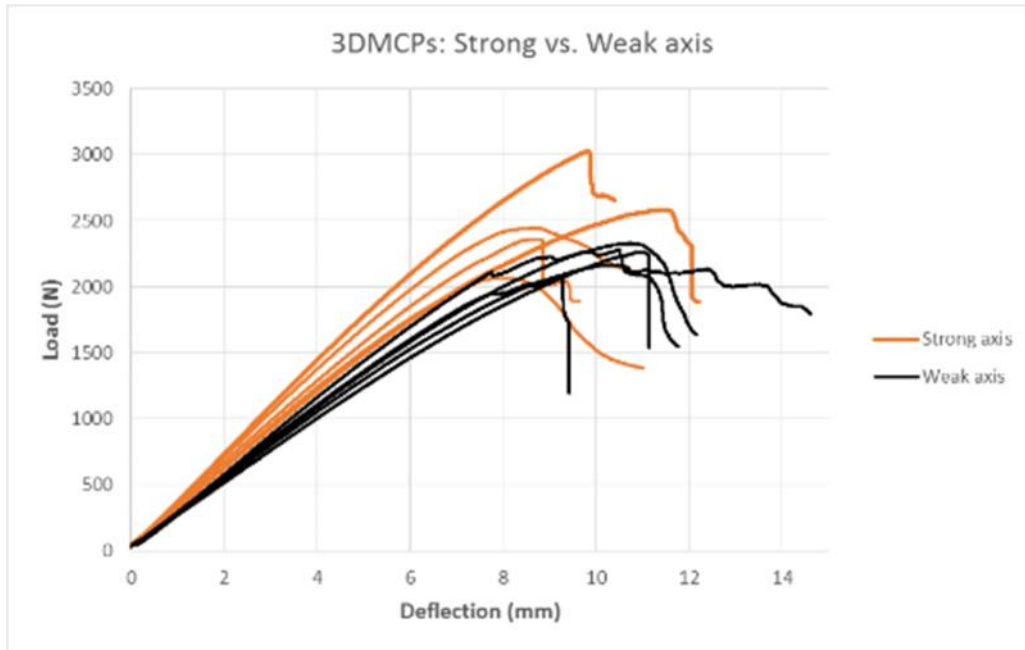


Figure B1. Load-deflection plot for some 3DMCPs in strong and weak axis bending

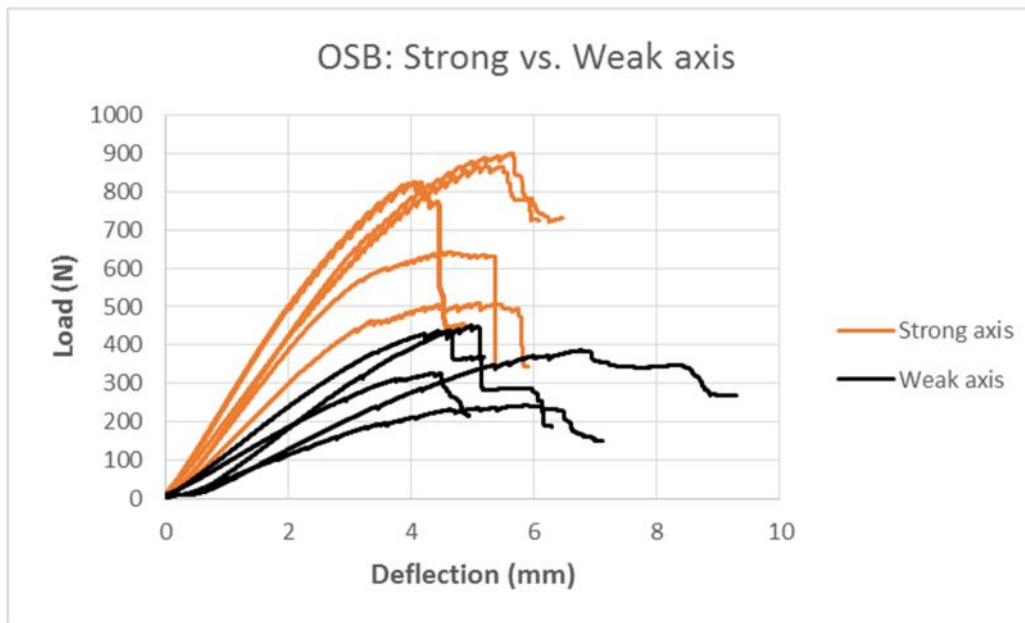


Figure B2. Load-deflection plot for some OSB in strong and weak axis bending

Table B1. ANOVA output comparing bending strength of strong axis specimens S2 and S3

<b>Specimen</b>	<b>DF</b>	<b>Sum Sq.</b>	<b>Mean Sq.</b>	<b>F-value</b>	<b>p-value</b>
<b>S2</b>	1	4.071	4.071	1.730	0.201
<b>S3</b>	24	56.458	2.352		

*Explanation of Box Plots*

Box plots that are presented herein were constructed using the following parameters:

- The top of the box is plotted at  $Q(0.75)$  and the bottom at  $Q(0.25)$ .
- The height of the box is  $Q(0.75)-Q(0.25)$ , or the interquartile range (IQR)
- The line located inside the box represents the median value [ $Q(0.5)$ ]
- The whiskers extend to the most extreme values that are less than  $1.5(IQR)$  from the box while extreme points are plotted individually

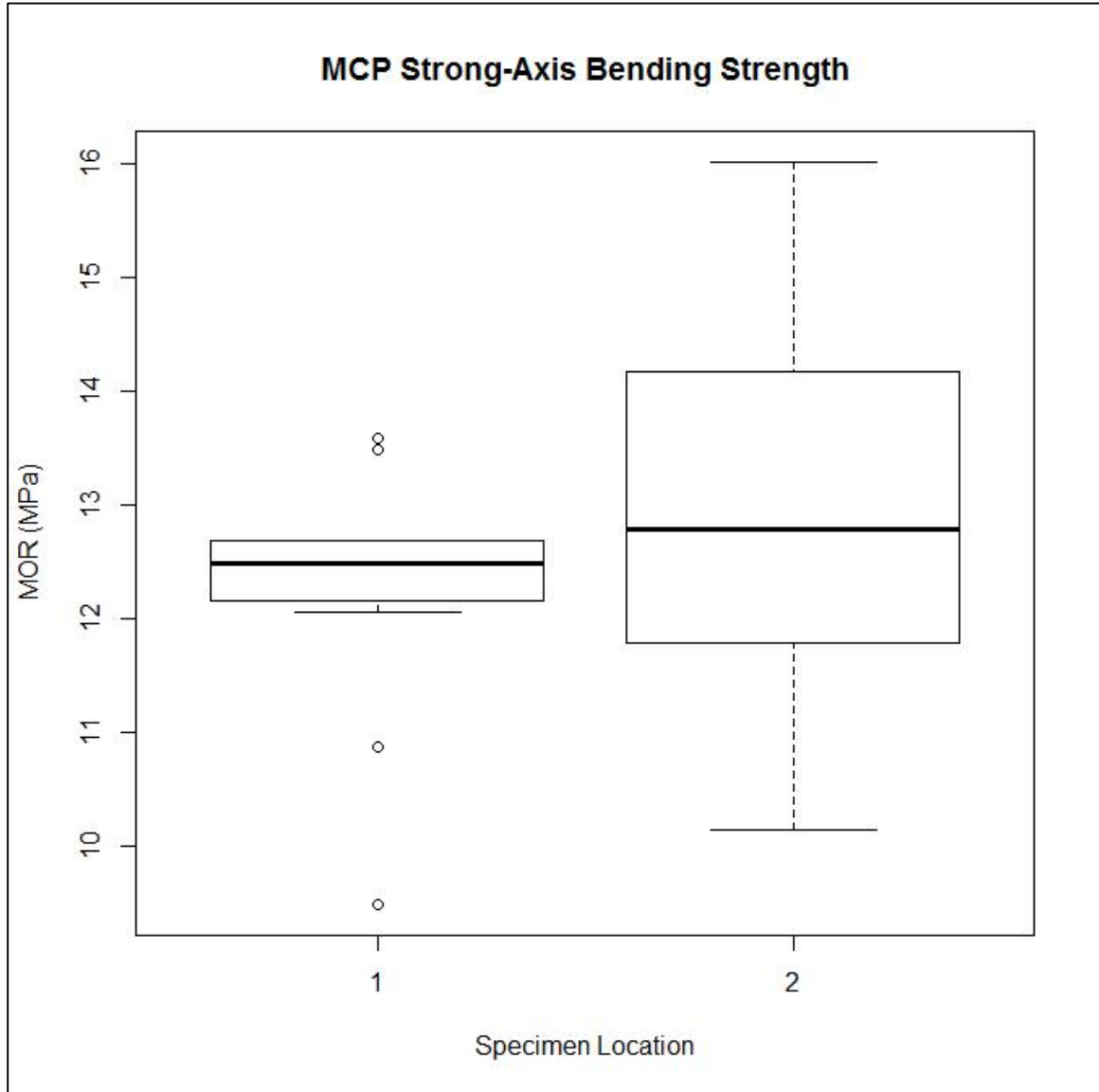


Figure B3. Boxplot comparing the bending strength of strong axis specimens S2 (#1) and S3 (#2)

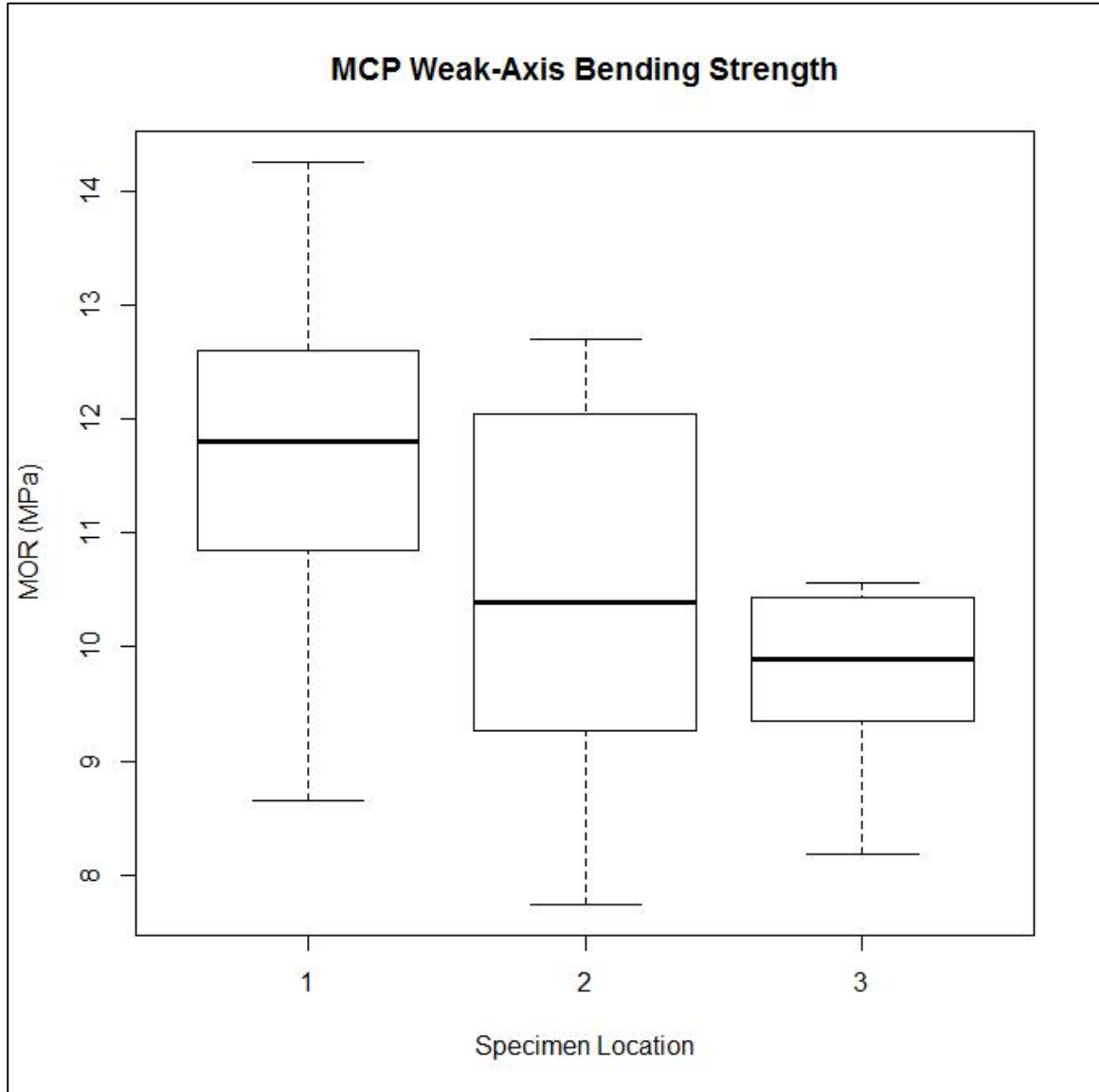


Figure B4. Boxplot comparing the bending strength of weak axis specimens W1 (#1), W2 (#2), and W3 (#3)

Table B2. Multiple linear regression output comparing bending strength of weak axis specimens W1, W2, and W3

Specimen	Estimate	Std. Error	t-value	p-value
<b>W1</b>	11.714	0.418	28.059	< 2e-16
<b>W2</b>	-1.200	0.578	-2.076	0.05
<b>W3</b>	-1.94	0.605	-3.229	0.003

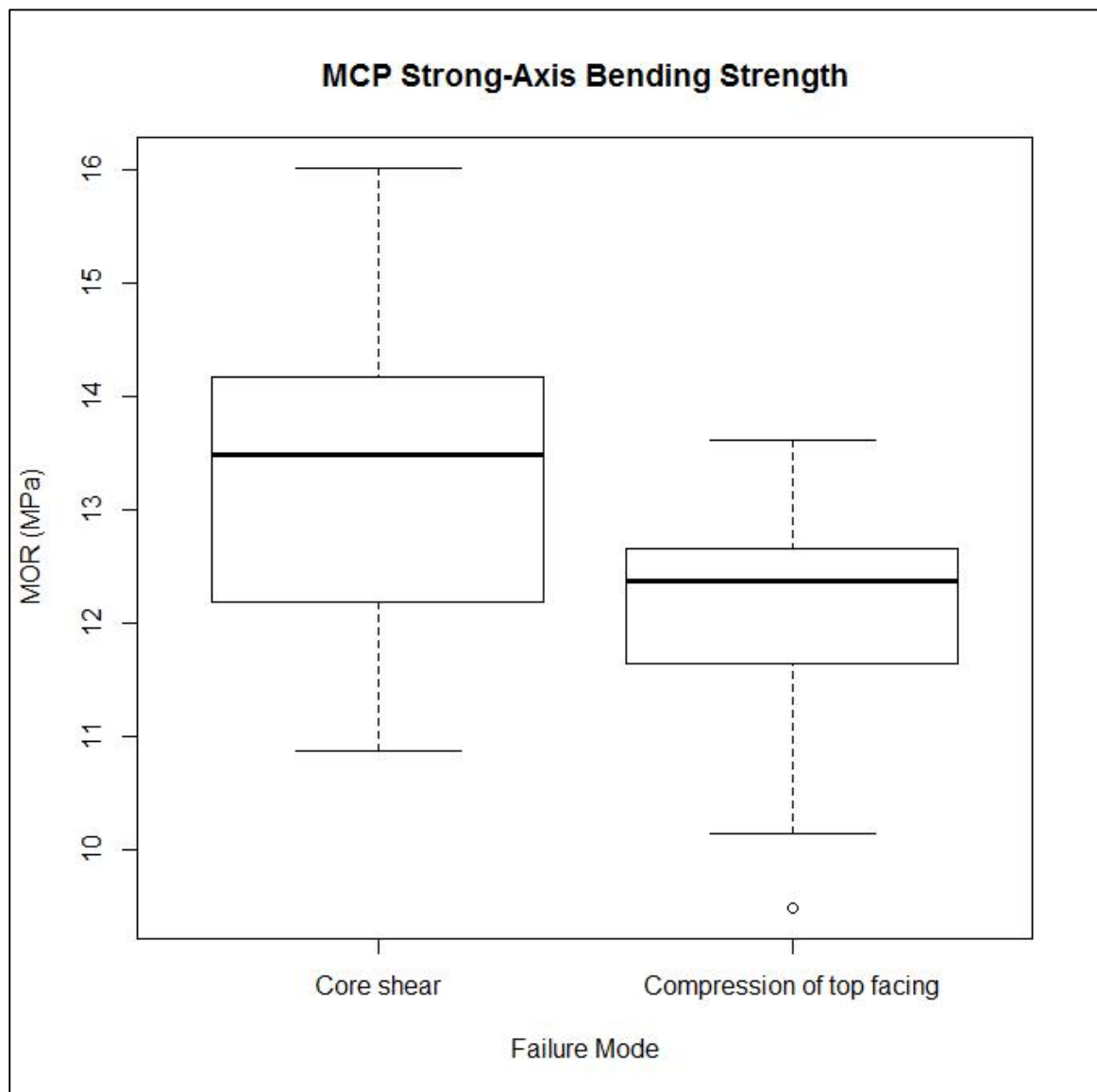


Figure B5. Boxplot comparing of strong axis bending strength by failure mode

Table B3. Multiple linear regression output comparing bending strength of strong axis bending specimens by failure mode

	Estimate	Std. Error	t-value	p-value
<b>Core shear</b>	13.387	0.390	34.318	< 2e-16
<b>Failure in top facing</b>	-1.417	0.552	-2.569	0.017

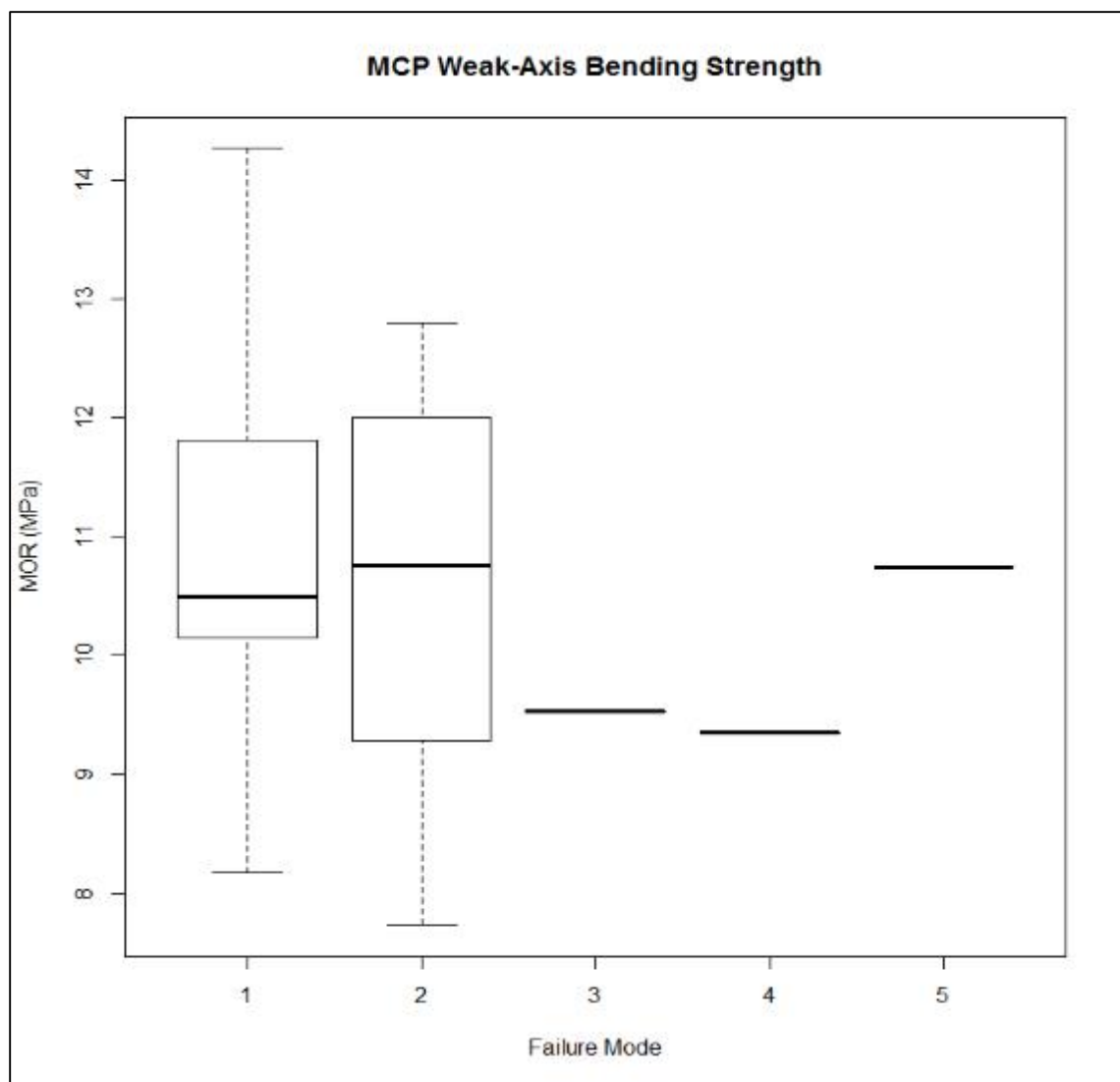


Figure B6. Boxplot comparing weak axis bending strength by failure mode: (1) failure of top facing, (2) flexural failure in bottom facing, (3) delamination at core-facing interface, (4) shear failure in facing, and (5) shear failure in core

Table B4. Multiple linear regression output comparing bending strength of weak axis bending specimens by failure mode

	<b>Estimate</b>	<b>Std. Error</b>	<b>t-value</b>	<b>p-value</b>
<b>Failure in top facing</b>	10.893	0.452	24.097	< 2e-16
<b>Failure in bottom facing</b>	-0.223	0.601	-0.371	0.714
<b>Delamination</b>	-1.357	1.692	-0.802	0.429
<b>Facing shear failure</b>	-1.544	1.692	-0.913	0.369
<b>Core shear failure</b>	-0.154	1.692	-0.091	0.928



Figure B7. Comparison of weak axis bending specimens. W1 (left), W2 (middle), and W3 (right). Red lines represent the location of the loading head, which are marked on the side of the specimens.

**APPENDIX C***In-Plane Shear*

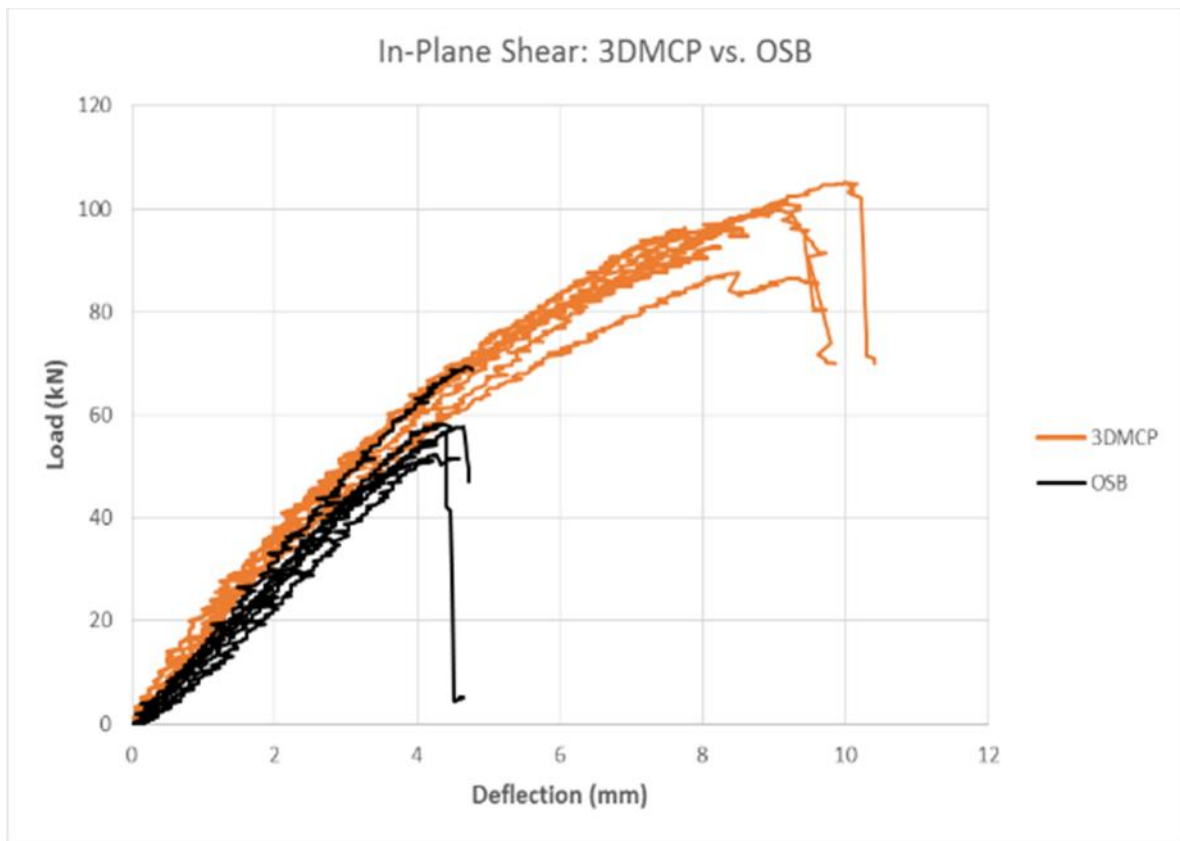


Figure C1. In-plane shear load-deflection plot comparing 3DMCPs and OSB

**APPENDIX D***Flatwise Compression*

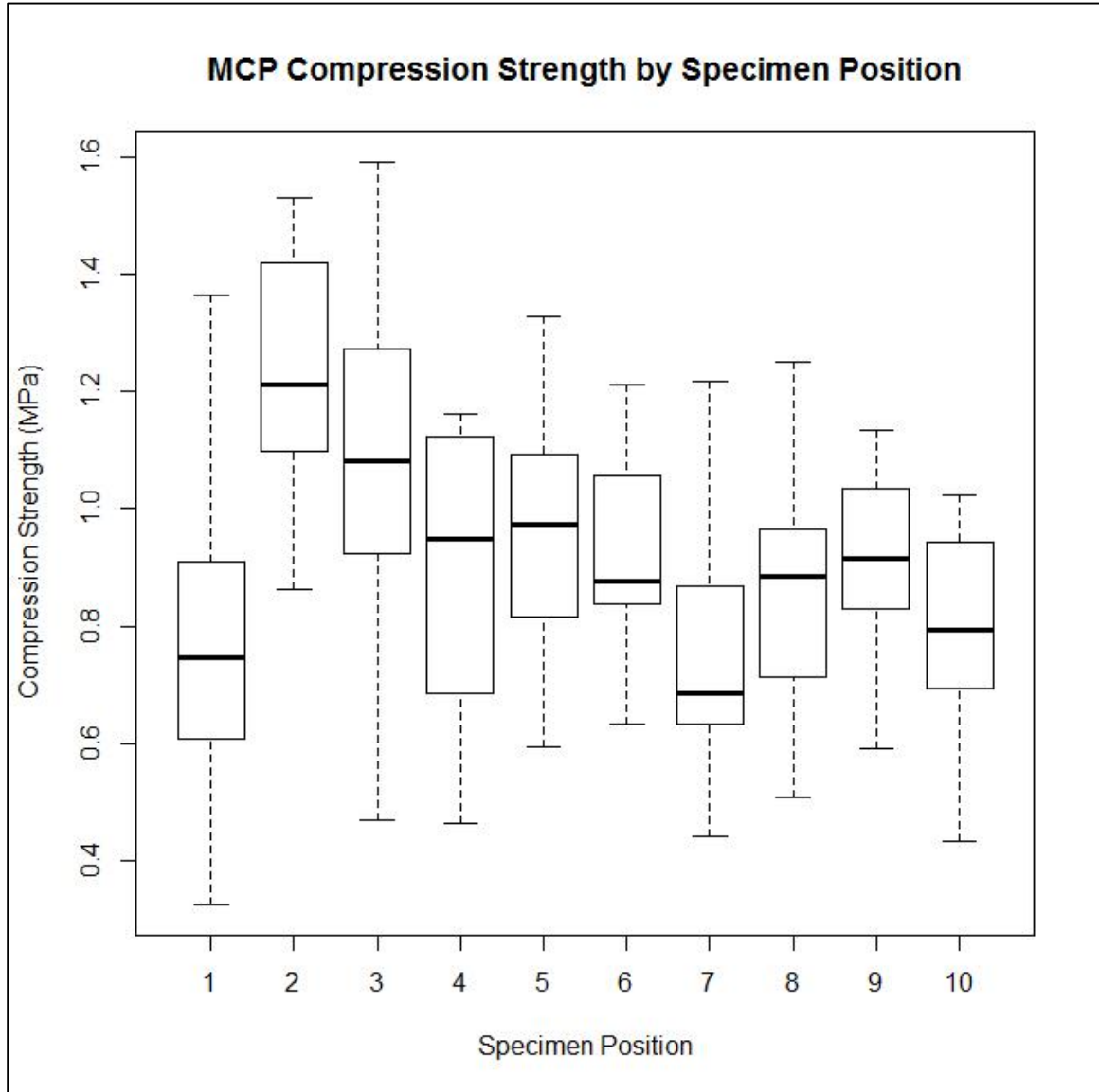


Figure D1. Boxplot comparing compression strength for compression specimens W4 (#1), W5 (#2), W6 (#3), W7 (#4), W8 (#5), W9 (#6), W10 (#7), W11 (#8), W12 (#9), and W13 (#10)

Table D1. Multiple linear regression output comparing flatwise compression specimen panel placement to strength

	<b>Estimate</b>	<b>Std. Error</b>	<b>t-value</b>	<b>p-value</b>
<b>W4</b>	0.775	0.071	10.90	< 2e-16
<b>W5</b>	0.455	0.101	4.53	1.65e-5
<b>W6</b>	0.310	0.101	3.09	0.003
<b>W7</b>	0.120	0.101	1.19	0.237
<b>W8</b>	0.173	0.101	1.72	0.088
<b>W9</b>	0.158	0.101	1.57	0.120
<b>W10</b>	-0.021	0.101	-0.21	0.834
<b>W11</b>	0.061	0.101	0.60	0.547
<b>W12</b>	0.130	0.101	1.29	0.200
<b>W13</b>	0.018	0.101	0.18	0.856



Figure D2. Buckling failure at rounded portion of the rib in flatwise compression specimen



Figure D3. Core shear failure in flatwise compression specimen



Figure D4. Flexural failure of bottom peak in flatwise compression specimen

**APPENDIX E***Mechanical Fasteners*



Figure E1. Nail yielding in lateral connection tests. Mode III<sub>m</sub> yielding (left) and mode III<sub>s</sub> yielding (right).



Figure E2. Example of main member bearing yielding in lateral connection tests



Figure E3. Example of nail contacting rib and deflecting upon further insertion

Table E1. Multiple linear regression output comparing withdrawal resistance based on nail position in the core of 3DMCPs

	Estimate	Std. Error	t-value	p-value
<b>Top peak</b>	24.988	2.559	9.765	7.71e-9
<b>Bottom peak</b>	12.442	3.536	3.519	0.002

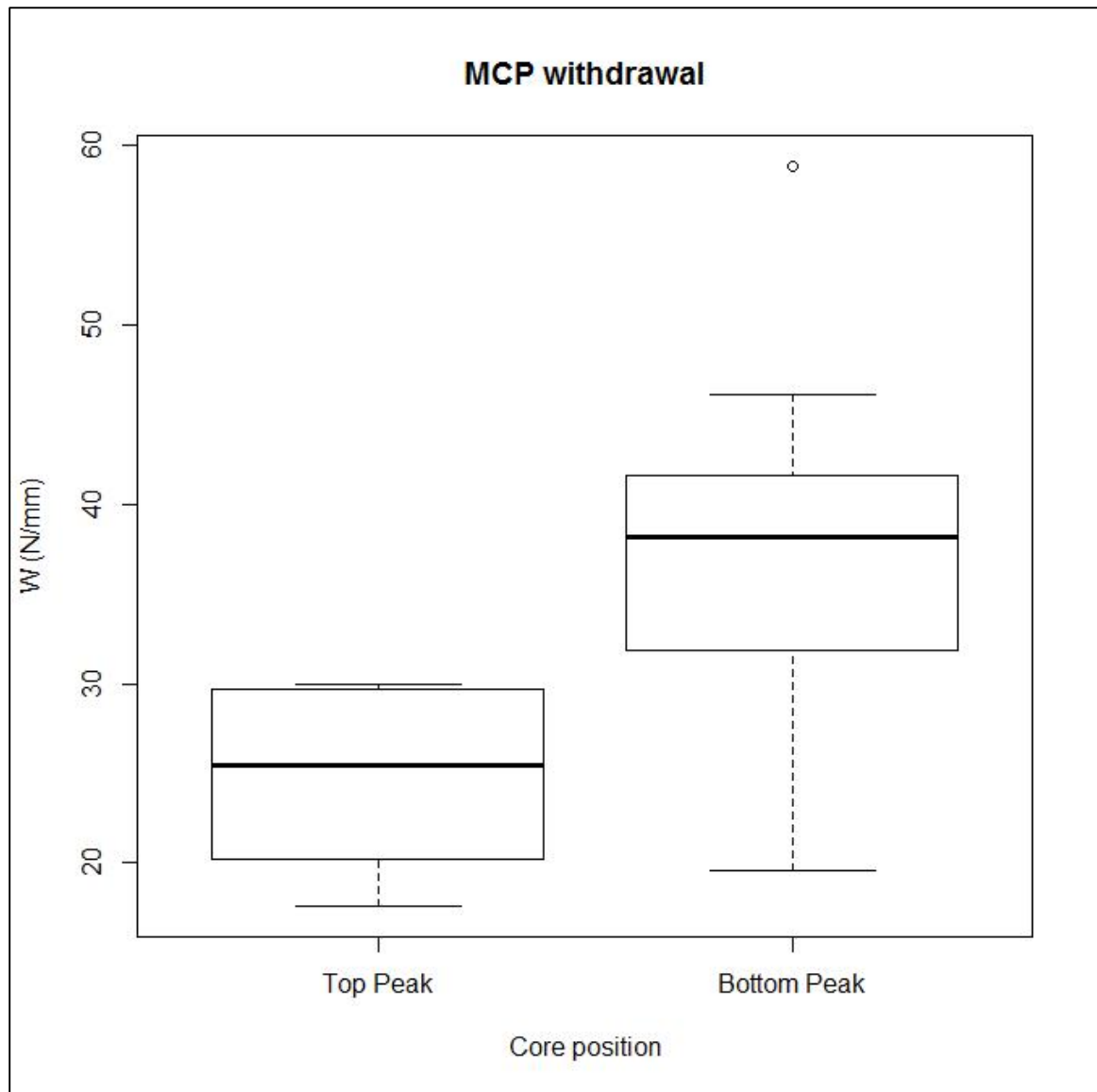


Figure E4. Boxplot comparing withdrawal resistance based on nail position in the core of 3DMCPs.

Table E2. Multiple linear regression output comparing dowel bearing strength of 3DMCPs vs. bearing direction

Bearing into	Estimate	Std. Error	t-value	p-value
<b>Strong axis</b>	40.90	2.37	17.23	1.28e-13
<b>Weak axis</b>	-2.66	3.36	-0.793	0.44

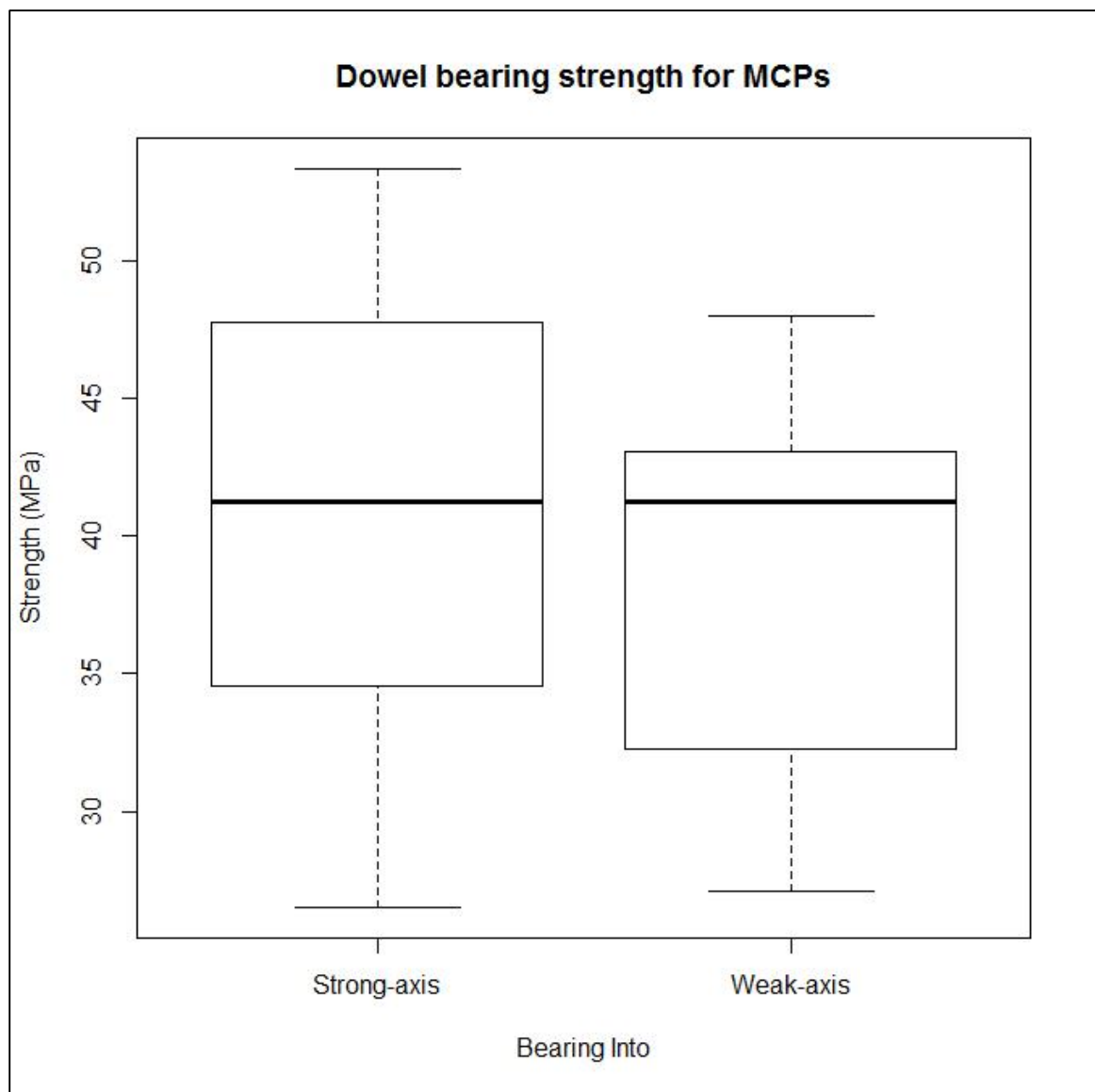


Figure E5. Boxplot comparing dowel bearing strength of 3DMCPs vs. bearing direction

Table E3. Multiple linear regression output comparing dowel bearing strength of OSB vs. bearing direction.

Bearing into	Estimate	Std. Error	t-value	p-value
Strong axis	40.90	2.61	15.70	3.85e-11
Weak axis	-3.12	4.18	-0.75	0.466

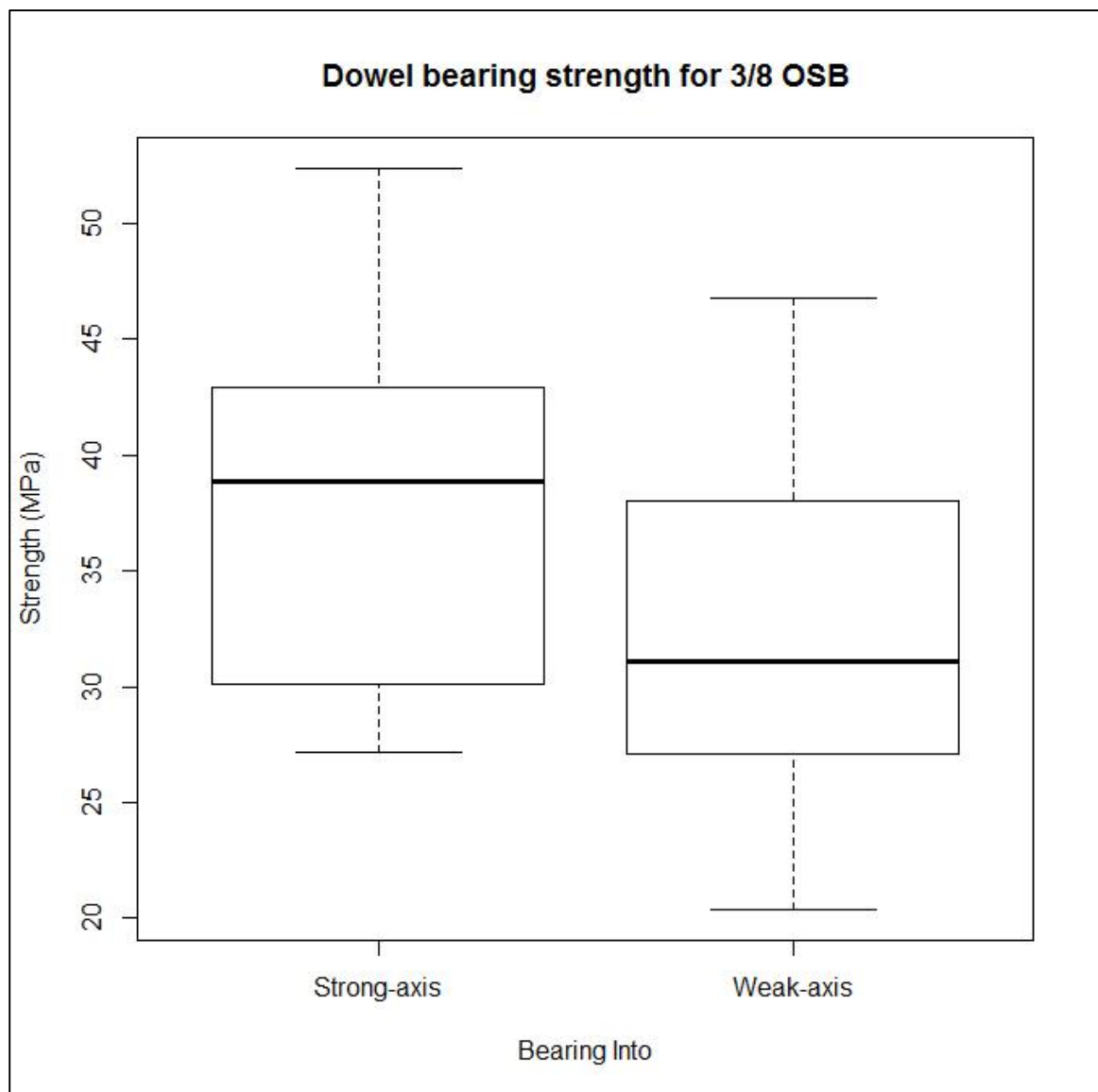


Figure E6. Boxplot comparing dowel bearing strength of OSB vs. bearing direction

**APPENDIX F***Small-Scale Shear Walls*

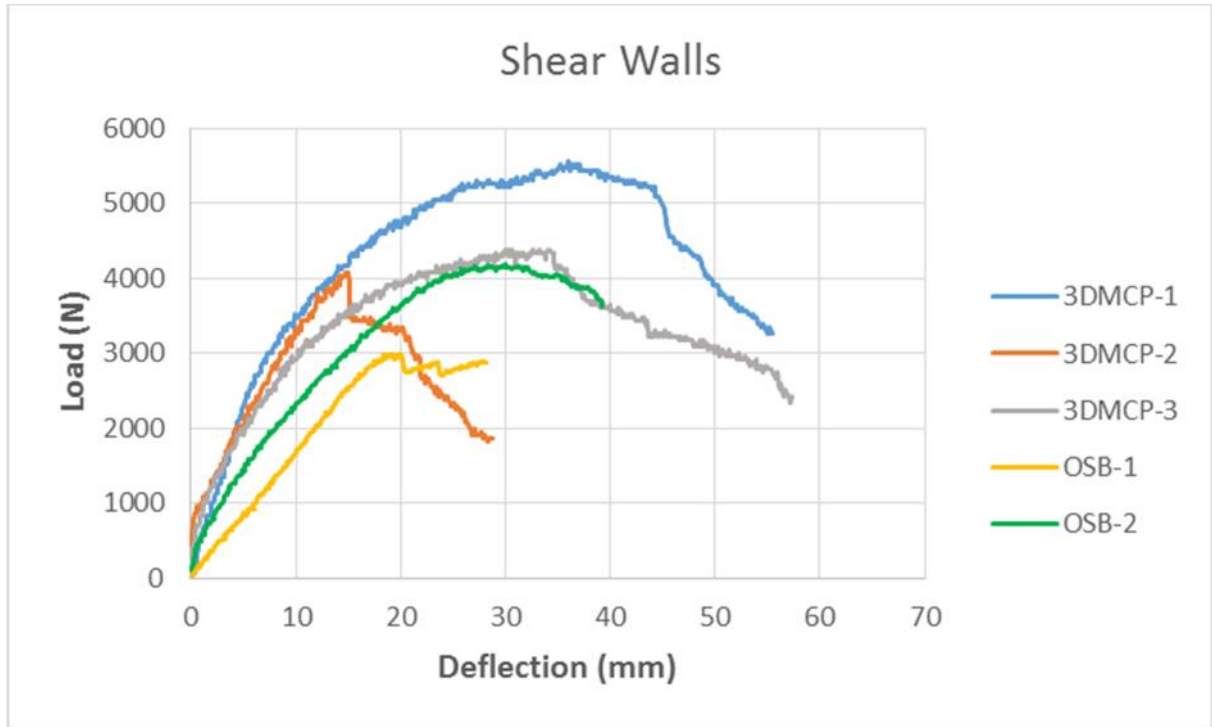


Figure F1. Load-deflection plot for all small-scale shear wall assemblies

Table F1. Small-scale shear wall results

ID	Peak load (N)	0.4 Peak (N)	0.9 Peak (N)	Yield (mm)	Peak (mm)	Fail (mm)	Slope, $K_e$ (N/mm)	Energy (J)
<b>OSB-1</b>	2986	1205	2736	7.5	20.0	21.0	161	41.2
<b>OSB-2</b>	4181	1672	3762	6.1	28.3	39.1	273	121.2
<b>MCP-1</b>	4387	1754	3948	4.1	30.0	36.5	429	107.6
<b>MCP-2</b>	4083	1633	3674	3.4	14.9	15.3	479	28.7
<b>MCP-3</b>	5560	2224	5004	4.9	36.0	44.8	454	196.5

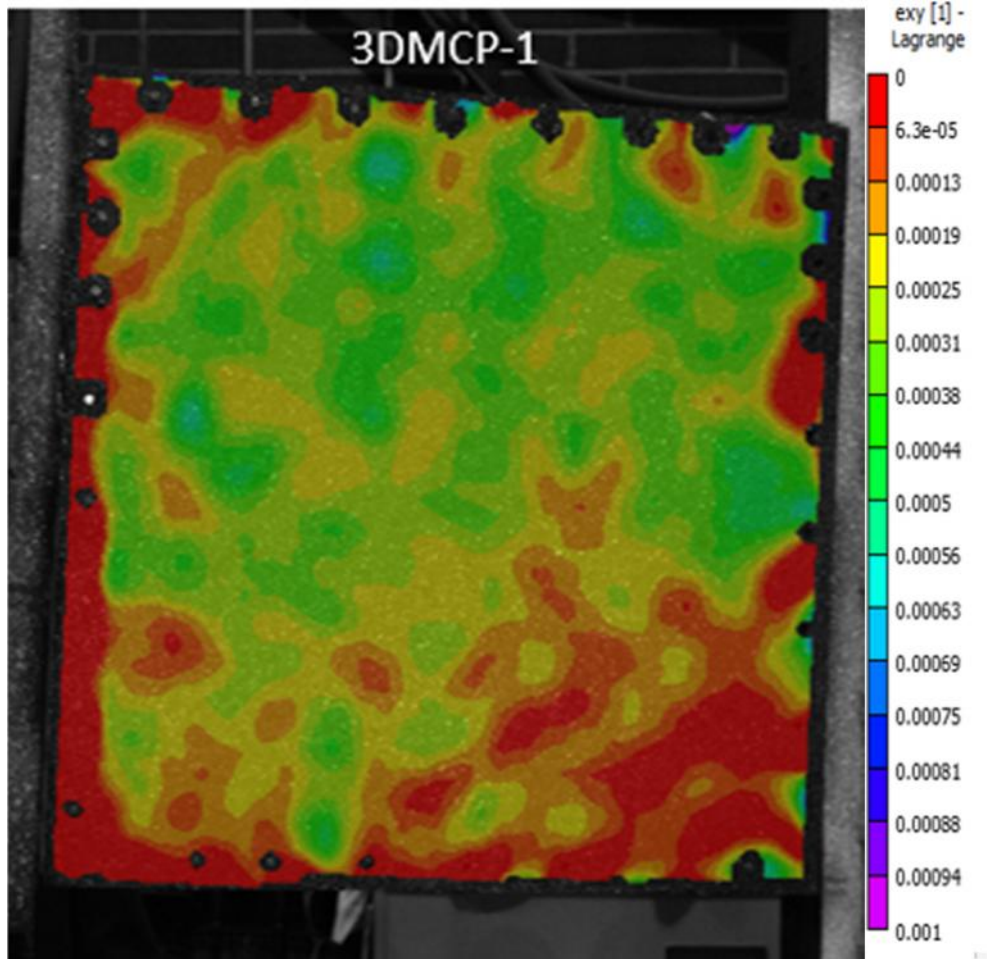


Figure F2. Strain contour plot for specimen 3DMCP-1 at peak load (4.39 kN)

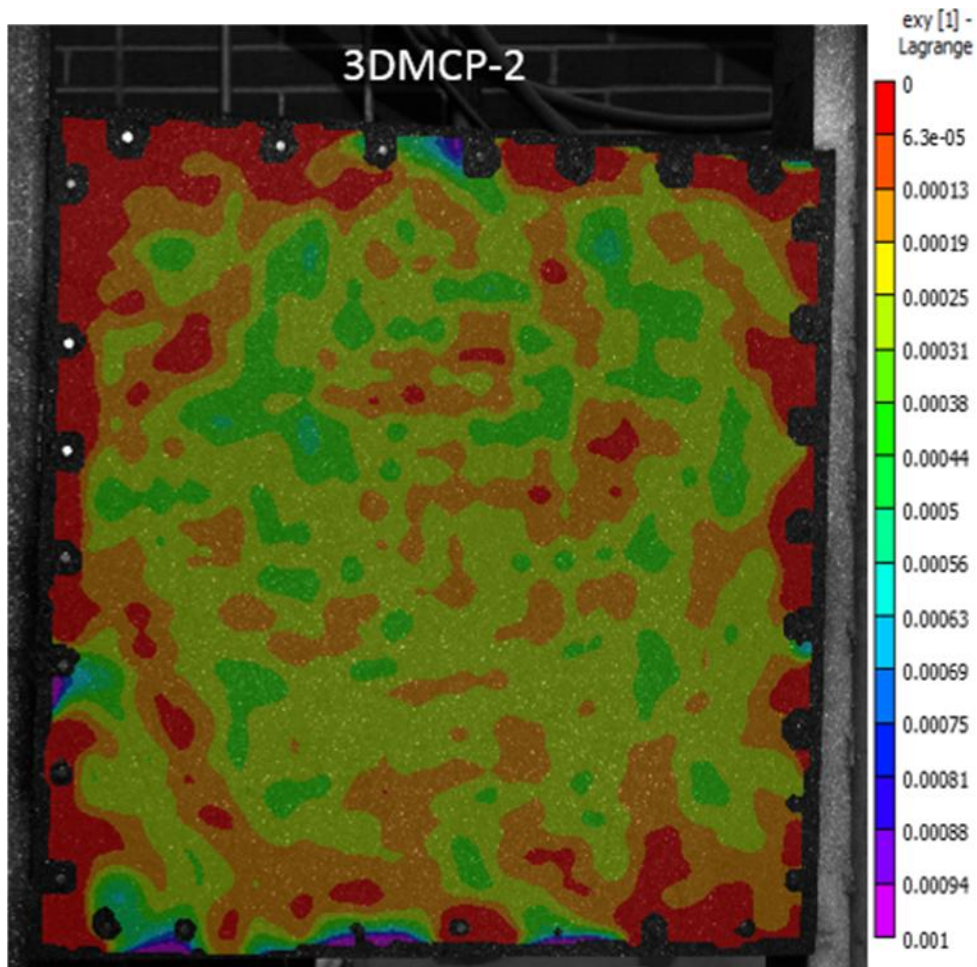


Figure F3. Strain contour plot for specimen 3DMCP-2 at peak load (4.08 kN)

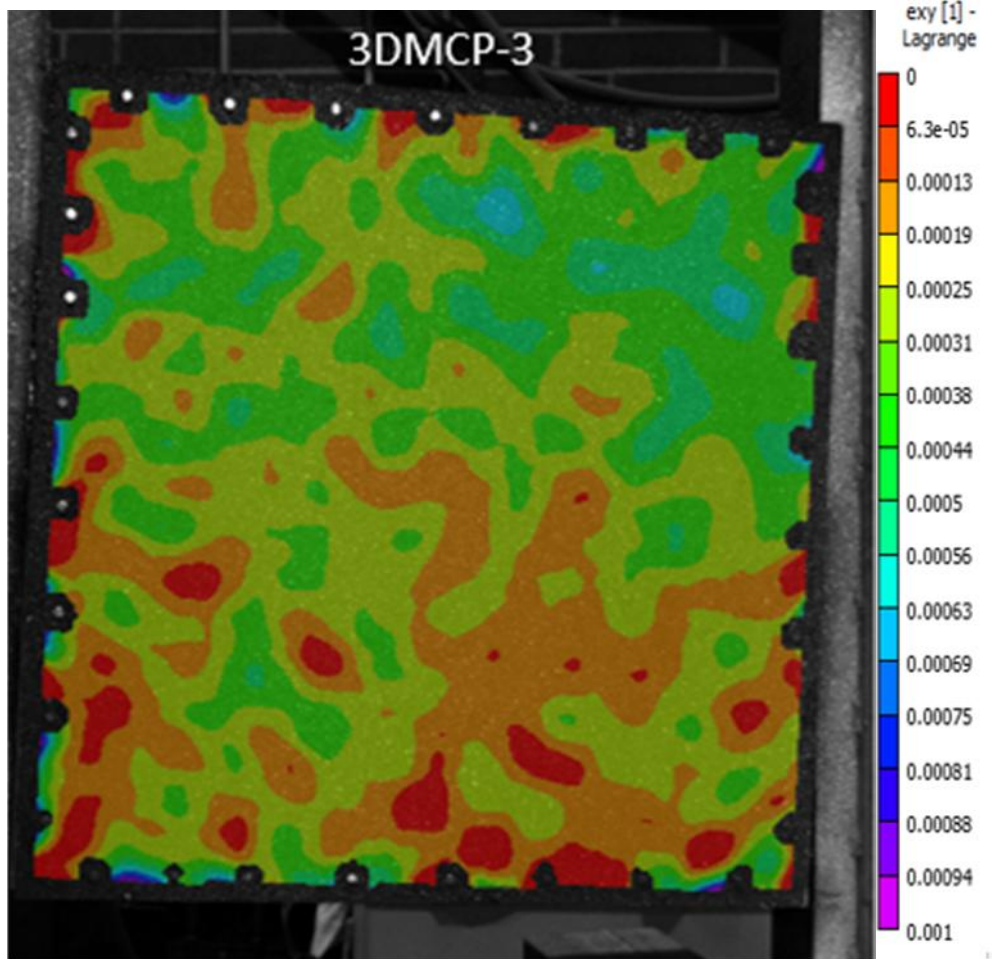


Figure F4. Strain contour plot for specimen 3DMCP-3 at peak load (5.56 kN)

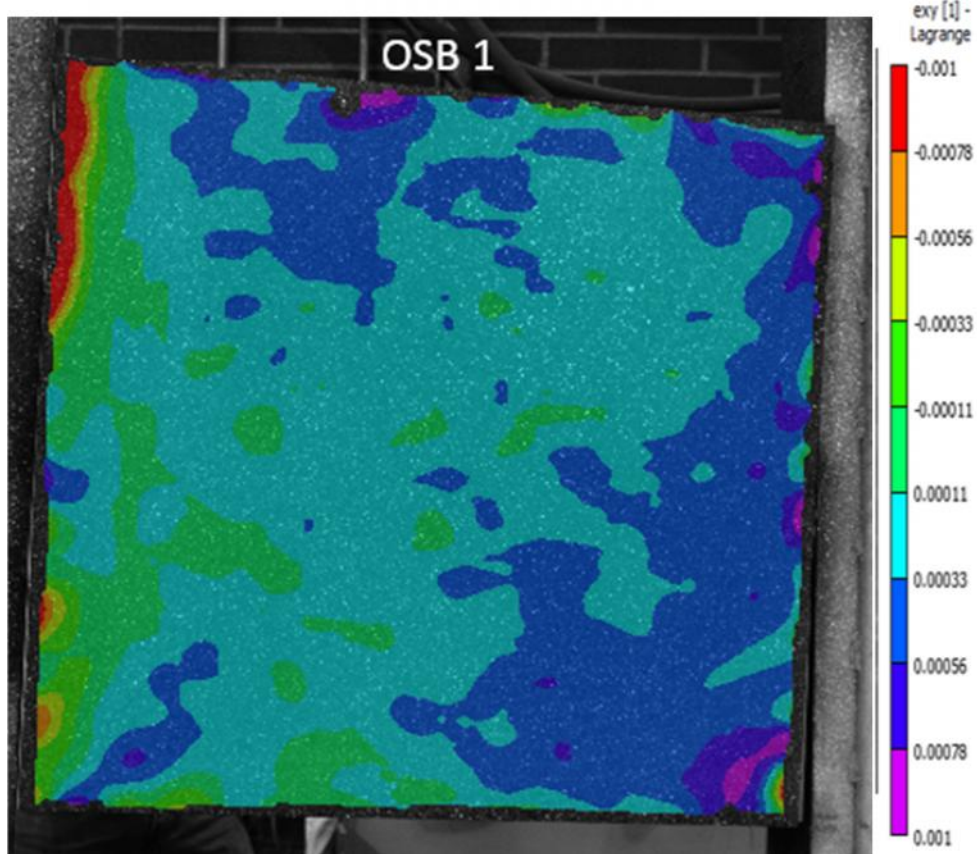


Figure F5. Strain contour plot for specimen OSB-1 at peak load (3.0 kN)

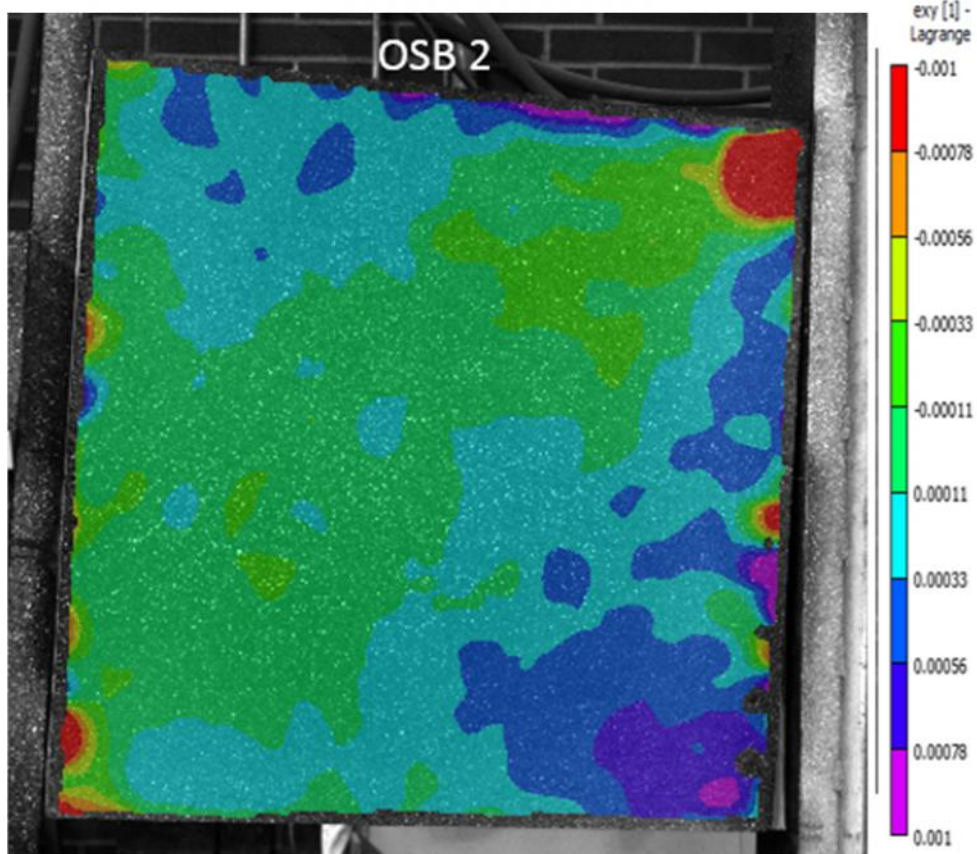


Figure F6. Strain contour plot for specimen OSB-2 at peak load (4.18 kN)